Visualizing and Characterizing Excited States from Time-Dependent Density Functional Theory

John M. Herbert*
Department of Chemistry & Biochemistry
The Ohio State University, Columbus, Ohio, 43210 USA

December 12, 2023

Abstract

Time-dependent density functional theory (TD-DFT) is the most widely-used electronic structure method for excited states, due to a favorable combination of low cost and (in many contexts) semi-quantitative accuracy. This Perspective describes various ways in which excited states from TD-DFT calculations can be visualized and analyzed, both qualitatively and quantitatively. This includes not just orbitals and densities but also well-defined statistical measures of electron–hole separation and of Frenkel-type exciton delocalization. Emphasis is placed on mathematical connections between methods that have often been discussed separately. Particular attention is paid to charge-transfer diagnostics, which provide indicators to diagnose when TD-DFT may not be trustworthy due to its categorical failure to describe long-range electron transfer. Measures of exciton size and charge separation that are directly connected to the underlying transition density are recommended over more *ad hoc* metrics for quantifying charge-transfer character.

*herbert@chemistry.ohio-state.edu

1 Introduction

Amongst various formulations of density functional theory (DFT) for electronic excited states,[1] by far the most widely used is linear-response DFT.[1–5] For historical reasons,[6] that formulation is commonly known as "time-dependent" (TD-)DFT,[1,5–8] despite the absence of time in its static, frequency-domain formulation. The latter formalism has a pleasing familiarity for chemists, as it can be cast as an eigenvalue problem in a space of singly-substituted Slater determinants, analogous to the method of configuration interaction with single substitutions (CIS)[9] but incorporating dynamical electron correlation. In favorable contexts, including the electronic spectroscopy of many medium-sized organic molecules, TD-DFT achieves a mean accuracy of ~ 0.3 eV for vertical excitation energies,[1,10] which is often sufficient for solution-phase spectroscopy. At the same time, TD-DFT's formal scaling and computational cost are comparable to ground-state DFT,[7,11] meaning that it is often the only *ab initio* method for excited states that can address large chemical systems. These considerations have made TD-DFT into the *de facto* workhorse of computational electronic spectroscopy.

The present work provides an overview of visualization methods for linear-response TD-DFT, going beyond molecular orbitals (MOs) and aiming to describe (and potentially quantify) how charge is rearranged upon electronic excitation. Both density-based and orbital-based visualization tools are considered, as are certain atomic partitions of the density change upon excitation,

$$\Delta\rho(\mathbf{r}) = \rho_{\mathrm{exc}}(\mathbf{r}) - \rho_0(\mathbf{r}) \; . \tag{1.1}$$

These can be used to characterize the nature of an excited state, in both qualitative and quantitative terms. Although many of these analysis and visualization methods have been around for a long time, only occassionally have the connections between them been discussed,[1,12–18] and often in a general form for correlated wave functions with arbitrary levels of excitation.[14–18] This obscures certain simplifications that are possible for CIS- and TD-DFT-type wave functions, where the particle–hole picture is clear and explicit. The present work is limited to those particular *ansätze*, with an emphasis on connections between different visualization tools that exist in the literature.

Especially relevant are a variety of charge-transfer (CT) metrics.[18–23] These can be used as prognosticators of (potentially catastrophic[1,24–28]) problems with conventional TD-DFT's description of long-range CT.[29] The practical effect is that TD-DFT significantly underestimates excitation energies for states having significant CT character,[1,9,30–32] including Rydberg states.[30,33] Significant progress has been made recently towards correcting this behavior,[34–36] via long-range corrected (LRC) density functionals,[37–39] yet it remains important to possess a means to diagnose problematic cases.

The remainder of this work is organized as follows. Section 2 provides a brief introduction to the formalism of linear-response TD-DFT and also introduces some visualization tools based on the density matrix, which are more incisive than simply plotting $\Delta\rho(\mathbf{r})$ in real space. Orbital-based visualization tools, which remain the most popular means for qualitative characterization of an excited state, are introduced in Section 3. To quantify charge rearrangement during excitation, it is useful to introduce an atomic partition of $\Delta\rho(\mathbf{r})$ that

can be made into a metric for CT but can also assist in understanding states that are delocalized across more than one chromophore. These tools are introduced in Section 4, and then Section 5 introduces additional ways to quantify exciton delocalization that have a direct connection to the underlying wave function or transition density. Finally, the CT problem in TD-DFT calculations is described in Section 6 along with a discussion of various metrics that can be used to indicate when (and for which excited states) this becomes an issue.

2 Theoretical Background

We begin with a brief recapitulation of the linear-response TD-DFT formalism (Section 2.1), then introduce densities and density matrices for ground and excited states (Section 2.2). Attachment and detachment densities,[40] which are important tools for excited-state visualization, are introduced in Section 2.3.

2.1 Linear-response TDDFT

Mathematical derivations of linear-response TD-DFT, starting from an explicitly time-dependent theory of a perturbed Kohn-Sham ground state, can be found elsewhere;[1–5] see Ref. 1 for a pedagogical version. The linear-response formalism is what is most often implied by "TD-DFT", as it is (by far) the most common form. An explicitly time-dependent or "real-time" formalism also exists,[1,41–43] which can be used to describe attosecond electron dynamics in an external electric field.[44–51] For excitation energies and most molecular electronic spectroscopy applications, however, the real-time method is much less efficient.[11] Real-time methods are not considered here, and visualization tools are somewhat different for that approach.[52–57]

Starting from the ground-state solution of the Kohn-Sham eigenvalue problem,[58]

$$\hat{F}\psi_r = \varepsilon_r \psi_r \ , \tag{2.1}$$

the basic equation of the linear-response formalism is

$$\begin{pmatrix} \mathbf{A} & \mathbf{B} \\ \mathbf{B}^* & \mathbf{A}^* \end{pmatrix} \begin{pmatrix} \mathbf{x}^{(n)} \\ \mathbf{y}^{(n)} \end{pmatrix} = \omega_n \begin{pmatrix} \mathbf{1} & \mathbf{0} \\ \mathbf{0} & -\mathbf{1} \end{pmatrix} \begin{pmatrix} \mathbf{x}^{(n)} \\ \mathbf{y}^{(n)} \end{pmatrix} \ . \tag{2.2}$$

This is a non-Hermitian eigenvalue problem for the excitation amplitudes $\mathbf{x}^{(n)} = (x_{ia}^{(n)})$ and de-excitation amplitudes $\mathbf{y}^{(n)} = (x_{ia}^{(n)})$, for the nth excited state whose vertical excitation energy is ω_n. Throughout this work, we use indices $i, j, \ldots$ to denote occupied MOs, $a, b, \ldots$ to indicate virtual (unoccupied) MOs, and $r, s, \ldots$ to denote arbitrary MOs. Spin indices are omitted here; see Ref. 1 for a version of these equations that includes them. The matrices $\mathbf{A}$ and $\mathbf{B}$ in Eq. (2.2) are Hessians with respect to orbital rotations.[1,59] In the canonical MO basis that diagonalizes the Fock matrix $\mathbf{F}$, their matrix elements are

$$A_{ia,jb} = (\varepsilon_a - \varepsilon_i)\delta_{ij}\delta_{ab} + \frac{\partial F_{ia}}{\partial P_{jb}} \tag{2.3a}$$

$$B_{ia,jb} = \frac{\partial F_{ia}}{\partial P_{bj}} \ , \tag{2.3b}$$

where $\mathbf{P}$ is the one-electron density matrix. Expressions for $\mathbf{A}$ and $\mathbf{B}$ in terms of electron repulsion integrals and the exchange-correlation kernel can be found elsewhere.[1,7,9] Lastly, the quantities $\varepsilon_a - \varepsilon_i$ in Eq. (2.3a) are differences between virtual (ε_a) and occupied (ε_i) Kohn-Sham energy levels defined by the ground-state eigenvalue problem, Eq. (2.1). The difference $\varepsilon_a - \varepsilon_i$ appears along the diagonal of $\mathbf{A}$ and constitutes a zeroth-order approximation to an electronic excitation energy, consistent with a zeroth-order picture in which an electronic transition consists in promotion of one electron from a single occupied MO into a single virtual MO, $\psi_i \rightarrow \psi_a$.

A TD-DFT calculation consists of the iterative solution of Eq. (2.2) for a certain number of excited states, each characterized by vectors $\mathbf{x}^{(n)}$ and $\mathbf{y}^{(n)}$. These are subject to an unconventional normalization,

$$\sum_{ia} (x_{ia}^2 - y_{ia}^2) = 1 \ , \tag{2.4}$$

consistent with the metric matrix in Eq. (2.2).[4,60–62] For brevity, we omit the state index n in Eq. (2.4) and subsequent expressions. Amplitudes $\{x_{ia}\}$ and $\{y_{ia}\}$ parameterize the *transition density matrix* (TDM) for the excitation in question. As a position-space kernel, that object is[4,7,61]

$$T(\mathbf{r},\mathbf{r}') = \sum_{ia}\Big[x_{ia}\,\psi_a(\mathbf{r})\,\psi_i^*(\mathbf{r}') + y_{ia}\,\psi_i(\mathbf{r})\,\psi_a^*(\mathbf{r}')\Big]\ . \tag{2.5}$$

It provides one possible visualization tool, usually in the form of the *transition density*, $T(\mathbf{r}) \equiv T(\mathbf{r},\mathbf{r})$.

Often, Eq. (2.2) is simplified by invoking the Tamm-Dancoff approximation (TDA),[3,63] in which the de-excitation amplitudes y_{ia} are neglected. These amplitudes arise naturally in the equation-of-motion formalism for the one-particle density matrix,[4,62] yet in molecular TD-DFT calculations they are typically $\sim 100\times$ smaller than the largest x_{ia}. (This this may not always be the case for solids.[64,65]) The matrix $\mathbf{B}$ is absent from the resulting TDA eigenvalue problem, which is simply

$$\mathbf{A}\mathbf{x} = \omega\mathbf{x}\ . \tag{2.6}$$

For historical reasons,[66] the original eigenvalue problem in Eq. (2.2) is sometimes called the *random phase approximation* (RPA),[9] in order to distinguish it from the simpler Hermitian eigenvalue problem in Eq. (2.6). That terminology is avoided here, however, so as not to confuse it with other methods known as RPA.[66–69] Where we need to make a distinction, we refer to Eq. (2.2) as "full" TD-DFT and Eq. (2.6) as TD-DFT/TDA.

Use of the TDA is often essential for avoiding triplet instabilities and obtaining accurate triplet excitation energies.[70–73] Triplet instabilities in the ground-state Kohn-Sham solution,[74] indicating that an unrestricted wave function would lower the energy with respect to the closed-shell solution, manifest as negative excitation energies.[75] This is common at bond-stretching geometries, where singlet and triplet states become quasi-degenerate,[76,77] but may also occur near the ground-state geometry, if the fraction of Hartree-Fock exchange is large,[78–83] or for large values of the range separation parameter in LRC functionals.[70,71,84–86] Beyond indicating an instability, solutions with negative excitation energies are not physically meaningful and can lead to convergence failure in solving Eq. (2.2), if the iterative algorithm is predicated on the excitation energies being positive. Invoking the TDA decouples the stability problem from the excitation energy problem and is used in most calculations that are described here.

The TDA simplifies the structure of the transition density into a form where one can imagine a Kohn-Sham wave function[2,87] (determinant) whose form is analogous to the CIS *ansatz*, namely

$$\big|\Psi_{\text{exc}}\big\rangle = \sum_{i}^{\text{occ}}\ \sum_{a}^{\text{vir}} x_{ia}\big|\Psi_i^a\big\rangle\ , \tag{2.7}$$

where $|\Psi_i^a\rangle$ is a Slater determinant that differs from the ground state by a single substitution. Given this form for $|\Psi_{\text{exc}}\rangle$, the real-space kernel $T(\mathbf{r},\mathbf{r}')$ in Eq. (2.5) can be connected to its more general definition in wave function theory,[13,61] which is

$$T(\mathbf{r},\mathbf{r}') = N\int \Psi_0^*(\mathbf{r}',\mathbf{r}_2,\ldots,\mathbf{r}_N)\ \Psi_{\text{exc}}(\mathbf{r},\mathbf{r}_2,\ldots,\mathbf{r}_N)\ d\mathbf{r}_2\cdots d\mathbf{r}_N \tag{2.8}$$

where $\Psi_0(\mathbf{r}_1,\ldots,\mathbf{r}_N)$ is the ground-state wave function. The definition of $T(\mathbf{r},\mathbf{r}')$ in Eq. (2.8) is valid for correlated wave functions also.[14]

It has been argued that eigenvalue differences $\varepsilon_a - \varepsilon_i$ should be good approximations to true excitation energies *in exact Kohn-Sham theory*,[87–90] albeit without spin coupling so there is no distinction between excitations to different spin multiplicities. As such, one might imagine that configuration mixing in Eq. (2.7) occurs to a lesser extent in TD-DFT as compared to CIS, and indeed this is observed to be the case.[91] For example, Figs. 1a and 1b compare amplitudes x_{ia} for $S_0 \rightarrow S_1$ excitation of formaldehyde, computed using TD-DFT/TDA with the PBE functional and also with the Hartree-Fock functional (*i.e.*, exact exchange and no correlation), the latter of which is equivalent to the CIS method. The TD-PBE eigenstate consists almost

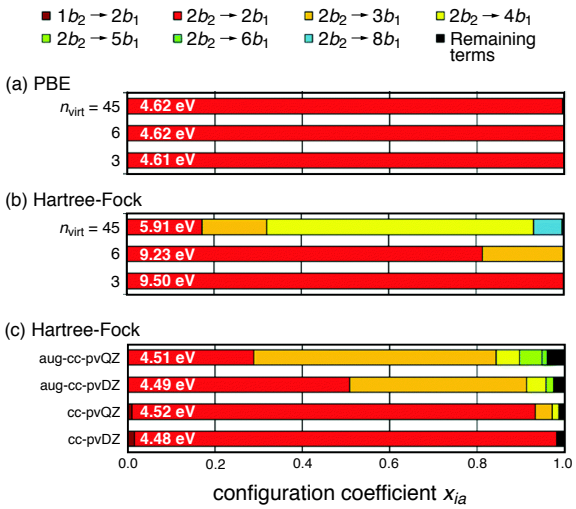

Figure 1: Bar graph of configuration mixing coefficients x_{ia} for TD-DFT/TDA calculations on the $1\,^1A_2$ state of formaldehyde: (a) calculations using the PBE functional using active spaces containing n_{virt} virtual orbitals, as implemented in a real-space (basis-set-free) electronic structure code; (b) CIS calculations using the same active spaces; and (c) conventional CIS calculations in Gaussian basis sets. Calculated excitation energies provide a measure of convergence with respect to active space or basis set. Adapted from Ref. 91; copyright 2015 The PCCP Owner Societies.

exclusively of the $2b_2 \rightarrow 2b_1$ amplitude whereas for a converged CIS calculation (including all virtual orbitals), this amplitude accounts for less than 20% of the norm of the transition eigenvector. (These calculations were performed using a real-space electronic structure code,[92] so there is not finite-basis approximation. CIS with conventional Gaussian basis sets are shown in Fig 1c.) Truncating the virtual space leads to a more compact expansion and a $2b_2 \rightarrow 2b_1$ coefficient in the CIS case, but has a disastrous effect on the excitation energy (Fig 1b). This is not a useful strategy.

That said, significant configuration mixing may be an unavoidable consequence of the use of hybrid functionals that contain some fraction of "exact" (Hartree-Fock) exchange. Because the Hartree-Fock virtual orbitals experience an N-electron potential rather than a $(N-1)$-electron potential,[93] the virtual levels ε_a are upshifted such that even frontier virtual orbitals are often unbound ($\varepsilon_a > 0$). These are discretized continuum states,[94] and a large number of them will need to mix together in order to generate the localized wave function of a bound excited state. Inclusion of diffuse basis functions, which are often necessary to obtain converged excitation energies,[8] also generate significant configuration mixing as shown in Fig. 1c.

Configuration mixing muddies the picture of electron and hole, thus it is desirable to have alternative ways of visualizing an excitation besides simply plotting each of the MOs whose amplitudes x_{ia} are significant. To that end, we next introduce excited-state electron densities that can be used to visualize an excitation in real space.

2.2 Densities and density matrices

Within TD-DFT, the density matrix for an excited state can be expressed as

$$\mathbf{P}_{\text{exc}} = \mathbf{P}_0 + \Delta\mathbf{P}^{\text{elec}} + \Delta\mathbf{P}^{\text{hole}} + \mathbf{Z}\,. \tag{2.9}$$

Here, $\mathbf{P}_0$ is the ground-state density matrix and

$$\Delta\mathbf{P} = \Delta\mathbf{P}^{\text{elec}} + \Delta\mathbf{P}^{\text{hole}} \tag{2.10}$$

is the (unrelaxed) difference density matrix. Lastly, $\mathbf{Z}$ is the so-called Z-vector contribution that accounts for orbital relaxation in the excited state.[7,82,95] The "particle" (or electron) and "hole" components of $\Delta\mathbf{P}$

are available from the TD-DFT response vectors:[82,95–97]

$$\Delta\mathbf{P}^{\text{elec}} = \tfrac{1}{2}\Big[(\mathbf{x}+\mathbf{y})^\dagger(\mathbf{x}+\mathbf{y}) + (\mathbf{x}-\mathbf{y})^\dagger(\mathbf{x}-\mathbf{y})\Big] \tag{2.11a}$$

$$\Delta\mathbf{P}^{\text{hole}} = -\tfrac{1}{2}\Big[(\mathbf{x}+\mathbf{y})(\mathbf{x}+\mathbf{y})^\dagger + (\mathbf{x}-\mathbf{y})(\mathbf{x}-\mathbf{y})^\dagger\Big] \,. \tag{2.11b}$$

These formulas correct thosse written down intuitively in previous work,[98] which include the $(\mathbf{x}+\mathbf{y})^\dagger(\mathbf{x}+\mathbf{y})$ term of Eq. (2.11) but not the $(\mathbf{x}-\mathbf{y})^\dagger(\mathbf{x}-\mathbf{y})$ term. Expressions for the matrix elements in the MO basis can be simplified to afford[96]

$$(\Delta\mathbf{P}^{\text{elec}})_{ab} = \sum_i (x^*_{ia}x_{ib} + y^*_{ia}y_{ib}) \tag{2.12a}$$

$$(\Delta\mathbf{P}^{\text{hole}})_{ij} = -\sum_a (x_{ia}x^*_{ja} + y_{ia}y^*_{ja}) \,. \tag{2.12b}$$

These quantities are normalized such that

$$\text{tr}(\Delta\mathbf{P}^{\text{elec}}) = 1 = -\,\text{tr}(\Delta\mathbf{P}^{\text{hole}}) \,. \tag{2.13}$$

Although we have not been explicit about spin indices, the spin-orbital indices (i, a, etc.) could be limited to either α or β spin, *e.g.*, to obtain a spin density matrix for either the particle ($\Delta\mathbf{P}^{\text{elec}}_{\boldsymbol{\alpha}} - \Delta\mathbf{P}^{\text{elec}}_{\boldsymbol{\beta}}$) or hole ($\Delta\mathbf{P}^{\text{hole}}_{\boldsymbol{\alpha}} - \Delta\mathbf{P}^{\text{hole}}_{\boldsymbol{\beta}}$).

Whereas $\Delta\mathbf{P}$ in Eq. (2.9) is available from $\mathbf{x}$ and $\mathbf{y}$ alone, calculation of $\mathbf{Z}$ requires solution of the coupled-perturbed equations that are associated with the TD-DFT excited-state gradient.[82,97] The density matrix $\mathbf{P}_{\text{exc}}$ that includes $\mathbf{Z}$ is known as the "relaxed" density matrix, whereas

$$\mathbf{P}_{\text{unrlx}} = \mathbf{P}_0 + \Delta\mathbf{P} \tag{2.14}$$

is the unrelaxed density matrix.

As the notation implies, the quantities $\Delta\mathbf{P}^{\text{elec}}$ and $\Delta\mathbf{P}^{\text{hole}}$ can be conceptualized as separate densities for the excited electron and the hole that it leaves behind in the occupied space. More precisely, this is true of the real-space densities $\Delta\rho_{\text{elec}}(\mathbf{r})$ and $\Delta\rho_{\text{hole}}(\mathbf{r})$ that are encoded by these density matrices. Unlike the difference density

$$\Delta\rho(\mathbf{r}) = \Delta\rho_{\text{elec}}(\mathbf{r}) + \Delta\rho_{\text{hole}}(\mathbf{r}) \,, \tag{2.15}$$

which has both positive and negative regions in space, $\Delta\rho_{\text{elec}}(\mathbf{r}) \geq 0$ everywhere, and $\Delta\rho_{\text{hole}}(\mathbf{r}) \leq 0$. Sometimes it is more informative to visualize these two quantities separately. It is therefore suggested that $\Delta\rho_{\text{elec}}(\mathbf{r})$ should be called the *particle density* and $\Delta\rho_{\text{hole}}(\mathbf{r})$ the *hole density*. (These terms are sometimes used differently,[14] but our usage is consistent with the idea of $\Delta\mathbf{P}^{\text{hole}}$ as the density matrix for the hole.[60]) An example is depicted in Fig. 2, where the particle and hole densities can be visually superimposed by the reader to suggest the difference density, which is also shown. The $\mathbf{Z}$-vector contribution is omitted in this example, making these unrelaxed densities.

The molecule in Fig. 2 is a polyfluorene oligomer with a single keto defect (fluorenone) as one of the terminal monomer units.[99] It provides an example of how particle and hole densities are useful for interpreting excited states that are strongly mixed in the canonical MO basis, meaning there are numerous amplitudes x_{ia} that are similar in magnitude. In this particular example, each of the valence MOs is completely delocalized along the length of the oligomer, which is not atypical for π-conjugated chromophores. Nevertheless, it is obvious from the densities in Fig. 2 that the excited state in question is localized as a result of the defect. This is not obvious within the canonical MO basis, however, wherein the transition density consists of a roughly equal mixture of four different $\psi_i \rightarrow \psi_a$ excitations as shown in Fig. 3a. Localization arises from phase interference in a coherent superposition of four terms, but this would be essentially impossible to discern by inspecting the relevant MOs alone.

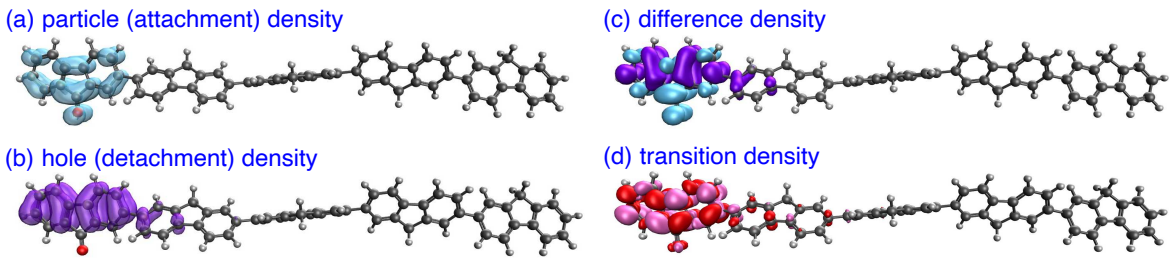

Figure 2: Unrelaxed densities for (a) the particle ($\Delta\rho_{\text{elec}}$) and (b) the hole ($\Delta\rho_{\text{hole}}$), along with (c) their sum $\Delta\rho$ [Eq. (2.15)] and (d) the transition density $T(\mathbf{r})$. The excitation in question is the lowest dipole-allowed transition ($S_0 \rightarrow S_2$) of a five-unit, fluorenone-terminated polyfluorene whose leftmost fluorene unit contains a carbonyl defect. TD-DFT/TDA calculations were performed at the CAM-B3LYP/3-21G* level. Adapted from Ref. 1; copyright 2023 Elsevier.

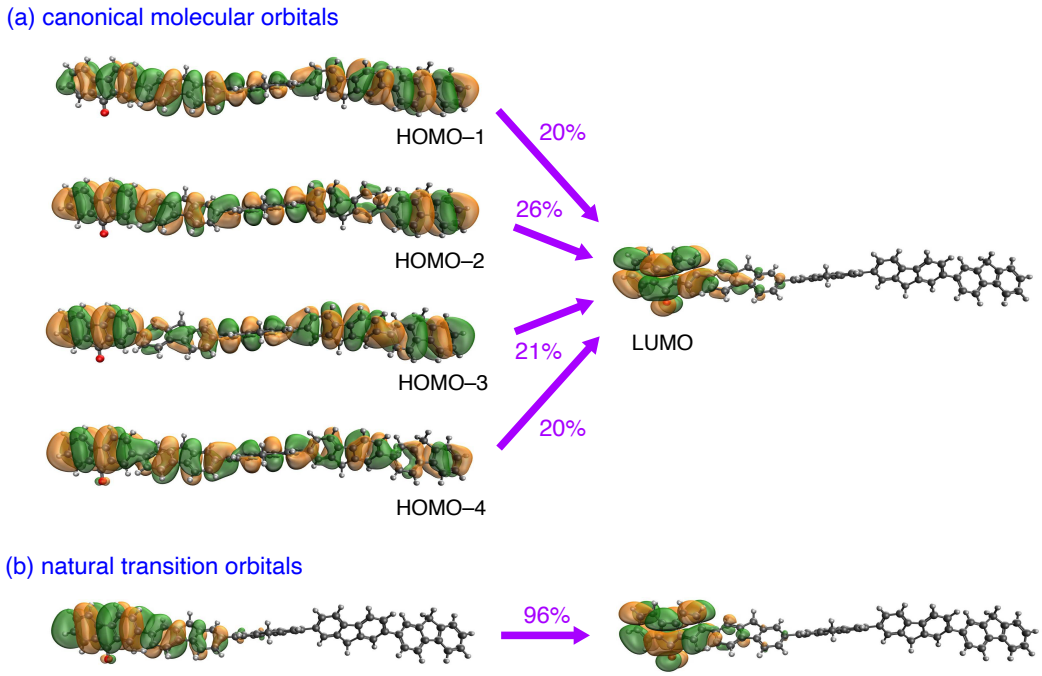

Figure 3: Transition density for the fluorenone-terminated polyfluorene oligomer that is also depicted in Fig. 2, viewed here in two different representations: (a) the canonical MO representation, with weights x_{ia}^2 given as percentages, and (b) the NTO representation, with weight λ_1^2 that is also given as a percentage. TD-DFT/TDA calculations were performed at the CAM-B3LYP/3-21G* level. Adapted from Ref. 1; copyright 2023 Elsevier.

2.3 Attachment and detachment densities

For CIS and TD-DFT calculations, the particle and hole densities defined in Section 2.2 coincide precisely with the *attachment density* and the *detachment density*, respectively, quantities that were originally defined in a manner that is not be limited to single-excitation theories.[40] This definition sheds additional light on the nature of $\Delta\mathbf{P}^{\text{elec}}$ and $\Delta\mathbf{P}^{\text{hole}}$ in TD-DFT, and is the topic of this section First, let us diagonalize a difference density matrix $\Delta\mathbf{P}$ and express the result in the form

$$\mathbf{U}^{\dagger}(\Delta\mathbf{P})\mathbf{U} = \begin{pmatrix} \mathbf{a} & \mathbf{0} \\ \mathbf{0} & \mathbf{d} \end{pmatrix} , \tag{2.16}$$

where the nonzero blocks $\mathbf{a}$ and $\mathbf{d}$ are diagonal matrices that contain the positive and the negative eigenvalues of $\Delta\mathbf{P}$, respectively. Density matrices affording the attachment and detachment densities are then defined as[12,13,40]

$$\Delta\mathbf{P}^{\text{attach}} = \mathbf{U} \begin{pmatrix} \mathbf{a} & \mathbf{0} \\ \mathbf{0} & \mathbf{0} \end{pmatrix} \mathbf{U}^{\dagger} \tag{2.17a}$$

and

$$\Delta\mathbf{P}^{\text{detach}} = \mathbf{U} \begin{pmatrix} \mathbf{0} & \mathbf{0} \\ \mathbf{0} & \mathbf{d} \end{pmatrix} \mathbf{U}^{\dagger} . \tag{2.17b}$$

Note that $\Delta\mathbf{P}^{\text{attach}}$ is positive semidefinite and $\Delta\mathbf{P}^{\text{detach}}$ is negative semidefinite.

The procedure above could be followed for any difference density matrix, including the relaxed one from a TD-DFT calculation or one that is obtained from a correlated wave function. In the special case that $\Delta\mathbf{P}$ is the unrelaxed difference density matrix from a TD-DFT calculation [Eq. (2.10)], it follows that $\Delta\mathbf{P}^{\text{attach}} \equiv \Delta\mathbf{P}^{\text{elec}}$ and $\Delta\mathbf{P}^{\text{detach}} \equiv \Delta\mathbf{P}^{\text{hole}}$. Although this equivalence has been noted before,[1,13] it does not seem to be widely appreciated. It arises from a unique feature of single-excitation theories, namely, a direct correspondence between CI coefficients and matrix elements of the TDM.[14,61,62,100] For example, $x_{ia} = \langle\Psi_{\text{exc}}|\hat{a}_a^{\dagger}\hat{a}_i|\Psi_0\rangle$ in the CIS case.

Considering the specific case of $\Delta\mathbf{P}$ in Eq. (2.10), qualitative insight into the nature of an excited state can often be gleaned by analyzing its particle and hole components $\Delta\mathbf{P}^{\text{elec}}$ and $\Delta\mathbf{P}^{\text{hole}}$, but it must be borne in mind that electron/hole separation does not survive the contribution from orbital relaxation, *i.e.*, from $\mathbf{Z}$ in Eq. (2.9). Nonzero matrix elements $Z_{ia} = Z_{ai}$ introduce occupied–virtual coupling, in contrast to the occupied–occupied and virtual–virtual terms that define the unrelaxed difference density [Eq. (2.12)]. However, one may construct the *relaxed* difference density,

$$\Delta\mathbf{P}_{\text{rlx}} = \mathbf{P}_{\text{exc}} - \mathbf{P}_0 = \Delta\mathbf{P} + \mathbf{Z} , \tag{2.18}$$

and substitute this for $\Delta\mathbf{P}$ in Eq. (2.16). This defines attachment and detachment components of the relaxed density and recovers a particle/hole picture that includes includes orbital relaxation.

Relaxation effects can be especially significant for states with CT character, as demonstrated in Fig. 4 for the case of a donor–acceptor complex consisting of naphthalene and tetracyanoquinone. Unrelaxed particle and hole densities (on the left in Fig. 4) suggest that the S_1 state of the complex has almost perfect CT character, with the excited electron localized on the acceptor (tetracyanoquinone) and the hole localized on the donor (naphthalene). A dipole moment change of $\Delta\mu = 14.9$ D upon excitation underscores this CT character. However, both of the relaxed densities (on the right in Fig. 4) are delocalized over both monomers. The change in dipole moment ($\Delta\mu = 10.9$ D) is substantially reduced although still quite large. Note that the excitation energy is precisely the same regardless of which densities are used to visualize the transition in question, as is the ground-state dipole moment of 1.3 D, however the excited-state dipole moment changes significantly when computed using the relaxed density matrix for the excited state.

This example underscores the fact that using $\Delta\mathbf{P}_{\text{rlx}}$ rather than $\Delta\mathbf{P}$ can have a significant effect on excited-state properties,[95,101,106] especially for states with a high degree of CT character.[95] The relaxed

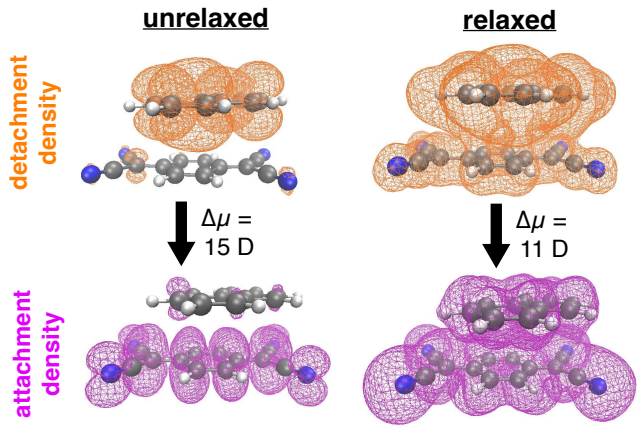

Figure 4: Relaxed and unrelaxed detachment densities (upper images, in orange) and attachment densities (lower images, in magenta) for the $S_0 \rightarrow S_1$ excitation of a donor–acceptor complex between naphthalene and tetracyanoquinone, computed at the TD-ωB97X-D/6-31G* level within the TDA. All densities are plotted using 90% isoprobability contours. Unrelaxed densities (on the left), which are equal to $\Delta\rho_{\text{elec}}(\mathbf{r})$ and $\Delta\rho_{\text{hole}}(\mathbf{r})$ in Eq. (2.15), consist of donor and acceptor densities localized on naphthalene and tetracyanoquinone, respectively. Relaxed densities (on the right) are delocalized over both molecules although the state maintains significant CT character as evidenced by the dipole moment change upon excitation, $\Delta\mu$.

Table 1: Excitation energies and excited-state dipole moments compared to experiment.[a]

Molecule & Method	ΔE (eV)	μ (D)[b] unrelaxed	μ (D)[b] relaxed
formaldehyde ($^1A_2$)			
TD-BLYP	3.82	−0.05	−1.34
TD-B3LYP	3.98	−0.22	−1.40
TD-BH&HLYP	4.08	−0.39	−1.40
TD-HF	4.39	−0.60	−1.26
CASSCF(12,10)			−1.29
experiment	4.07[c]		-1.56 ± 0.07[d]
p-nitroaniline (^{1}CT)			
TD-BLYP	3.61	23.57	11.71
TD-B3LYP	4.07	20.81	12.40
TD-BH&HLYP	4.63	16.81	12.43
TD-HF	4.89	11.53	10.71
CASSCF(12,12)			16.35
experiment	4.24[e]		13.35[f]

[a]Data from Ref. 101 except where indicated. [b]Sign convention set by the ground-state dipole moment. [c]Ref. 102. [d]Ref. 103. [e]Ref. 104. [f]Ref. 105.

dipole moment, for example, which is the *correct* dipole moment for the excited state according to linear response theory, is computed as $\mu_x^{\text{rlx}} = \text{tr}(\boldsymbol{\mu}_x \mathbf{P}_{\text{exc}})$ for the x component, and its unrelaxed analog is $\mu_x^{\text{unrlx}} = \text{tr}(\boldsymbol{\mu}_x \mathbf{P}_{\text{unrlx}})$. In Table 1, these two quantities are juxtaposed for the first excited state of formaldehyde ($^1A_2$), and for an excited state of *p*-nitroaniline that is characterized by excitation from the highest occupied MO (HOMO) to the lowest unoccupied MO (LUMO) that transfers charge from the amino group to the nitro group. Even for the comparatively benign case of formaldehyde, use of the relaxed density alters the total dipole moment by more than 1 D for several different density functionals, bringing it much closer to experiment. The contrast is more dramatic for *p*-nitroaniline, where ^{1}CT state exhibits a large dipole moment ($\mu \approx 13$ D),[105,107] and one might therefore expect significant orbital relaxation effects. Unrelaxed densities overestimate this dipole moment by more than a factor of two in some cases, although the effect decreases as the fraction of exact exchange is increased. (Relaxed and unrelaxed dipole moments differ by more than a factor of two for formaldehyde as well,[101,106] but the dipole moment is much smaller.)

Although relaxed densities are required for reliable and quantitative excited-state property calculations, there is much qualitative information to be gleaned from the unrelaxed density. The CT nature of the donor $\rightarrow$ acceptor transition in the naphthalene:tetracyanoquinone dimer (Fig. 4), for example, comes through in both the relaxed and unrelaxed dipole moments, even if orbital relaxation serves to delocalize both particle and hole across both monomers. Other examples considered below will neglect the **Z**-vector contribution, which is adequate for a quick survey of the nature of the predicted excited states.

3 Natural Transition Orbitals

Densities reveal how overall charge is moved about upon excitation but they sacrifice the phase (sign) information that is contained in the orbitals, which might have been helpful for understanding the character of an excited state. If the number of significant amplitudes x_{ia} is small, then the canonical Kohn-Sham MOs are a good way to visualize the state in question but often this is not the case, especially when hybrid functionals are employed. A quantity that *does* contain phase information is the transition density $T(\mathbf{r}, \mathbf{r}')$ that is defined in Eqs. (2.5) and (2.8), which can be plotted in three-dimensional space by setting $\mathbf{r} = \mathbf{r}'$. This quantity, however, cannot be interpreted directly in terms of the movement of charge in the same way that the particle, hole, and difference densities can be. For example, consider the transition density $T(\mathbf{r}) \equiv T(\mathbf{r}, \mathbf{r})$ for the fluorenone-terminated polyfluorene oligomer that was considered above (Fig. 2d). Although its nodal structure contains elements of the nodal structures of both $\Delta\rho_{\text{elec}}$ and $\Delta\rho_{\text{hole}}$, $T(\mathbf{r})$ is clearly distinct from the difference density. What can be gleaned from $T(\mathbf{r})$ is the nature of the transition moment for the excitation in question, which must lie along the long axis of the molecule because the negative and positive lobes of $T(\mathbf{r})$ approximately cancel along the short axis. Clearly, the result of the fluorenone defect is that this particular excited state is a property of the terminal monomer (fluorenone), not a property of the whole polymer. This fact is not obvious from the canonical MOs that participate in the transition, which are shown in Fig. 3a. The *natural transition orbitals* (NTOs),[108] which are introduced below, will help to recover an electron/hole picture within a representation that contains phase information.

3.1 Theory

Starting from $\Delta\mathbf{P}^{\text{elec}}$ and $\Delta\mathbf{P}^{\text{hole}}$ defined in Eq. (2.12), phase information can be restored (in a manner that maximally preserves the qualitative characteristics of these densities) by using their eigenvectors to define a change-of-basis for the MOs. The transformation $\mathbf{U}_{\text{o}}$ that diagonalizes $\Delta\mathbf{P}^{\text{elec}}$ defines a transformation of the canonical occupied MOs that we express as

$$\mathbf{U}_{\text{o}}^{\dagger}(\Delta\mathbf{P}^{\text{elec}})\mathbf{U}_{\text{o}} = \underbrace{\begin{pmatrix} \lambda_1^2 & 0 & 0 & \cdots \\ 0 & \lambda_2^2 & 0 & \cdots \\ & & \ddots & 0 \\ 0 & \cdots & 0 & \lambda_N^2 \end{pmatrix}}_{\boldsymbol{\Lambda}^2} . \tag{3.1}$$

The $n_{\rm occ} \times n_{\rm occ}$ diagonal matrix $\mathbf{\Lambda}^2$ contains the eigenvalues of $\Delta\mathbf{P}^{\rm elec}$. (It is the square of a diagonal matrix $\mathbf{\Lambda}$ that will be used in Section 3.2, where we will discover that the values λ_i have their own significance.) Eigenvalues of $\Delta\mathbf{P}^{\rm elec}$ are strictly non-negative, which we indicate by writing them as λ_i^2, and they are normalized such that $\sum_i \lambda_i^2 = 1$ [Eq. (2.13)]. In similar fashion, we introduce a matrix $\mathbf{U}_{\rm v}$ that diagonalizes $\Delta\mathbf{P}^{\rm hole}$:

$$\mathbf{U}_{\rm v}^\dagger(\Delta\mathbf{P}^{\rm hole})\mathbf{U}_{\rm v} = \begin{pmatrix} -\mathbf{\Lambda}^2 & \mathbf{0} \\ \mathbf{0} & \mathbf{0} \end{pmatrix} . \tag{3.2}$$

This defines a transformation of the canonical virtual MOs. For single-excitation wave functions, the matrices $\Delta\mathbf{P}^{\rm elec}$ and $\Delta\mathbf{P}^{\rm hole}$ have the same eigenvalues, up to a sign,[99,108] so $\mathbf{\Lambda}^2$ is the same matrix $n_{\rm occ} \times n_{\rm occ}$ in both Eqs. (3.1) and (3.2). (Extra zeros in the latter are needed to dimension the matrices consistently.)

The matrix $\mathbf{U}_{\rm o}$ transforms the canonical occupied MOs into a set of "hole" orbitals that we will call $\{\psi_i^{\rm hole}(\mathbf{r})\}$, while $\mathbf{U}_{\rm v}$ transforms the canonical virtual MOs into a corresponding set of "particle" (or "electron") orbitals $\{\psi_i^{\rm elec}(\mathbf{r})\}$ where $i = 1, \ldots, n_{\rm occ}$ in both cases, because even for the virtual orbital transformation in eq. (3.2) there are only $n_{\rm occ}$ nonzero eigenvalues. These transformed orbitals are the NTOs for the hole and for the excited electron, respectively. These are useful analysis tools because they reduce the $2n_{\rm occ}n_{\rm virt}$ excitation amplitudes x_{ia} and y_{ia} into just $n_{\rm occ}$ unique amplitudes, as will be discussed further in Section 3.2. For now, we simply note that the particle and hole densities are diagonal in the NTO representation, which in real space means

$$\Delta\rho_{\rm elec}(\mathbf{r}) = \sum_{i=1}^{n_{\rm occ}} \lambda_i^2 \left|\psi_i^{\rm elec}(\mathbf{r})\right|^2 \tag{3.3a}$$

$$\Delta\rho_{\rm hole}(\mathbf{r}) = -\sum_{i=1}^{n_{\rm occ}} \lambda_i^2 \left|\psi_i^{\rm hole}(\mathbf{r})\right|^2 . \tag{3.3b}$$

Examples of NTOs are provided in Sections 3.3 and 3.4.

The name NTOs was first suggested by Martin in 2003,[108] but this form of analysis was actually introduced much earlier by Luzanov and co-workers.[109,110] It has since be rediscovered (and expressed in the notation used above) by others.[100,108,111] The terminology for these orbitals reflects the sense in which "natural" is used in quantum chemistry to mean eigenfunctions of a density matrix.[112–114] Just as *natural orbitals* are eigenfunctions of $\mathbf{P}$ (even in the case of a correlated wave function),[112] with eigenvalues that constitute *natural occupation numbers*, the NTOs diagonalize the TDM. Within a single-excitation model, this is equivalent to diagonalizing the difference density matrix $\Delta\mathbf{P}$, although that equivalence is lost in the case of a correlated wave function. (In that case, one must distinguish between NTOs that diagonalize the TDM and *natural difference orbitals* that diagonalize the difference density matrix.[14,15]) Similarly, *natural ionization orbitals* diagonalize the difference density obtained upon electron removal.[115] None of these quantities should be confused with *natural bond orbitals* or any of the other "natural" concepts introduced by Weinhold and co-workers.[116–118]

3.2 Interpretation

The transformations in Eqs. (3.1) and (3.2) fully defines the NTOs in TTDFT, but an equivalent and illustrative definition is possible. Keeping to the TDA case for simplicity, we considder $\mathbf{x}$ to be a rectangular matrix of dimension $n_{\rm occ} \times n_{\rm virt}$. Hole and particle NTOs are defined by separate unitary transformations of the occupied and virtual MOs ($\mathbf{U}_{\rm o}$ and $\mathbf{U}_{\rm v}$, respectively), and an equivalent definition of these two transformations involves a singular value decomposition (SVD) of $\mathbf{x}$:

$$\mathbf{U}_{\rm o}^\dagger\,\mathbf{x}\,\mathbf{U}_{\rm v} = \begin{pmatrix} \mathbf{\Lambda} & \mathbf{0} \\ \mathbf{0} & \mathbf{0} \end{pmatrix} . \tag{3.4}$$

Here, $\mathbf{\Lambda}$ is the $n_{\rm occ} \times n_{\rm occ}$ matrix of singular values λ_i, but is the same matrix that appears (as $\mathbf{\Lambda}^2$) in eqs. (3.1) and (3.2). According to Eq. (3.4), the matrices $\mathbf{U}_{\rm o}$ and $\mathbf{U}_{\rm v}$ contain the left and right singular

vectors of $\mathbf{x}$, respectively, but they are identical to the eponymous transformations defined as eigenvectors of $\Delta\mathbf{P}^{\text{hole}}$ and $\Delta\mathbf{P}^{\text{elec}}$.

As compared to the definitions in Section 3.1, the construction in Eq. (3.4) demonstrates more clearly why no more than n_{occ} of the singular values are non-zero, and that eigenvalues of $\Delta\mathbf{P}^{\text{hole}}$ and $\Delta\mathbf{P}^{\text{elec}}$ occur in pairs.[108] From yet another point of view, Eq. (3.4) is a special case of a *corresponding orbitals* transformation,[119–121] which selects a subset of virtual orbitals in one-to-one correspondence with the occupied orbitals, diagonalizing the TDM in the process.

If $\Delta\mathbf{P}^{\text{hole}}$ is dominated by a single NTO, it follows that so is $\Delta\mathbf{P}^{\text{elec}}$, which is a consequence of the correspondence between amplitudes x_{ia} and elements of the one-particle density matrix that was discussed in Section 2.3. As a result, for single-excitation theories (only), the NTOs are equivalent to excited-state natural orbitals.[100] For CIS wave functions, the corresponding eigenvalues in the natural orbital basis (natural occupation numbers) can be specified in terms of the singular values of the transition amplitudes:[100]

$$n_r = \begin{cases} 1-\lambda_r^2, & 1 \leq r \leq N \\ \lambda_r^2, & N < r \leq 2N \\ 0, & r > 2N \end{cases} . \tag{3.5}$$

The values $n_r = 1-\lambda_r^2$ represent the hole that is created and $n_r = \lambda_r^2$ correspond to the excited electron, which demonstrates why $\Delta\mathbf{P}^{\text{elec}}$ and $\Delta\mathbf{P}^{\text{hole}}$ have the same eigenvalues up to a sign. Redundant orbitals ($n_r = 0$) have been eliminated by the SVD in Eq. (3.4). Although the direct connection between the excitation amplitudes, transition density, and one-electron density matrix for the excited state is a unique feature of the single-excitation *ansatz*, the concept of attachment and detachment densities as eigenfunctions of $\Delta\mathbf{P}$, separable based on the sign of the eigenvalues in Eqs. (2.16) and (2.17), is generalizable to wave functions of arbitrary complexity. The individual eigenfunctions of $\Delta\mathbf{P}$, which are the NDOs,[14] then generalize the concept of NTOs for many-body theories, without the need to introduce "correlated NTOs".[122]

Notice also that the TDM is diagonal in the NTO basis:

$$T(\mathbf{r},\mathbf{r}') = \sum_{i}^{n_{\text{occ}}} \lambda_i \, \psi_i^{\text{elec}}(\mathbf{r}) \left[\psi_i^{\text{hole}}(\mathbf{r}')\right]^* . \tag{3.6}$$

This constitutes another proof that the transformation to NTOs distills a given excitation into the smallest possible number of occupied/virtual orbital pairs. In a well-defined sense, the NTO basis is the best choice for conceptualizing excited states in terms of a one-electron promotion from an occupied MO into a virtual MO. Note that the NTOs are state-specific, so this optimal basis changes from one excited state to the next. (State-averaged NTOs have been suggested as a compact basis for correlated wave function expansions.[14]) In Eqs. (3.1) and (3.2), we have written the eigenvalues of $\Delta\mathbf{P}^{\text{elec}}$ and $\Delta\mathbf{P}^{\text{hole}}$ as λ_r^2 in order to emphasize the correspondence with x_{ia}^2 in the canonical MO basis, whereas the singular values λ_r in Eq. (3.4) are the amplitudes themselves, rotated into the NTO basis.

For chemists, there exists a temptation to designate the orbitals comprising the first NTO pair (having the largest singular values λ_i) as "HONTO" and "LUNTO",[123–145] in analogy to HOMO and LUMO. (The terms "HOTO" and "LUTO" have also been used occassionally.[99,146]) This seems to be especially prevalent in the literature on thermally-activated delayed fluorescence (TADF) emitters.[132–145] As even some who use this terminology have acknowledged,[125] this usage is incorrect insofar as "highest" and "lowest" are typically used in the context of the *aufbau* principle, whereas orbital energies are undefined in the NTO basis because the Fock matrix is not diagonal. As such, it makes no sense to discuss the energies of NTOs, and this makes the "HONTO" and "LUNTO" terminology especially confusing when discussed alongside HOMO/LUMO energy gaps, as is often done in the TADF literature. In this author's view, the terms "HONTO/LUNTO" should be avoided, so that visual descriptions of NTOs are kept separate from arguments based on one-electron energy levels. In discussing the NTO pairs with the largest singular values, a more appropriate term is *principle transition orbitals*, or perhaps *principle NTOs* (pNTOs). The full set of NTOs can be labeled $\text{pNTO}, \text{pNTO}-1, \text{pNTO}-2, \ldots$, in order of decreasing singular values $\lambda_1 > \lambda_2 > \lambda_3 > \cdots$. That is the nomenclature used herein.

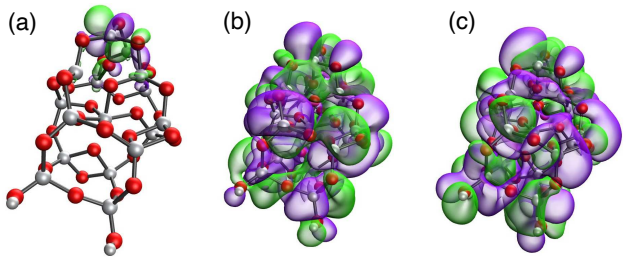

Figure 5: Orbitals participating in the lowest titanium K-edge transition in $Ti_{16}O_{32}H_2$, computed using TD-DFT/TDA (PBE0/def2-ma-SVP): (a) the principle electron NTO $\psi_1^{\rm elec}(\mathbf{r})$, for which $\lambda_1^2 = 1.00$, and (b) two canonical virtual MOs $\psi_a(\mathbf{r})$, for which $x_{ia}^2 = 0.19$ and 0.09. Isosurfaces plotted here encapsulate 85% of the probability density $|\psi(\mathbf{r})|^2$.

3.3 Examples

Equation (3.3) demonstrates how the NTOs extract the most important contributions to the particle and hole densities, or in other words the most significant contributions to the unrelaxed attachment and detachment densities. In the case where there is only one significant singular value ($\lambda_1^2 \approx 1$), then $|\psi_1^{\rm elec}(\mathbf{r})|^2$ and $|\psi_1^{\rm elec}(\mathbf{r})|^2$ are equivalent to the particle and hole densities $\Delta\rho_{\rm elec}(\mathbf{r})$ and $\Delta\rho_{\rm hole}(\mathbf{r})$, respectively, or in other words they are equivalent to unrelaxed attachment and detachment densities. This connection does not seem to be widely appreciated.

In some cases the use of densities may be more convenient, especially in the opposite limit where several singular values are significant, a situation that is discussed in Section 3.4. On the other hand, the NTOs preserve phase information that is lost upon squaring the orbitals, and that information may be useful in some situations, *e.g.*, to distinguish $n\pi^*$ from $\pi\pi^*$ in cases of significant orbital mixing, or to reveal the $\pi \rightarrow \pi^*$ in a case with complicated nodal structure, as in the example of Fig. 3b, to which we return below.

For a very different example, we turn to x-ray spectroscopy at the titanium K-edge. Calculations on a $Ti_{16}O_{32}H_2$ cluster[11] were performed at the PBE0/def2-ma-SVP level where the basis set is an augmented one,[147] intended to describe any nascent band structure. The K-edge consists of transitions from Ti(1s) to valence virtual orbitals at almost 5,000 eV, and to access core-level excitations these calculations invoke the core/valence separation approximation.[148] Here, one omits amplitudes x_{ia} unless ψ_i corresponds to a core orbital of interest, meaning Ti(1s) in the present example, while retaining the full virtual space. The principle particle NTO in this example exhibits just one nonzero singular value ($\lambda_1^2 = 1.00$) and is depicted in Fig. 5a, where its Ti(3d) character is evident along with some admixture of O(2p). The hole NTO is not shown but corresponds to the Ti(1s) on a nearby atom, meaning that the asymmetry of the cluster has localized this Ti(1s) $\rightarrow$ Ti(3d) pre-edge feature to one end of the $Ti_{16}O_{32}H_2$ cluster.

In the canonical MO basis, the same transition is completely scrambled and essentially uninterpretable. Two of the relevant canonical virtual orbitals are shown in Figs. 5b and 5c but there are 17 distinct amplitudes with $|x_{ia}| \geq 0.1$, the largest of which contributes only 19% of the norm of the transition eigenvector. and all of which collectively contribute only 85%. Note that Fig. 5 indicates the fraction of $|\psi(\mathbf{r})|^2$ that is encapsulated within each isosurface, which is necessary in order to make meaningful side-by-side comparisons of orbital localization or size. Isoprobability surfaces are be readily computed,[149] given volumetric data on a grid (*e.g.*, in the format of a "cube" file),[94] and this functionality is available in some visualization programs.[150]

It is thus conceivable that $\mathbf{x}$ is characterized by just one singular value with $\lambda_1^2 \approx 1$. In such cases, the principle NTO pair can be used to distill the picture into one that involves just one occupied and one virtual orbital, without loss of information. Such is also the case in the $S_0 \rightarrow S_2$ transition of the fluorenone-terminated polyfluorene that is shown in Fig. 3, for which $\lambda_1^2 = 0.96$. In contrast to the simple picture in the NTO basis, in the canonical MO basis four different amplitudes x_{ia} contribute significantly to the same transition. The latter are highly delocalized in the occupied space and form a localized hole only upon coherent superposition, whereas the localization is immediately evident in the NTO basis. Higher-lying states of polyfluorenes do involve a larger number of significant NTO pairs,[124] which is not unusual. Since

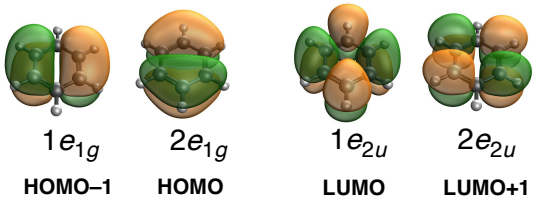

Figure 6: Frontier MOs for benzene (B3LYP/6-31G* level). The two occupied orbitals are degenerate, as are the two virtual orbitals.

NTOs are the optimal particle/hole basis, the presence of more than one significant singular value λ_i is a signature of unresolvable multideterminant character in the excited-state wave function, which cannot simply be rotated away by unitary change of basis.[14,15,100] The next section considers this in more detail.

3.4 Static correlation

The presence of more than one significant λ_i in the SVD of $\mathbf{x}+\mathbf{y}$ can be driven by symmetry-induced orbital degeneracies. Such is the case for benzene, whose frontier MOs (Fig. 6) consist of a pair of degenerate e_{1g} orbitals (HOMO and HOMO $-$ 1) along with a pair of degenerate e_{2u} orbitals (LUMO and LUMO + 1). In small basis sets, there is essentially no difference between the canonical MOs and the NTOs for the low-lying excited states and they can be used interchangeably in the following discussion. Four singly-excited determinants can be constructed from the four aforementioned orbitals, and together these make up the first four singlet excited states of benzene. These states are:

$$|\mathrm{S}_1(B_{2u})\rangle = \left(\left|\Psi^{1e_{2u}}_{1e_{1g}}\right\rangle + \left|\Psi^{2e_{2u}}_{2e_{1g}}\right\rangle\right)/\sqrt{2} \tag{3.7a}$$

$$|\mathrm{S}_2(B_{1u})\rangle = \left(\left|\Psi^{1e_{2u}}_{1e_{1g}}\right\rangle - \left|\Psi^{2e_{2u}}_{2e_{1g}}\right\rangle\right)/\sqrt{2} \tag{3.7b}$$

$$|\mathrm{S}_3(E_{1u})\rangle = \left(\left|\Psi^{1e_{2u}}_{2e_{1g}}\right\rangle + \left|\Psi^{2e_{2u}}_{1e_{1g}}\right\rangle\right)/\sqrt{2} \tag{3.7c}$$

$$|\mathrm{S}_3{}'(E_{1u})\rangle = \left(\left|\Psi^{1e_{2u}}_{2e_{1g}}\right\rangle - \left|\Psi^{2e_{2u}}_{1e_{1g}}\right\rangle\right)/\sqrt{2}\,. \tag{3.7d}$$

States S_1 and S_2 are optically dark in one-photon spectroscopy but S_3 is dipole-allowed and doubly-degenerate.[152] Calculations at the TD-B3LYP/6-31G* level conform to this simple four-orbital model with $> 99\%$ fidelity, and though the TD-DFT results might at first seem complex, in the sense that there is no excited state that is primarily HOMO($2e_{1g}$) $\rightarrow$ LUMO($1e_{2u}$) in nature, given the symmetry of the system there is little else that these states could have been. Symmetry here is a parlor trick that makes the situation seem more complicated than it really is, leading to unresolvable multiconfigurational character. wherein a minimum of four orbitals and two determinants is required to describe the low-lying excited states, even within the single-excitation *ansätze* of CIS and TD-DFT.

A more interesting example, which is not driven by symmetry, is the keto-defect polyfluorene oligomer whose $\mathrm{S}_0 \rightarrow \mathrm{S}_2$ transition was considered in Figs. 2 and 3 and whose $\mathrm{S}_0 \rightarrow \mathrm{S}_3$ transition is depicted in Fig. 7a. There is interest in these molecules for fabrication of organic light-emitting devices,[153–158] as this is one of the few classes of materials that can span the whole range of visible wavelengths at low operating voltage,[153] and also one of the few classes of materials with good emission properties for blue light.[154] These properties arise from highly delocalized excited states of the π system that may exhibit large polarizabilities and hyperpolarizabilities, giving rise to nonlinear optical properties.[159] In the present example, such states are accessed at higher excitation energies such as $\omega = 4.5$ eV for $\mathrm{S}_0 \rightarrow \mathrm{S}_3$. The oscillator strength for this delocalized transition ($f = 4.5$) is about 25 times greater than that of the defect-localized $\mathrm{S}_0 \rightarrow \mathrm{S}_2$ excitation.

For $\mathrm{S}_0 \rightarrow \mathrm{S}_3$, even the principle NTOs are delocalized over the length of the molecule (Fig. 7a), meaning that this is genuine delocalization and is not an artifact of the representation. The principle NTO pair accounts for only 67% of the transition density, with a second NTO pair contributing another 20%. Irreducible mixing of more than one NTO pair is a signature of static correlation in the excited state.[14,15,100] (Note

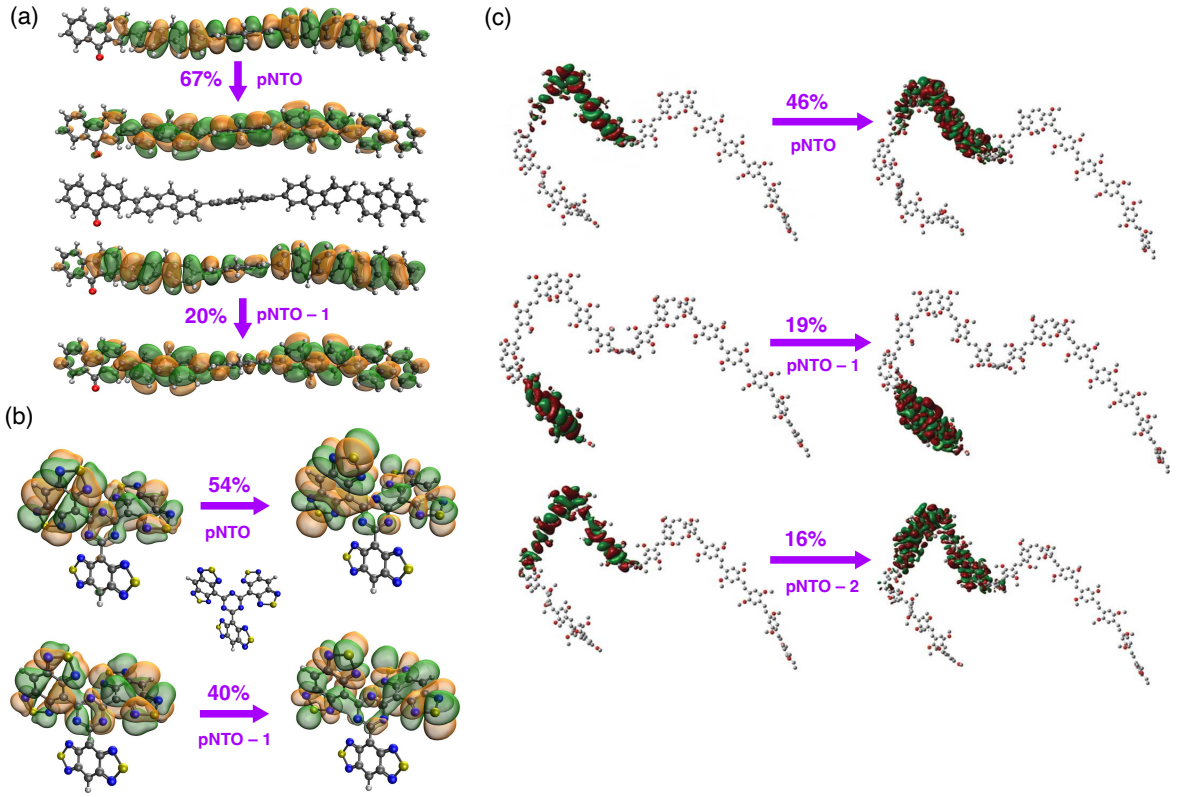

Figure 7: NTOs for transitions that exhibit significant static correlation in the excited state: (a) $S_0 \rightarrow S_3$ excitation ($\omega = 4.5$ eV, $f = 4.5$) of a five-unit polyfluorene polymer with a keto defect (as in Figs. 2 and 3), computed using TD-DFT/TDA at the CAM-B3LYP/3-21G* level; (b) $S_0 \rightarrow S_1$ excitation ($\omega = 2.8$ eV, $f = 0.4$) of a 1,3,5-triazene derivative,[133] computed at the ωB97X-D/6-31+G* level; and (c) $S_0 \rightarrow S_2$ excitation of a 20-unit MEH-PPV polymer, computed at the ωB97X-D/6-31G* level. Panel (c) is adapted from Ref. 151; copyright 2014 American Chemical Society.

that there is no contradiction with the use of a single-determinant formalism for the ground state, because the CIS wave function *ansatz* is multideterminantal.) From another point of view, the presence of more than one significant singular value in the TDM indicates that the natural orbitals of the ground state differ significantly from those in the excited state.[100] A close examination of the NTOs in Fig. 7a reveals that $\psi_1^{\text{hole}}(\mathbf{r})$ and $\psi_2^{\text{hole}}(\mathbf{r})$ are out of phase with one another, on the left end of the molecule, but evolve across its length such that they are in phase on the right end of the molecule. The same is true of $\psi_1^{\text{elec}}(\mathbf{r})$ and $\psi_2^{\text{elec}}(\mathbf{r})$, which suggests that the excited state in question can only properly be described using a minimum of two determinants. This would not be obvious from attachment/detachment density analysis.

Formal analysis suggests that static correlation, manifesting as more than one significant NTO pair, may occur in cases where a molecule consists of what amounts to two weakly-interacting chromophores,[160] even if these are but different chemical moieties within the same molecule. An example is the molecule shown in Fig. 7b that consists of three identical ligands connected to a central 1,3,5-triazene moiety in a propeller motif, wherein each ligand may be considered a distinct chromophore. (This and other triazene derivatives have been investigated[133] in the context of optoelectronic applications such as triplet-triplet annihilation and TADF.[161–165]) Canonical MOs for this molecule are not shown but are mostly delocalized over all three ligands, nevertheless the NTOs for the $S_0 \rightarrow S_1$ transition are delocalized over just two of the three ligands (Fig. 7b). Although this could be inferred also from the particle and hole densities, what those densities cannot reveal is the role of static correlation: this excited state is evidently an irreducible combination of two

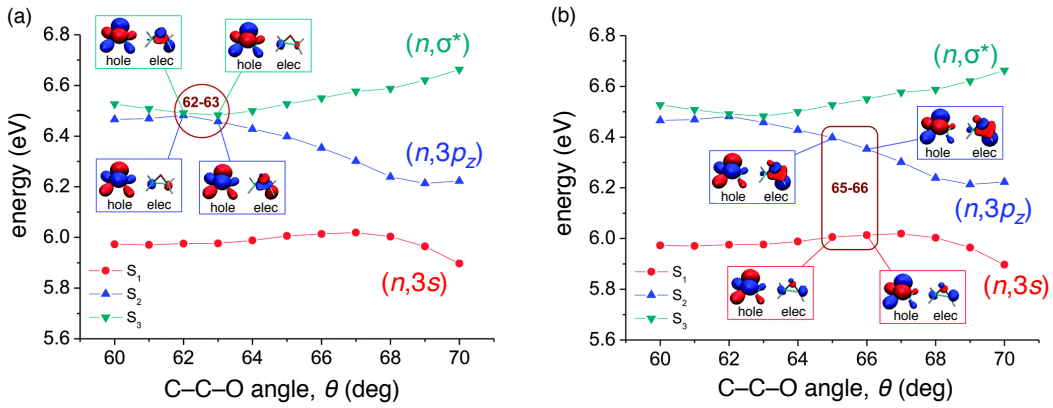

Figure 8: Energy profiles along the electrocyclic ring-opening coordinate of oxirane (CH_2CH_2O), illustrating changes in the dominant NTO pairs at different points along the reaction coordinate. (a) Near the S_2/S_3 intersection at $\theta = 62°$, the hole remains consistent on both states as the system passes through the conical intersection, whereas the excited electron switches its character abruptly, from $3p_z$ to σ^*. (b) Where the electronic states are well-separated (*e.g.*, for $\theta = 65°$), the dominant NTOs remain qualitatively consistent as the system moves along the potential surface. Adapted from Ref. 166; copyright 2015 the PCCP Owner Societies.

particle/hole pairs. Another example with multiple chromophores within the same molecule is the poly[2-methoxy-5-(2-ethylhexyloxy)-1,4-phenylene vinylene] (MEH-PPV) polymer that is shown in Fig. 7c.[151] Here, breaks in the conjugation divide the polymer into several effective intramolecular chromophores, yet electronic coupling between them is sufficient to maintain coherence of the exciton across these gaps in conjugation.

The close connection between significant NTO pairs and static correlation suggests that the NTOs can be used to infer electron configurations, and in particular to detect changes in electron configuration across a potential energy surface. (In fact, a more descriptive name for the NTOs might be *natural electron configurations*.[167]) Consider the electrocyclic ring-opening of oxirane (C_2H_4O), a prototypical reaction for which the Woodward-Hoffmann rules were developed.[168,169] Potential energy curves along the C–C–O bond angle of the ring are plotted in Fig. 8 and isosurface plots of the principle NTO pair are provided at various points, for transitions to S_2 and S_3.[166] The reaction involves a conical intersection between these two excited states, at an angle $\theta_{CCO} \approx 62°$, and the the nonadiabatic transition that occurs there is accompanied by an abrupt switch in the qualitative nature of $\psi_1^{elec}(\mathbf{r})$, as shown in Fig. 8a. On the other hand, $\psi_1^{hole}(\mathbf{r})$ remains qualitatively unchanged as the system passes through the intersection. By means of these NTOs, one may assign the diabatic character of either state: for $\theta_{CCO} < 62°$, the S_2 state is $n \rightarrow \sigma^*$ and the S_3 state is $n \rightarrow 3p_z$, whereas this character is reversed for $\theta_{CCO} > 62°$. Away from any near-degeneracy between Born-Oppenheimer potential surfaces, no such abrupt change is seen in the nature of the dominant NTOs, as illustrated in Fig. 8b.

4 Atomic Partitions

Orbitals and densities introduced above provide convenient tool to visualize excited states in real space. The present section describes tools that attempt to quantify charge rearrangement in $\Delta\rho(\mathbf{r})$, by partitioning the density change into atomic contributions.

4.1 Mulliken analysis

Consider the ^{1}CT state of *p*-nitroaniline whose dipole moment change is listed in Table 1. Although the HOMO is nominally located on the amino group and the LUMO on the nitro group, both orbitals extend over a significant portion of this small molecule, thus the CT nature of the state in question may not be immediately obvious. A Mulliken-style[170–172] partition of $\Delta\mathbf{P}^{elec}$ and $\Delta\mathbf{P}^{hole}$ might help to quantify the

nature and extent of the charge rearrangement. In this approach, the charge that is transferred to atom A by electronic excitation is defined as

$$\Delta q_A^{\mathrm{elec}} = \sum_{\mu \in A} (\mathbf{S}\Delta\mathbf{P}^{\mathrm{elec}})_{\mu\mu} \; , \tag{4.1}$$

where $\mathbf{S}$ is the atomic orbital (AO) overlap matrix. Simultaneously, atom A may lose some charge if it contributes to the hole, and that quantity of charge is defined as

$$\Delta q_A^{\mathrm{hole}} = \sum_{\mu \in A} (\mathbf{S}\Delta\mathbf{P}^{\mathrm{hole}})_{\mu\mu} \; . \tag{4.2}$$

Other common atomic partitions of a density matrix can be applied equally well, to obtain Löwdin charges,[93] for example. These decompositions are subject to the same variability with respect to the choice of AO basis set that characterizes ground-state Mulliken or Löwdin atomic charges, and are intended only to aid qualitative understanding. For reproducing electrostatic properties (such as dipole moments) of electronically-excited states, charges derived from the molecular electrostatic potential are much more reliable.[20]

4.2 Charge-transfer numbers

A different sort of atomic partition are the *CT numbers* that were first suggested by Luzanov and coworkers.[60,109,110,173–175] Like the difference charges $\Delta q_A^{\mathrm{elec}}$ and $\Delta q_A^{\mathrm{hole}}$, these quantities attempt to identify and quantify charge flow upon electronic excitation, based on atomic indices. For atoms or groups of atoms A and B, one might intuitively define an $A \to B$ charge transfer number according to[60,175]

$$l_{A\to B} = \sum_{\mu \in A} \sum_{\nu \in B} (x_{\mu\nu}^2 + y_{\mu\nu}^2) \tag{4.3}$$

where

$$x_{\mu\nu} = \sum_{ia} c_{\mu i} \, x_{ia} \, c_{\nu a} \tag{4.4}$$

is a transition amplitude expressed in the AO basis,[175] also known as a pseudo-density for the excitation.[176,177] (The quantity $y_{\mu\nu}$ is defined analogously.) The idea is that squared amplitudes $x_{\mu\nu}^2$ and $y_{\mu\nu}^2$ are associated with probabilities for transfer of charge from $\mu \in A$ to $\nu \in B$. However, the formula in Eq. (4.3) accounts neither for the normalization condition in Eq. (2.4), nor for the fact that the AOs are not orthogonal. This may not be an issue when $l_{A\to B}$ is used to analyze semi-empirical calculations,[174,178–184] where the inherent minimal basis might be assumed to be orthonormal, but the same formula has been put forward for all-electron TD-DFT calculations in arbitrary basis sets.[60,175] Normalization could be enforced in a straightforward fashion,[185]

$$\tilde{l}_{A\to B} = \frac{l_{A\to B}}{\sum_{\lambda\sigma}(x_{\lambda\sigma}^2 + y_{\lambda\sigma}^2)} \; . \tag{4.5}$$

However, failure to account for the AO overlap matrix leads to significant discrepancies in CT numbers computed in small versus large basis sets.[185]

For this reason, an alternative definition due to Plasser *et al.* is preferable,[14,186] as it accounts for nonorthogonality of the AO basis functions. This definition starts from the normalization condition

$$\int \left| T(\mathbf{r}, \mathbf{r}') \right|^2 d\mathbf{r} \, d\mathbf{r}' = 1 \; . \tag{4.6}$$

Rewriting this in terms of $\mathbf{S}\Delta\mathbf{P}$, as in Eqs. (4.1) and (4.2), suggests an atomic partition analogous to Mayer's bond-order matrix, $\mathbf{M}$.[187,188] For a closed-shell system, that quantity has matrix elements

$$M_{AB} = \sum_{\mu \in A} \sum_{\nu \in B} (\mathbf{PS})_{\mu\nu} (\mathbf{SP})_{\mu\nu} \tag{4.7}$$

and partitions $(\mathbf{SP})_{\mu\nu}$ into contributions $\mu \in A$ and $\nu \in B$. A change-in-bond-order matrix ($\Delta\mathbf{M}$) can then be obtained by swapping $\mathbf{S}\Delta\mathbf{P}$ for $\mathbf{SP}$ in Eq. (4.7):

$$(\Delta M)_{AB} = \sum_{\mu\in A}\sum_{\nu\in B}[(\Delta\mathbf{P})\mathbf{S}]_{\mu\nu}[\mathbf{S}(\Delta\mathbf{P})]_{\mu\nu} \; . \tag{4.8}$$

The quantity ΔM_{AB} can then be taken as an alternative definition of a CT number,[186] a convention that has since been adopted by others.[185,189–191] Alternatively, one might exploit trace invariance in $\mathrm{tr}(\Delta\mathbf{M}) = \sum_{A,B}(\Delta M)_{AB}$ to partition the summand in Eq. (4.8) in the spirit of a symmetric (Löwdin) orthogonalization of $\Delta\mathbf{P}$,[93,192–194] meaning two factors of $\mathbf{S}^{1/2}(\Delta\mathbf{P})\mathbf{S}^{1/2}$ as opposed to separate factors of $(\Delta\mathbf{P})\mathbf{S}$ and $\mathbf{S}(\Delta\mathbf{P})$ that in Eq. (4.8).[23] This leads to a definition

$$\Omega_{A\to B} = \sum_{\mu\in A}\sum_{\nu\in B}[\mathbf{S}^{1/2}(\Delta\mathbf{P})\mathbf{S}^{1/2}]^2_{\mu\nu} \tag{4.9}$$

to quantify the flow of charge from A to B, which amounts to a Löwdin-style partition of $\Delta\mathbf{P}$.[23] The quantity $\Omega_{A\to B}$ is a CT index in the spirit of $l_{A\to B}$ but corrected to take proper account of the nonorthogonal AO basis set. A Mulliken-style partition has also been formulated,[14] in the spirit of Eq. (4.8), however Löwdin populations are generally more stable and free of negative population artifacts.[23,172] That said, the value of $\Omega_{A\to B}$ certainly depends on the choice of AO basis set, just like any Löwdin population analysis.[172]

The method based on Eq. (4.9) has been called *fragment transition density analysis*,[185,189,195] because in the case of a correlated wave function one could imagine using the TDM in place of $\Delta\mathbf{P}$. For TD-DFT there is no distinction, although one could substitute $\Delta\mathbf{P}_{\mathrm{rlx}}$ in place of $\Delta\mathbf{P}$, thereby using the relaxed density to understand charge flow. In view of the discussion in Section 2.3, this is probably the better approach for quantitative analysis of CT states.

The CT indices $\Omega_{A\to B}$ satisfy the normalization condition

$$\sum_{A,B}\Omega_{A\to B} = 1 \tag{4.10}$$

for single-excitation wave functions. (The normalization condition is more complicated for other types of wave functions.[14]) An expression analogous to Eq. (4.10) has been suggested for $l_{A\to B}$,[175] yet this claim seems suspicious for all-electron TD-DFT calculations in nonorthogonal basis sets. Several other concepts introduced by Luzanov *et al.*[60,175] in the context of the CT indices $l_{A\to B}$ would seem to be rigorously valid only when the alternative definition $\Omega_{A\to B}$ is used instead. These include a *gross excitation localization index* (GLI),[60,175]

$$\mathrm{GLI}_A = \Omega_{A\to A} + \mathrm{CT}_A \tag{4.11}$$

where

$$\mathrm{CT}_A = \frac{1}{2}\sum_{B\neq A}(\Omega_{A\to B} + \Omega_{B\to A}) \; . \tag{4.12}$$

The quantity CT_A is a measure of charge that is shifted around in ways that involve atom A, such that

$$N_{\mathrm{CT}} = \sum_A \mathrm{CT}_A \tag{4.13}$$

is a measure of the total CT character of the excited state in question.[186] It follows that

$$\sum_A \mathrm{GLI}_A = 1 \; , \tag{4.14}$$

which suggests that GLI_A provides an atomic or functional group partition of the excited electron. As such, it is also possible to use the quantities $\Omega_{A\to B}$ to define the size of an exciton, although we postpone that discussion until Section 4.5.

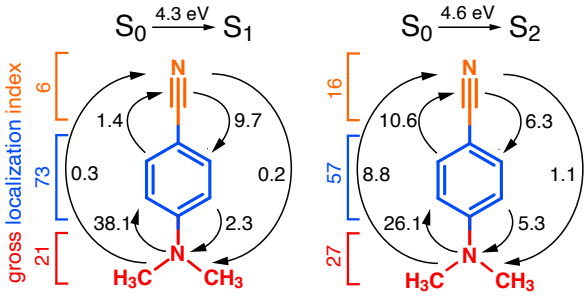

Figure 9: CT numbers $\tilde{l}_{A\to B}$ for selected atoms (given here in percentages, in black, at the arrows) and gross excitation localization indices GLI_A (on the left, at the brackets) for the color-coded fragments A, for the lowest excitations of the DMABN molecules. Calculations were performed at the TD-B3LYP/aug-cc-pVDZ level. Adapted from Ref. 60; copyright 2010 John Wiley and Sons.

4.3 Example: DMABN molecule

Examples illustrating the use of CT numbers $\Omega_{A\to B}$ in complicated cases of photochemical reactions involving transition metal complexes have been considered in Ref. 23. Here, we consider a relatively simple example, 4-(dimethylamino)benzonitrile (DMABN), which has something of a history within TD-DFT. Its spectroscopy which consists primarily of the usual $^1\mathrm{L}_a$ and $^1\mathrm{L}_b$ states,[98,196–198] often discussed in the context of polycyclic aromatic hydrocarbons (PAHs).[17,199–203] Setting aside detailed symmetry considerations, these two states have roughly perpendicular transition moments (along axes "a" and "b"). The former is primarily a HOMO $\to$ LUMO excitation, with significant ionic character in PAHs, while $^1\mathrm{L}_b$ is a mixture of (HOMO $-$ 1) $\to$ LUMO and HOMO $\to$ (LUMO + 1).[204] TD-DFT calculations often afford an unbalanced treatment of these two states,[98,204,205] which are quite close in energy in the case of DMABN.[206]

The DMABN molecule is a canonical example of the phenomenon of *dual fluorescence*,[197,198,207–209] or the appearance of two fluorescence bands whose intensity ratio is highly sensitive to solvent polarity.[197,207–209] Other donor–π–acceptor (or "push-pull") systems also exhibit this behavior,[210–212] and examples such as push-pull porphyrins and thiophene-based push-pull polymers have been widely studied as potential photosensitizers for solar cells.[213–220] Often, TD-DFT calculations have been used in an attempt to establish design principles.[221–225] Other categories of push-pull systems may be useful as dopants to produce devices with novel optoelectronic properties, including photoswitchable molecules,[226] and molecules that exhibit TADF without the use of heavy metals.[227–229]

Dual fluorescence represents an exception to Kasha's rule,[230–232] which states that emission typically occurs in a single band originating from the lowest excited state, insofar as radiationless internal conversion from higher-lying excited states is usually rapid and efficient. The dependence on solvent polarity has long been been interpreted in terms of excited-state dynamics that access a twisted intramolecular CT (TICT) state, characterized by rotation of the $-\mathrm{N(CH_3)_2}$ group out of the phenyl plane.[197,207,233–241] In this picture, the TICT state is stabilized in polar solvents, relative to the "locally excited" (LE) or $^1\pi\pi^*$ state, and is the origin of the longer-wavelength fluorescence band. This interpretation has been questioned, however, in both DMABN[242–249] and similar donor–π–acceptor systems.[250–253]

What is not in dispute is that the S_1 and S_2 states of DMABN exhibit different degrees of CT upon vertical excitation. In the gas phase, S_1 is the LE state and S_2 is the CT state, as evidenced by a dipole moment that is ≈ 6 D larger in S_2 than S_1, whose dipole moment is ≈ 3 D larger than that of the ground state.[206] This interpretation is furthered by examining the CT numbers and GLIs for both states, which are provided in Fig. 9 based on Luzanov's definition ($l_{A\to B}$), normalized as percentages to sidestep issues with the normalization of Eq. (4.3). These quantities suggest that the $\mathrm{S}_0 \to \mathrm{S}_1$ transition is characterized by a single large CT number corresponding to electron transfer from the amino lone pair into the phenyl ring, yet the GLI analysis suggests that 73% of the excited electron is localized on the phenyl ring, consistent with the idea that S_1 is the $\pi\pi^*$ state. For the S_2 state, the CT numbers provide clear evidence of amino

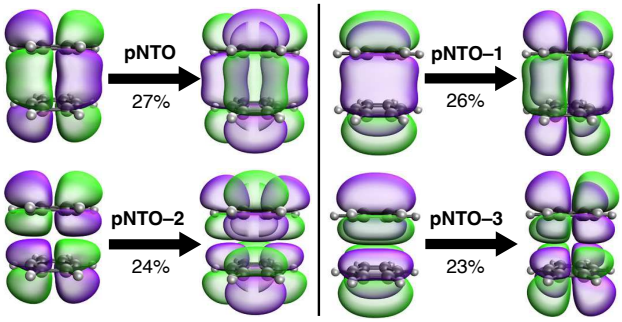

Figure 10: Principle NTO pairs pairs for the lowest dipole-allowed FE state of the benzene dimer, in a cofacial D_{6h} arrangement. Calculations were performed at the TD-DFT/TDA level using CAM-B3LYP/6-31G* and the orbital isosurfaces contain 80% of the corresponding orbital densities.

$\rightarrow$ phenyl $\rightarrow$ cyano electron transfer, with smaller fractions of the excited electron is localized on the amino and phenyl groups as compared to S_1, and a larger fraction transferred to the cyano moiety.

4.4 Frenkel excitons and charge-resonance states

New forms of complexity emerge in systems having multiple electronic chromophores that are identical or near-identical and whose vertical excitation energies are therefore quasi-degenerate. If the electronic coupling between chromophores is sufficiently strong, then the monomer excitations will mix and the excited-state wave function for the aggregate system will be delocalized across more than one chromophore.[254–257] Consider the case of two identical monomers in a high-symmetry arrangement, such as a cofacial benzene dimer with D_{6h} symmetry, for which the pNTOs are illustrated in Fig. 10. In Section 3.4, it was discussed that a minimum of four Slater determinants is required to describe the frontier excitations of the benzene monomer [Eq. (3.7)], and the same is true for the dimer but the relevant pNTOs are delocalized over both monomers.

Collective excitations of electronically coupled chromophores can be conceptualized as linear combinations of basis states $|\Psi_1^*\Psi_2\rangle$ and $|\Psi_1\Psi_2^*\rangle$, in which one monomer or the other is excited. These are the *Frenkel exciton* (FE) states, as in the classic case of H- and J-aggregates of PAH molecules.[258] In a high-symmetry system such as the benzene dimer, the mixing coefficients are equal:

$$\left|\Psi_{\pm}^{\mathrm{FE}}\right\rangle = \frac{1}{\sqrt{2}}\Big(\left|\Psi_1^*\Psi_2\right\rangle \pm \left|\Psi_1\Psi_2^*\right\rangle\Big) \,. \tag{4.15}$$

In a lower-symmetry example, the isolated-monomer excitations may not be exactly degenerate. In quasi-degenerate cases the monomer-excited basis states may still mix, though perhaps not equally. A more general expression might thus be

$$\left|\Psi^{\mathrm{FE}}\right\rangle = c_1\left|\Psi_1^*\Psi_2\right\rangle + c_2\left|\Psi_1\Psi_2^*\right\rangle \,, \tag{4.16}$$

for some mixing coefficients c_1 and c_2.

When the chromophores are at close-contact (van der Waals) separation, there is also the possibility of intermolecular CT, which we might represent using basis states $|\Psi_1^+\Psi_2^-\rangle$ and/or $|\Psi_1^-\Psi_2^+\rangle$. For highly symmetric systems, these these forward and backward CT states may be degenerate, leading to the formation *charge-resonance* (CR) states,

$$\left|\Psi_{\pm}^{\mathrm{CR}}\right\rangle = \frac{1}{\sqrt{2}}\Big(\left|\Psi_1^+\Psi_2^-\right\rangle \pm \left|\Psi_1^-\Psi_2^+\right\rangle\Big) \,, \tag{4.17}$$

which are characterized by equal amounts of forward and backward CT.[255,259,260] Furthermore, if the electron-transfer process is similar in energy to the $S_0 \rightarrow S_1$ monomer excitation energy then either CT excitons or else localized CT states may further mix with FE states. This type of mixing has been widely discussed in the theory of excimers and photoluminescence.[254,255,261–263] These various scenarios are illustrated schematically in Fig. 11.

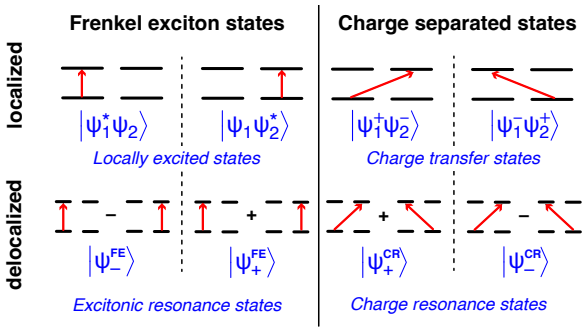

Figure 11: Different representations of FE (or excitonic resonance) excited states versus CT excited states, in a symmetric dimer whose ground-state wave function is denoted $|\Psi_1\Psi_2\rangle$. Adapted from Ref. 186; copyright 2012 American Chemical Society.

Interaction between various types of states that are illustrated in Fig. 11 may lead to some mixing, such that the real picture is more muddled. An important case where both types of states are in play are π-stacked nucleobase dimers,[26,27,264–266] leading to interplay between optically-allowed FE states and optically-dark CT states in single-stranded DNA.[267–272] Low-lying excited states of tetracene and pentacene also exhibit this type of mixing[259,273–277] which is relevant to the singlet fission process.[278–282] In the perylene diimide dimer, which is a common singlet fission (SF) chromophore,[283,284] there has been much discussion of solvent-induced symmetry breaking that can convert CR states into localized CT states.[285,286] Within a quantum chemistry calculation, even low-polarity dielectric boundary conditions ($\epsilon = 3$, as in organic thin films) can provide sufficient polarization to break the electronic symmetry and localize the CT states.[260]

In cases where mixing is significant, it can be challenging to develop a conceptual picture based on detailed calculations. Because each of the four wave functions $|\Psi_\pm^{\rm FE}\rangle$ and $|\Psi_\pm^{\rm CR}\rangle$ is delocalized over both chromophores, FE states cannot be distinguished from CR states on the basis of particle/hole (or attachment/detachment) densities.[110] The key to differentiating them is to recognize that the CT numbers $\Omega_{A\to B}$ or $l_{A\to B}$ contain information about correlations between particle and hole that are averaged away in the densities $\Delta\rho_{\rm elec}$ and $\Delta\rho_{\rm hole}$. This has been analyzed in terms of the cumulant of the two-particle density matrix,[287] but a more straightforward analysis is to use a 2×2 matrix ($\boldsymbol{\Omega}$ or $\boldsymbol{l}$) comprised of the quantities $\Omega_{A\to B}$ or $l_{A\to B}$, in which the fragments A and B represent monomers.[186] This matrix is presented in Table 2 for the delocalized states $|\Psi_\pm^{\rm FE}\rangle$ and $|\Psi_\pm^{\rm CR}\rangle$ that appear Fig. 11, along with the four basis states that contribute to them. By means of the matrix $\boldsymbol{\Omega}$, these states become easily distinguishable: diagonal character is associated with charge-neutral excitations (FE states, where only $\Omega_{A\to A}$ is significant), whereas off-diagonal character indicates charge separation. The metric $N_{\rm CT}$ [Eq. (4.13)] differentiates charge-neutral excitations (both localized and delocalized) from charge-separated ones. Note that the full matrix $\boldsymbol{\Omega}$ is necessary in order to make these distinctions; the GLI in Eq. (4.11) is insufficient.

This analysis has been idealized in the sense that it assumes orthonormal basis functions, and is intended to demonstrate simply that the aforementioned metrics are capable of distinguishing between delocalized states and thus providing information that $\Delta\rho_{\rm elec}$ and $\Delta\rho_{\rm hole}$ do not. As discussed also in Section 4.2, these metrics rely on our ability to assign amplitudes $x_{\mu\nu}$ to atoms and are susceptible to all of the usual problems with Mulliken and Löwdin charge analysis. That said, this type of analysis has been used in real calculations to classify the excited states of π-stacked dimers of naphthalene,[186] adenine,[186,265] and pyridine,[288] for example.

4.5 Participation ratio

Table 2 also introduces the *participation ratio* (PR) as a means to distinguish between localized and delocalized states. This is a measure of delocalization over sites that is used in a wide variety of contexts.[14,289–292]

Table 2: Descriptors for the excimer states of a symmetric dimer.[a]

State[b]	N_{CT}[c]	$\mathrm{PR}_{\text{e-h}}$[d]	$\boldsymbol{\Omega}$[e]
$\lvert\Psi_1^*\Psi_2\rangle$	0	1	$\begin{pmatrix} 1 & 0 \\ 0 & 0 \end{pmatrix}$
$\lvert\Psi_1\Psi_2^*\rangle$	0	1	$\begin{pmatrix} 0 & 0 \\ 0 & 1 \end{pmatrix}$
$\lvert\Psi_1^-\Psi_2^+\rangle$	1	1	$\begin{pmatrix} 0 & 0 \\ 1 & 0 \end{pmatrix}$
$\lvert\Psi_1^+\Psi_2^-\rangle$	1	1	$\begin{pmatrix} 0 & 1 \\ 0 & 0 \end{pmatrix}$
$\lvert\Psi_-^{\mathrm{FE}}\rangle$	0	2	$\begin{pmatrix} 1/2 & 0 \\ 0 & 1/2 \end{pmatrix}$
$\lvert\Psi_+^{\mathrm{FE}}\rangle$	0	2	$\begin{pmatrix} 1/2 & 0 \\ 0 & 1/2 \end{pmatrix}$
$\lvert\Psi_+^{\mathrm{CR}}\rangle$	1	2	$\begin{pmatrix} 0 & 1/2 \\ 1/2 & 0 \end{pmatrix}$
$\lvert\Psi_-^{\mathrm{CR}}\rangle$	1	2	$\begin{pmatrix} 0 & 1/2 \\ 1/2 & 0 \end{pmatrix}$

[a] Adapted from Ref. 186. [b] See Fig. 11. [c] Eqn. (4.13). [d] Eqn. (4.23). [e] $\Omega_{AB} = \Omega_{A\to B}$ [Eq. (4.9)], where A and B refer to monomers 1 and 2.

A generic definition is

$$\mathrm{PR} = \left(\sum_{i=1}^{n} p_i^2 \right)^{-1} \tag{4.18}$$

where p_i is the probability of localization on site i, in a system with n possible sites. In quantum mechanics, p_i is usually the square of some coefficient that expresses the wave function as a linear combination of localized basis functions assignable to sites, say,

$$|\psi_k\rangle = \sum_{i=1}^{n} a_{ki} \, |\phi_i\rangle \; . \tag{4.19}$$

The summation in Eq. (4.18) then involves the fourth power of the amplitudes a_{ki} and is often expressed as

$$\mathrm{PR}(\psi_k) = \frac{\left(\sum_{i=1}^{n} a_{ki}^2 \right)^2}{\sum_{j=1}^{n} a_{kj}^4} \; . \tag{4.20}$$

We assume normalized coefficients henceforth, in which case the numerator in this expression equals unity, as in Eq. (4.18). If $p_i = 1/n$, indicating equal probabilities at each site, then Eq. (4.18) affords $\mathrm{PR} = n$. In general, the PR may be interpreted as the number of sites over which the wave function delocalizes, and for that reason it has sometimes been called a *collectivity index*.[60]

The presence of a reciprocal in Eq. (4.18) seems to have led to some confusion, whereby this quantity is sometimes called the *inverse* participation ratio (IPR).[293–298] However, calling the quantity defined in Eq. (4.18) a PR is consistent with the earliest examples in the literature,[289,290,299,300] and perhaps more importantly it means that the PR increases (rather than decreases) as more and more monomers participate

in the excitation. With Eq. (4.18) taken to define the PR, then its inverse is

$$\mathrm{IPR} = \sum_{i=1}^{n} p_i^2 \tag{4.21}$$

and $\mathrm{IPR} = 1/n$ if $p_i = 1/n$. That is consistent with the idea of the inverse of participation by n chromophores, and also appears to be standard notation in the literature on localization phenomena.[290,291,300–304] However, both Mukamel and co-workers,[292–294] as well as Fleming and co-workers,[295,305] are inconsistent in whether Eq. (4.18) defines the PR or the IPR. In view of the arguments above, PR should be defined as in Eq. (4.18) and its inverse, if needed, can be called 1/PR.

For TD-DFT, one might define separate PRs for the electron and the hole:[186]

$$\mathrm{PR}_{\mathrm{elec}} = \left[\sum_B \left(\sum_A \Omega_{A\to B} \right)^2 \right]^{-1} \tag{4.22a}$$

$$\mathrm{PR}_{\mathrm{hole}} = \left[\sum_A \left(\sum_B \Omega_{A\to B} \right)^2 \right]^{-1} . \tag{4.22b}$$

(Note carefully the order of the summation indices and the fact that $\mathbf{\Omega}$ need not be symmetric, hence $\mathrm{PR}_{\mathrm{elec}}$ and $\mathrm{PR}_{\mathrm{hole}}$ are distinct.) Combining these two quantities affords a PR for the electron–hole pair:[186]

$$\mathrm{PR}_{\text{e-h}} = \frac{1}{2}(\mathrm{PR}_{\mathrm{elec}} + \mathrm{PR}_{\mathrm{hole}}) . \tag{4.23}$$

Following appropriate coordinate transformations, each of these PRs involves a summation over $x_{\mu\nu}^4$, as in the general definition of Eq. (4.20). In the idealized case of the states presented in Fig. 11, one finds that the four localized states are characterized by $\mathrm{PR}_{\text{e-h}} = 1$ and are thus distinguishable from the four delocalized states, for which $\mathrm{PR}_{\text{e-h}} = 2$. This is indicated in Table 2.

The quantities $\mathrm{PR}_{\mathrm{elec}}$ and $\mathrm{PR}_{\mathrm{hole}}$ measure the size of the exciton in terms of the coordinates of the electron ($\mathbf{r}_{\mathrm{elec}}$) and hole ($\mathbf{r}_{\mathrm{hole}}$), respectively. Their average, $\mathrm{PR}_{\text{e-h}}$, thus contributes to overall exciton size along the extracule[306] (center-of-mass) coordinate, $\mathbf{r}_{\mathrm{elec}} + \mathbf{r}_{\mathrm{hole}}$. A complementary metric is the *coherence length* of the exciton (L_{coh}),[186,292] which measures exciton size in terms of the intracule coordinate,[306] $\mathbf{r}_{\mathrm{elec}} - \mathbf{r}_{\mathrm{hole}}$. That quantity may be defined using the CT indices according to[186]

$$L_{\mathrm{coh}} = \left[(\mathrm{PR}_{\text{e-h}}) \sum_{A,B} (\Omega_{A\to B})^2 \right]^{-1} . \tag{4.24}$$

Note how off-diagonal elements of $\mathbf{\Omega}$ (or $\Delta\mathbf{P}$) characterize coherences between atoms or fragments in the electronic excitation. A value $L_{\mathrm{coh}} = 1$ indicates no off-diagonal contributions to $\mathbf{\Omega}$, which implies either that the excitation is localized on a single site or else that it is a superposition of localized excitations, *i.e.*, a FE state.[186] (Consult the schematic $\mathbf{\Omega}$ matrices in Table 2.) The length scale over which the FE state is delocalized is measured in the extracule coordinate and a sensible definition of a PR for this is[186]

$$\mathrm{PR}_{\mathrm{adiag}} = \frac{(\sum_A \Omega_{A\to A})^2}{\sum_B (\Omega_{B\to B})^2} . \tag{4.25}$$

This has been called a "diagonal" PR,[186] or sometimes a diagonal length scale,[292] although the extracule coordinate lies along the *anti-diagonal* direction in the matrix representation $\mathbf{\Omega}$. A schematic view of how to interpret that matrix is provided in Fig. 12. As indicated in that figure, the CT indices $\Omega_{A\to B}$ (and the two-dimensional matrix $\mathbf{\Omega}$ formed from them) are essentially a coarse-graining of the transition density $T(\mathbf{r}_{\mathrm{elec}}, \mathbf{r}_{\mathrm{hole}})$ expressed in particle/hole coordinates. This is discussed further in Section 5.

Quantities such as the PR are often of interest in the study of conjugated polymers where they may be used to define an effective length scale for an exciton, which need not be the same as the conjugation length

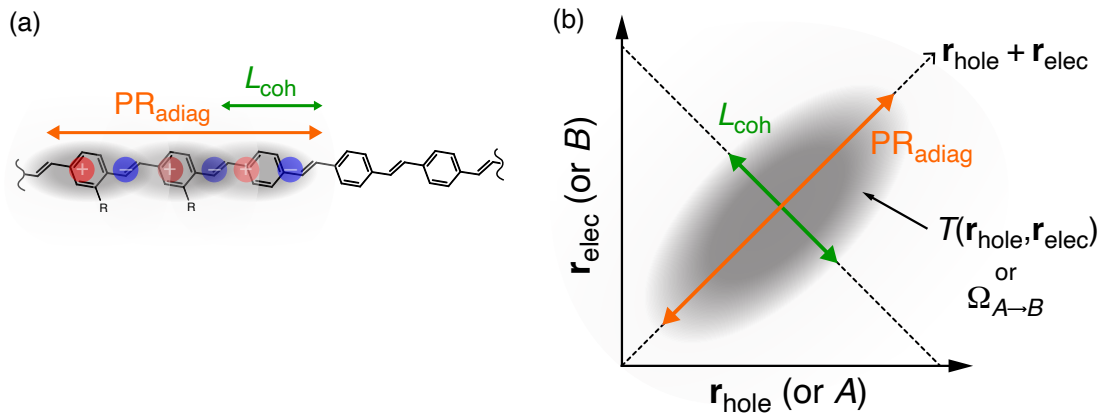

Figure 12: Guide to interpreting of $T(\mathbf{r}_{\text{hole}}, \mathbf{r}_{\text{elec}})$ as a two-dimensional probability distribution, or $\mathbf{\Omega}$ as a two-dimensional matrix, based on a similar figure in Ref. 292. (a) Schematic illustration of the coherence length L_{coh}, which measures electron–hole separation (intracule coordinate $\mathbf{r}_{\text{elec}} - \mathbf{r}_{\text{hole}}$), and the diagonal length PR_{adiag} that measures overall exciton size (extracule coordinate $\mathbf{r}_{\text{elec}} + \mathbf{r}_{\text{hole}}$), for a hypothetical excitation in a conjugated polymer. The whole exciton should be construed a superposition of electron–hole pairs, each of which has a characteristic separation L_{coh}, whereas the superposition extends over $\approx \text{PR}_{\text{adiag}}$ distinct chromophores, assuming that the indices in $\Omega_{A\to B}$ represent chromophores. (b) schematic illustration of a two-dimensional $|T(\mathbf{r}_{\text{hole}}, \mathbf{r}_{\text{elec}})|^2$ plot. Heat maps of $\mathbf{\Omega}$ (as in Table 3) can be interpreted as two-dimensional plots with the same axes $(\mathbf{r}_{\text{elec}}, \mathbf{r}_{\text{hole}})$. In that case, distance is measured in units of atoms or functional groups, depending on how the molecule is partitioned, Overall size of the exciton is limited by the size of the molecule as an upper bound, and L_{coh} is then limited by PR_{adiag}.

in the ground state. The PR also makes an appearance in certain analytic theories of exciton transport in organic photovoltaic materials.[296,297,307] For example, in a polymer with n repeat units, a simple analytic theory predicts that the effective Huang-Rys parameter (or linear exciton–phonon coupling constant) should be $S(n) = S(1)/\text{PR}$ where $S(1)$ is the Huang-Rys parameter for the monomer unit.[296]

An example is poly(*p*-phenylene vinylene) or PPV, which is the electroluminescent chromophore in one of the first organic light-emitting diodes fashioned from a polymeric material.[308–311] Excited states of a six-unit PPV polymer [$(\text{PV})_6\text{Ph}$] are considered in Table 3.[186] Although these states have been computed using a many-body wave function method, they are characterized in Table 3 using the descriptors introduced above, with indices A and B corresponding to PV monomer units. CT indices $\Omega_{A\to B}$ are arranged in the form of a matrix $\mathbf{\Omega}$ that is depicted as a grayscale heat map.

For the lowest few singlet excited states (including the S_1 bright state), $\text{PR}_{\text{e-h}}$ ranges from 3.8–6.7 with $\text{PR}_{\text{e-h}} > 5$ in all but one case, indicating nearly complete delocalization. The S_1, S_2, and S_3 states are characterized by zero, one, and two nodes along this coordinate, respectively, and could be interpreted as sequential states belonging to a single exciton band, with particle-in-a-box character along the center-of-mass coordinate. The S_4, S_5, and S_6 states (again with zero, one, and two nodes, respectively) constitute a second exciton band. This is consistent with the idea that the intracule and extracule coordinates $\mathbf{r}_{\text{elec}} \pm \mathbf{r}_{\text{hole}}$ sometimes behave as separable quasiparticle coordinates in conjugated polymers.[151,312] However, Plasser and Lischka[186] question whether these should indeed be characterized as FE states, given the fairly significant coherence lengths (*e.g.*, $L_{\text{coh}} = 3.9$ for S_1 and $L_{\text{coh}} = 5.0$ for S_4). These values quantify the anti-diagonal length in the $\mathbf{\Omega}$ heat maps and can be interpreted as electron–hole separation, measured in units of PV monomers, and the computed values suggest that the electron and hole are well separated, unlike the conventional FE picture of a tightly-bound electron and hole.

Evidence of static correlation in the PPV system can also be detected using the quantity

$$\text{PR}_{\text{NTO}} = \left(\sum_i \lambda_i^4 \right)^{-1} \tag{4.26}$$

Table 3: Excitation energies (ΔE), oscillator strengths (f), and various descriptors ($PR_{e\text{-}h}$, L_{coh}, PR_{NTO}, and $\mathbf{\Omega}$) for the lowest singlet excited states of $(PV)_6Ph$.[a]

	S_1 $1\,^1B_u$	S_2 $2\,^1A_g$	S_3 $2\,^1B_u$	S_4 $3\,^1A_g$	S_5 $4\,^1A_g$	S_6 $3\,^1B_u$
ΔE (eV)	3.15	3.56	4.00	4.22	4.39	4.47
f	5.66	0.00	0.61	0.00	0.00	0.02
$PR_{e\text{-}h}$[b]	5.53	6.32	6.69	5.14	6.30	3.80
L_{coh}[c]	3.90	3.38	3.03	4.98	3.04	2.20
PR_{NTO}[d]	1.59	2.14	2.99	2.39	4.00	4.16
$\mathbf{\Omega}$[e]						

[a] Calculations performed at the ADC(2) level and reprinted from Ref. 186; copyright 2012 American Chemical Society. [b] Eqn. (4.23). [c] Eqn. (4.24). [d] Eqn. (4.26) [e] $\Omega_{AB} = \Omega_{A\to B}$, monomer-based partition.

where the λ_i are the singular values associated with each NTO pair. The quantity PR_{NTO} is a participation ratio in the NTO basis; *cf.* Eq. (4.18). For the six-unit polymer described in Table 3, the quantity PR_{NTO} starts at a value of 1.6 for the S_1 state and increases monotonically as one moves up the excitation manifold, with $PR_{NTO} \geq 4$ for states S_5 and S_6. This means that S_5 and S_6 are each characterized by an average of four significant particle/hole pairs, indicating significant static correlation.

With this in mind, it is interesting to revisit the NTOs in Fig. 7c, which correspond to an excited state of a different polymer and where three pairs of NTOs are needed to recover 81% of the transition density. Interestingly, these NTOs demonstrate that the excitation delocalizes around the bent portion of the molecule, suggesting that a purely geometric definition of broken conjugation is insufficient to understand exciton localization in these molecules (and similarly inadequate to define the effective size of the chromophore), because other mechanisms such as dipole-dipole coupling and superexchange can drive delocalization even when geometric distortion leads to loss of conjugation.[151] With an excited-state wave function in hand, however, an effective chromophore size can be inferred by measuring the particle–hole separation for the exciton.[151] This is the anti-diagonal coordinate in the $\mathbf{\Omega}$ plots of Table 3, for a different PPV system. This analysis technique and other statistical measures of electron–hole correlation are described in the next section.

5 Exciton Wave Function

The concept of an "exciton" or bound particle/hole pair is ubiquitous in solid-state physics yet it can be difficult to connect that language to the MO-based concepts that are used in quantum chemistry,[16,313] since any excited state consists of an excited electron and a hole in the occupied space. A connection can be made by identifying virtual–occupied function pairs $\psi_a(\mathbf{r}_{elec})\,\psi_i^*(\mathbf{r}_{hole})$ as a quasiparticle basis. The transition density $T(\mathbf{r},\mathbf{r}')$ in Eq. (2.5), written in the form $T(\mathbf{r}_{elec},\mathbf{r}_{hole})$, is then identified as an electron/hole "wave function" for the exciton. That said, the true excited-state wave function in a many-body formalism is Ψ_{exc} in Eq. (2.8), which is be used to construct $T(\mathbf{r},\mathbf{r}')$. Nevertheless, the transition density $T(\mathbf{r}_{elec},\mathbf{r}_{hole})$ is often called a "wave function" in quasiparticle theories based on the two-particle Green's function and the Bethe-Salpeter equation.[314,315] Semantics aside, this quantity facilitates examination of the spatial correlation and separation between particle and hole. In quantum chemistry, this form of analysis was pioneered by Mukamel, Tretiak, and Chernyak,[99,292–294,316–318] and later used by others,[319–323] mostly in the context of organic photovoltaic materials and using semi-empirical CIS-type wave functions. These ideas were subsequently formalized, and generalized to wave functions of arbitrary complexity, and to the case of nonorthogonal basis functions, by Plasser and co-workers.[14,15,18,186,324] Those authors also studied organic photovoltaics,[288,325–327] albeit using TD-DFT and correlated wave functions rather than semi-empirical methods.

5.1 Electron–hole correlation

If $T(\mathbf{r}_{\text{elec}}, \mathbf{r}_{\text{hole}})$ is to serve as the excitonic wave function then it might seem that $|T(\mathbf{r}_{\text{elec}}, \mathbf{r}_{\text{hole}})|^2$ should be the corresponding probability density, although this analogy breaks down when one realizes that the normalization condition in Eq. (4.6) is not generally obeyed for correlated wave functions.[14,15] (This fact has occasionally been used to quantify deviation from one-particle character.[190,328,329]) For single-excitation wave functions, however, Eq. (4.6) is strictly valid and one may integrate over either $\mathbf{r} \equiv \mathbf{r}_{\text{elec}}$ or $\mathbf{r}' \equiv \mathbf{r}_{\text{hole}}$ to obtain separate one-particle densities for the electron and the hole.[14] For TD-DFT, these quantities are the same as the particle and hole densities defined in Section 2.2. In terms of $T(\mathbf{r}_{\text{elec}}, \mathbf{r}_{\text{hole}})$, they are

$$\Delta\rho_{\text{elec}}(\mathbf{r}_{\text{elec}}) = \int \left|T(\mathbf{r}_{\text{elec}}, \mathbf{r}_{\text{hole}})\right|^2 d\mathbf{r}_{\text{hole}} \tag{5.1a}$$

$$\Delta\rho_{\text{hole}}(\mathbf{r}_{\text{hole}}) = \int \left|T(\mathbf{r}_{\text{elec}}, \mathbf{r}_{\text{hole}})\right|^2 d\mathbf{r}_{\text{elec}} \ . \tag{5.1b}$$

with

$$\int \Delta\rho_{\text{elec}}(\mathbf{r})\ d\mathbf{r} = 1 = -\int \Delta\rho_{\text{hole}}(\mathbf{r})\ d\mathbf{r} \ , \tag{5.2}$$

where the normalization is consistent with Eq. (2.13). An atomic partition provides an equivalent definition of the CT numbers that were introduced in Section 4.2:[14,195]

$$\Omega_{A\to B} = \int_A d\mathbf{r}_{\text{hole}} \int_B d\mathbf{r}_{\text{elec}} \left|T(\mathbf{r}_{\text{hole}}, \mathbf{r}_{\text{elec}})\right|^2 \ . \tag{5.3}$$

Taking $|T(\mathbf{r}_{\text{elec}}, \mathbf{r}_{\text{hole}})|^2$ seriously as the probability distribution for the exciton, this quantity should afford the correlated probability of finding the hole at position $\mathbf{r}_{\text{hole}}$ given the presence of the excited electron at position $\mathbf{r}_{\text{elec}}$. A schematic view of $|T(\mathbf{r}_{\text{elec}}, \mathbf{r}_{\text{hole}})|^2$ as a two-dimensional probability distribution is presented in Fig. 12. According to Eq. (5.3), this plot conveys the same qualitative information, in the same way, as does a heat-map plot of $\mathbf{\Omega}$ (*e.g.*, in Table 3), but does so in real space whereas $\Omega_{A\to B}$ does so in atom or functional-group space. Either way, the diagonal direction in a plot of $\mathbf{r}_{\text{elec}}$ versus $\mathbf{r}_{\text{hole}}$ measures charge separation, with a characteristic length scale L_{coh} [Eq. (4.24)]. The anti-diagonal direction measures the total size of the exciton, *i.e.*, delocalization over atoms, and can be measured using PR_{adiag} [Eq. (4.25)].

This type of analysis can be used to demonstrate how different exchange-correlation functionals may predict qualitatively divergent behavior for excitonic states in multichromophore systems.[259] In such cases, FE states can mix with either localized CT states or delocalized CR states and the extent of mixing is sensitive to the long-range behavior of the functional in question, especially with regard to the fraction (if any) of Hartree-Fock exchange. The energetic position of CT and/or CR states is sensitive to this fraction,[31] to a much greater extent than localized excitations such as $\pi\pi^*$ or $n\pi^*$,[26] so adjusting the fraction of exact exchange has the effect of tuning charge-separated states in or out of resonance. As an example, Fig. 13 shows heat maps of $\mathbf{\Omega}$ for the lowest four singlet excited states of a $(\text{pentacene})_4$ cluster taken from a supercell of the crystalline material, computed using four different density functionals.[259]

Significant discrepancies are observed amongst different functionals in these data. Using the ωB97X-V functional,[330] for example, the states S_1 to S_4 are mostly CR states, which is evident from the strong anti-diagonal character of the $\mathbf{\Omega}$ heat maps; consult Table 2 for a guide. For example, the S_1 and S_4 states primarily involve mixing basis states $|\Psi_1\Psi_2^+\Psi_3^-\Psi_4\rangle$ and $|\Psi_1\Psi_2^+\Psi_3^-\Psi_4\rangle$. Range-separated hybrid (RSH) functionals,[1] including LRC-ωPBE and a screened RSH approach (sRSH-ωPBE) that respects asymptotic behavior within a low-dielectric crystal medium,[331] exhibit a much greater degree of FE character, with amplitude along the diagonal of the $\mathbf{\Omega}$ matrix. There is still some charge-separation character in these cases although it is asymmetric, indicative of localized (directional) CT. In centrosymmetric systems, localized CT is not possible due to symmetry and dipole moment changes vanish for the same reason, but $\mathbf{\Omega}$ heat maps can still be used to infer charge-separated character.[259]

To examine excitonic states in conjugated polymers of interest for organic electronics, Tretiak and co-workers have made extensive use of atomic partitions of the TDMs from semi-empirical electronic structure

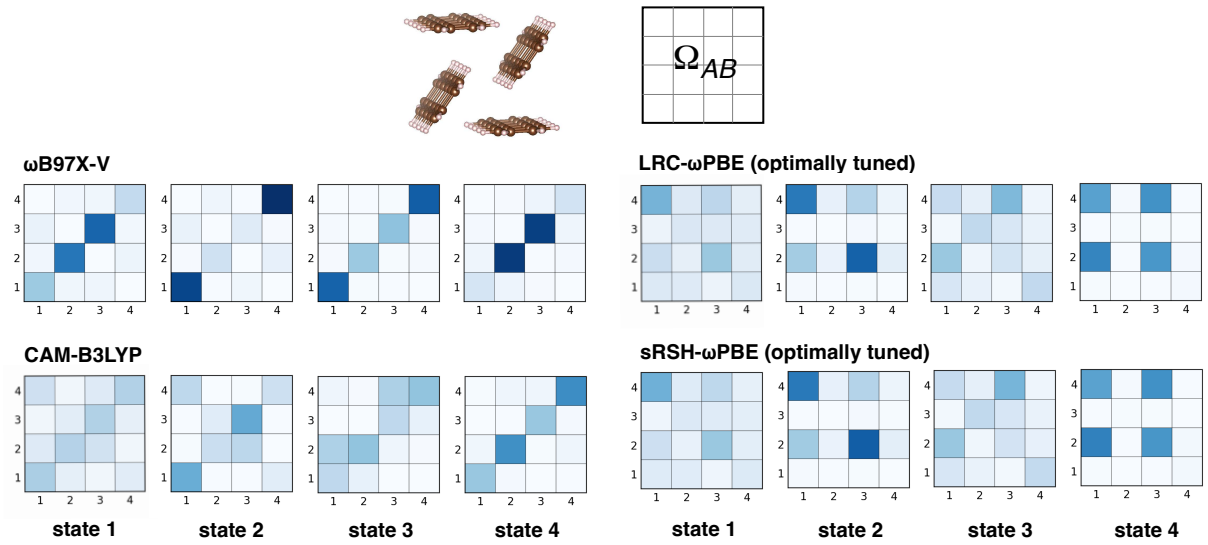

Figure 13: Heat maps of the CT matrix $\mathbf{\Omega}$, obtained from a monomer-based partition of $|T(\mathbf{r}_{\text{elec}}, \mathbf{r}_{\text{hole}})|^2$, for each of the first four singlet excited states of the $(\text{pentacene})_4$ model that is shown at the top. Results from four different density functionals are shown. Darker blue color indicates larger values of $\Omega_{A\to B}$ whereas white indicates that $\Omega_{A\to B} \approx 0$, and the indices A and B represent different pentacene monomers. Adapted from Ref. 259; copyright 2020 American Chemical Society.

calculations.[99,292,294,316–318,332,333] (This analysis has sometimes been ported to all-electron TD-DFT calculations without recognition of the need to consider the AO overlap matrix.[334,335]) Neglecting $\mathbf{S}$ or else using an orthogonalized minimal basis, there is little distinction between $l_{A\to B}$ in Eq. (4.3) and $\Omega_{A\to B}$ in Eq. (4.9), if normalization is ignored for the purpose of inferring spatial correlations between particle and hole. Tretiak and co-workers use slightly modified CT indices,[292] namely

$$\xi_{AA} = \left| \sum_{\mu\in A} (\Delta\mathbf{P})_{\mu\mu} \right| \tag{5.4}$$

in place of $l_{A\to A}$ and

$$\xi_{AB} = \left[\sum_{\mu\in A} \sum_{\nu\in B} [(\Delta\mathbf{P})_{\mu\nu}]^2 \right]^{1/2} \quad \text{for } A \neq B \tag{5.5}$$

in place of $l_{A\to B}$. When collected into a matrix $\boldsymbol{\xi}$ the diagonal and anti-diagonal axes measure electron–hole separation (intracule coordinate) and overall exciton size (extracule coordinate), respectively. This is analogous to the way that the $\mathbf{\Omega}$ matrix is analyzed; see Fig. 12.

Heat maps of $\boldsymbol{\xi}$ are depicted in Fig. 14 for a 20-unit PPV oligomer,[318] where indices A and B in ξ_{AB} refer to PPV units. In these examples, the length PR_{adiag} in the anti-diagonal direction (extracule coordinate $\mathbf{r}_{\text{elec}} + \mathbf{r}_{\text{hole}}$) signifies that the excitation is delocalized over essentially the entire oligomer, regardless of the exchange-correlation functional that is employed. On the other hand, the coherence length (in the diagonal direction), which indicates charge separation, is rather sensitive to the fraction of Hartree-Fock exchange, as it was for $(\text{pentacene})_4$. For functionals with a large fraction of exact exchange, including Hartree-Fock theory itself, L_{coh} approaches a limiting value of ≈ 2 monomer units, but for semilocal functionals such as BLYP and PBE, the coherence length approaches the length of the entire polymer. This is observed in other conjugated polymers as well.[95,325–327,336]

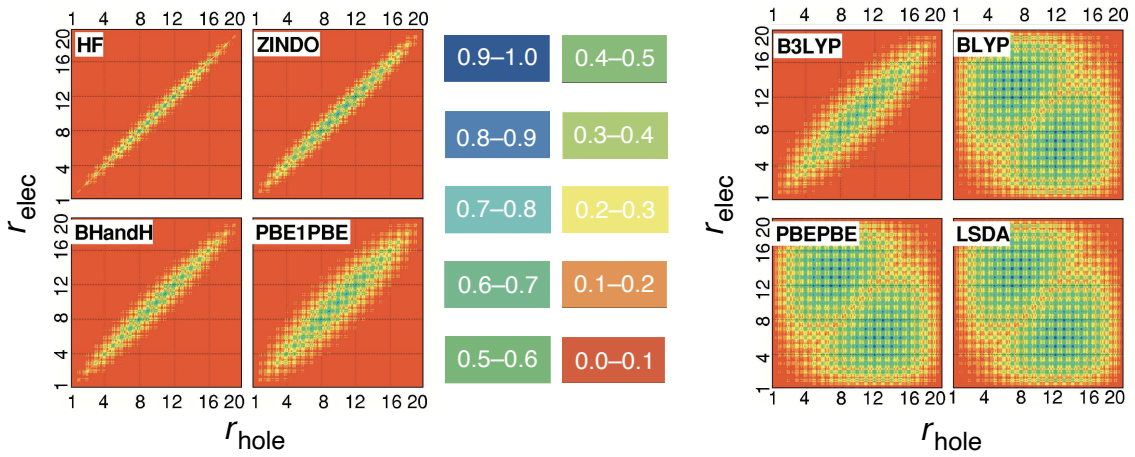

Figure 14: Heat maps of $\boldsymbol{\xi}$ for $(PPV)_{20}$, for calculations using various density functionals. The $\boldsymbol{\xi}$ matrix is defined in Eqs. (5.4) and (5.5) but is essentially the matrix $\boldsymbol{\Omega}$ defined in Section 4.2. Equivalently, this information is a spatial representation of the transition density $T(\mathbf{r}_{\text{hole}}, \mathbf{r}_{\text{elec}})$, with both axes measured in units of PPV monomers. The horizontal axis represents the hole coordinate (amplitude represents a hole located on the site in question) and the vertical axis presents the complementary information for the excited electron. Equivalently, the heat map represents the probability of transferring charge from the site indicated on the horizontal axis to the site indicated on the vertical axis. Adapted from Ref. 318; copyright 2007 American Institute of Physics.

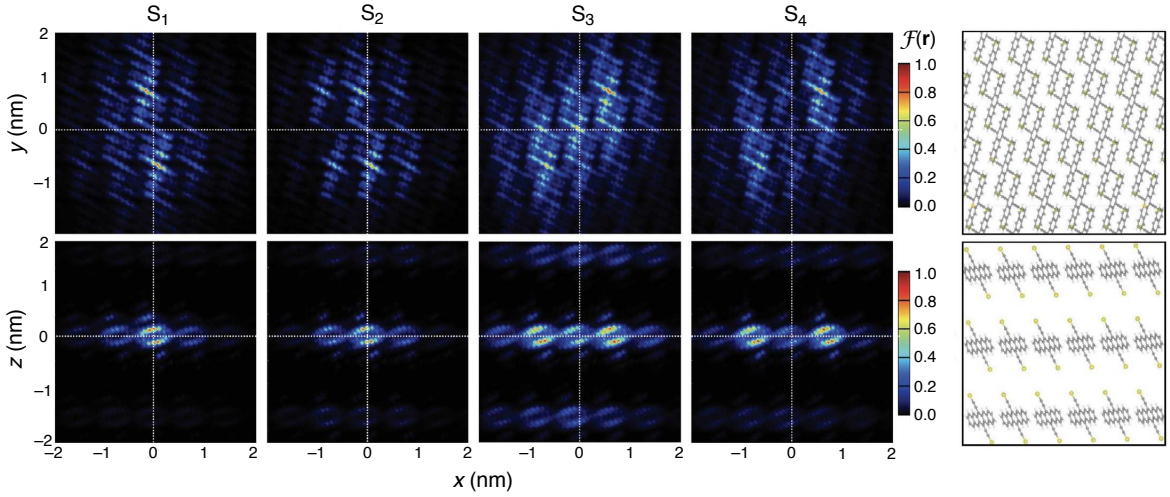

Figure 15: Electron–hole correlation functions $\mathcal{F}(\mathbf{r})$ [Eq. (5.6)] for the first four singlet excited states of a periodic crystal of 6,13-bis(triisopropylsilylethynyl) (TIPS) pentacene. These have been projected onto either the xy plane (upper panels) or the xz plane (lower panels). Corresponding cuts through the crystal structure are shown at the far right, with methyl groups have been removed from the TIPS side chains, for clarity. Reprinted from Ref. 274; copyright 2015 John Wiley & Sons.

5.2 Quantifying exciton size

A one-particle probability distribution that preserves certain aspects of electron–hole information is the *electron–hole correlation function*,[315]

$$\mathcal{F}(\mathbf{r}) = \int \left|T(\mathbf{r}+\mathbf{r}_{\text{hole}}, \mathbf{r}_{\text{hole}})\right|^2 d\mathbf{r}_{\text{hole}} \ , \tag{5.6}$$

representing the probability of finding the centroids of the electron and the hole separated by a vector $\mathbf{r}$. The electron–hole distance (exciton length) can then be sensibly defined as the expectation value of the vector between their barycenters,

$$R_{\text{e-h}} = \left\langle \|\mathbf{r}_{\text{elec}} - \mathbf{r}_{\text{hole}}\| \right\rangle \ , \tag{5.7}$$

which is computable by means of $\mathcal{F}(\mathbf{r})$:

$$R_{\text{e-h}} = \int r\, \mathcal{F}(r)\ dr \ . \tag{5.8}$$

(Here, $r = \|\mathbf{r}\|$.) The CT character of the excitation in question can be estimated in terms of the fraction of an electron that is transferred (Q_{CT}), which can be defined as

$$Q_{\text{CT}} = 1 - \int_{\mathbf{r}\in V_{\text{molec}}} \mathcal{F}(\mathbf{r})\ d\mathbf{r} \ . \tag{5.9}$$

The notation $\mathbf{r} \in V_{\text{molec}}$ indicates integration of the volume occupied by a single molecule in the crystal.[315]

Figure 15 plots $\mathcal{F}(\mathbf{r})$ for the lowest few singlet excitons in a periodic calculation of a functionalized pentacene derivative, which is perhaps the most widely-investigated SF material.[278–282] The SF process amounts to rapid spin-allowed conversion of a singlet excited state on one molecule into a correlated pair of triplet excitations on two neighboring molecules,

$$\mathrm{S}_0 \xrightarrow{h\nu} \mathrm{S}_1 \xrightarrow{\text{SF}} {}^1(\mathrm{T}_1\mathrm{T}_1) \rightarrow \mathrm{T}_1 + \mathrm{T}_1 \ . \tag{5.10}$$

The correlated triplet-pair or "multi-exciton" state, ${}^1(\mathrm{T}_1\mathrm{T}_1)$, represents a true double excitation in electronic structure terms.[337–339] Following decoherence, SF ultimately results in two charge carriers (T_1 + T_1) for the price of a single photon. This photochemical two-for-one has the potential to overcome the thermodynamic limit on conversion efficiency for one-to-one processes.[340,341] However, there are basic mechanistic questions that are still being investigated, including the role of low-energy CT states,[259,273–277] vibronic coherence,[338,342–348] the nature of exciton/phonon couplings,[349] and whether the ${}^1(\mathrm{T}_1\mathrm{T}_1)$ state may represent a trap rather than an intermediate.[350]

In the electron–hole correlation plots shown in Fig. 15, the origin ($\mathbf{r} = \mathbf{0}$) corresponds to zero net separation between electron and hole ($\mathbf{r}_{\text{elec}} = \mathbf{r}_{\text{hole}}$), but the plots do not indicate significant probability there. Rather, the regions of highest probability in the xy plane are those around ($x = 0, y = \pm 1$ nm), indicative of charge separation between nearest-neighbor molecules, although the extent of $\mathcal{F}(\mathbf{r})$ indicates delocalization over as many as three molecules.[274] This leads to an exciton length of > 5 Å, as determined by Eq. (5.8), with $\approx 50\%$ CT charactert according to the definition in Eq. (5.9).[315] In contrast, plots in the xz plane of the crystal indicate no delocalization in the z direction, which is attributable to the large intermolecular arising from bulky substituent groups.

The quantity $T(\mathbf{r}_{\text{elec}}, \mathbf{r}_{\text{hole}})$ can also be used to evaluate a variety of statistical properties of the joint electron/hole probability distribution,[16,18] which are indicated schematically in Fig. 16. These measures include root-mean-square (RMS) sizes of the electron and the hole,

$$\sigma_{\text{elec}} = \left(\langle \mathbf{r}_{\text{elec}} \cdot \mathbf{r}_{\text{elec}} \rangle - \langle \mathbf{r}_{\text{elec}} \rangle \cdot \langle \mathbf{r}_{\text{elec}} \rangle\right)^{1/2} \tag{5.11a}$$

$$\sigma_{\text{hole}} = \left(\langle \mathbf{r}_{\text{hole}} \cdot \mathbf{r}_{\text{hole}} \rangle - \langle \mathbf{r}_{\text{hole}} \rangle \cdot \langle \mathbf{r}_{\text{hole}} \rangle\right)^{1/2} \ , \tag{5.11b}$$

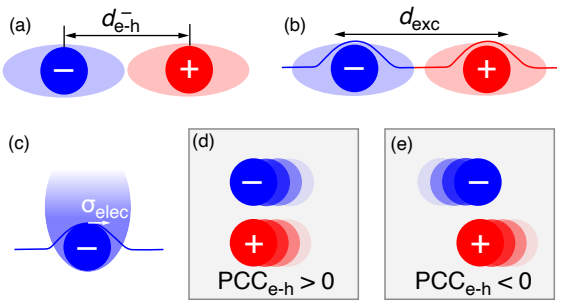

Figure 16: Schematic depictions of some statistical measures of electron–hole correlation, including (a) the average electron–hole separation, $d^-_{\text{e-h}}$; (b) the RMS electron–hole separation, d_{exc}; (c) the RMS size of the electron, σ_{elec}; and (d)–(e) Pearson's correlation coefficient for electron and hole, $\text{PCC}_{\text{e-h}}$. Adapted from Ref. 324; copyright 2018 American Chemical Society.

and the RMS value of the electron–hole separation,

$$d_{\text{exc}} = \left\langle \|\mathbf{r}_{\text{elec}} - \mathbf{r}_{\text{hole}}\|^2 \right\rangle^{1/2} . \tag{5.12}$$

The latter provides an alternative to $R_{\text{e-h}}$ in Eq. (5.8), or L_{coh} in Eq. (4.24), for characterizing the size of an exciton. Each of these measures electron–hole separation along the anti-diagonal direction in Fig. 12, but they are numerically distinct. These quantities play a central role in attempts to quantify the CT character of a given excited state, which will be explored below.

To explore these definitions a bit further, we define

$$d^{\pm}_{\text{e-h}} = \left\| \langle \mathbf{r}_{\text{elec}} \rangle \pm \langle \mathbf{r}_{\text{hole}} \rangle \right\| , \tag{5.13}$$

where $\langle \mathbf{r}_{\text{elec}} \rangle$ and $\langle \mathbf{r}_{\text{hole}} \rangle$ are the centroids of the attachment and detachment densities, respectively. Equivalently, these are the expectation values of the position operator, averaged over $\Delta\rho_{\text{elec}}(\mathbf{r})$ or $\Delta\rho_{\text{hole}}(\mathbf{r})$. For example, the x component of $\langle \mathbf{r}_{\text{elec}} \rangle$ is

$$\langle x_{\text{elec}} \rangle = \int x \, \Delta\rho_{\text{elec}}(\mathbf{r}) \, dx . \tag{5.14}$$

The quantity $d^+_{\text{e-h}}$ in Eq. (5.13) is the average of the extracule coordinate $\mathbf{r}_{\text{elec}} + \mathbf{r}_{\text{hole}}$ for the electron/hole pair. This value depends on the choice of laboratory-fixed coordinate frame but can be used to assess how the exciton migrates upon change in molecular geometry. The average inter-particle (intracule) distance is $d^-_{\text{e-h}}$ (Fig. 16a), however this vanishes for any centrosymmetric system,[18] meaning that it cannot detect charge separation in any system with inversion symmetry. This can have important implications in solid-state systems, where $d^-_{\text{e-h}}$ (and correspondingly, the dipole moment change upon excitation) is zero or small, yet there may still be significant charge separation.[259] In view of this, the quantity d_{exc} in Eq. (5.12) is a more robust measure of electron–hole separation. The latter satisfies the bounds

$$d^2_{\text{exc}} \geq (d^-_{\text{e-h}})^2 + (\sigma_{\text{elec}} - \sigma_{\text{hole}})^2 \tag{5.15a}$$

$$d^2_{\text{exc}} \leq (d^-_{\text{e-h}})^2 + (\sigma_{\text{elec}} + \sigma_{\text{hole}})^2 . \tag{5.15b}$$

The physical interpretation of these mathematical bounds is that the RMS exciton size (d_{exc}) is not larger than the sum of the RMS sizes of the electron and the hole ($\sigma_{\text{elec}} + \sigma_{\text{hole}}$).

For MEH-PPV polymers (Fig. 7c), examination of d_{exc} and $d^{\pm}_{\text{e-h}}$ leads to the conclusion that excitations in this system can be viewed as two independent quasiparticles in the intracule and extracule coordinates of the electron/hole pair.[151] As compared to geometric considerations, the RMS exciton size proves to be a better diagnostic for the effective size of the chromophore in a long, disordered polymer. That length

scale (measured by d_{exc}) is sometimes longer than what might have been anticipated simply by counting conjugated bonds, due to electronic coupling between conjugatively distinct segments of the polymer. The value of d_{exc} is effectively constant for the low-lying excited states of interest for optoelectronic applications, whereas exciton delocalization that is measured by $d^{+}_{\text{e-h}}$ is found to increase with excitation energy.[151]

Other statistical descriptors of an exciton include the covariance between the vectors $\mathbf{r}_{\text{elec}}$ and $\mathbf{r}_{\text{hole}}$, defined as

$$\text{COV}(\mathbf{r}_{\text{hole}}, \mathbf{r}_{\text{elec}}) = \langle \mathbf{r}_{\text{hole}} \cdot \mathbf{r}_{\text{elec}} \rangle - \langle \mathbf{r}_{\text{hole}} \rangle \cdot \langle \mathbf{r}_{\text{elec}} \rangle \ . \tag{5.16}$$

From this, one may compute Pearson's correlation coefficient (PCC) between the probability distributions for the electron and the hole:

$$\text{PCC}_{\text{e-h}} = \frac{\text{COV}(\mathbf{r}_{\text{hole}}, \mathbf{r}_{\text{elec}})}{\sigma_{\text{elec}}\, \sigma_{\text{hole}}} \ . \tag{5.17}$$

This quantity is defined such that

$$-1 \leq \text{PCC}_{\text{e-h}} \leq 1 \ , \tag{5.18}$$

with positive values indicating concerted motion of the two quasiparticles (Fig. 16d) and negative values indicating that they avoid each other dynamically (Fig. 16e).[18]

Analysis of correlations between the size of the electron and hole quasiparticles as a function of conjugation length suggests that the semilocal TD-DFT results for $(\text{PPV})_{20}$ in Fig. 14 are consistent with quasiparticles avoiding one another, or in other words, more consistent with a CT state than with a bound exciton.[327] Reducing the fraction of Hartree-Fock exchange is tantamount to eliminating electron–hole attraction, or equivalently, to an effectively repulsive interaction between the excited electron and the hole.[318] As a result, *TD-DFT using semilocal functionals contains no electron–hole interaction!* Semilocal DFT, meaning generalized gradient approximations (GGAs),[1] is thus inherently unable to describe bound excitons. This explains large errors for excitations energies in conjugated π systems that had been observed in previous TD-DFT calculations.[98,205,351,352] The origin of this failure cannot be deduced from the MOs alone, because the anti-diagonal length scales (PR_{adiag}) are essentially identical for all functionals. Instead, real-space analysis of the transition density (*i.e.*, visualization of electron–hole correlation) is required.[14,327]

5.3 CT metrics

Results for conjugated polymers allude to systemic problems with the description of long-range CT in TD-DFT calculations.[1,9,24–32] These will be considered further in Section 6, and will ultimately require one or more metrics that can quantify the extent of CT character in a given excited state, to use as a diagnostic for when problems should be anticipated. A variety of CT metrics have been proposed and several of them are closely related to statistical measures of electron–hole separation that were introduced in Section 5.2, although these connections have seldom been made clear in the literature. For that reason, we introduce a few of these metrics here, in order to illustrate how they are connected to the physically-meaningful metrics introduced above.

Much of the work on CT metrics for TD-DFT has been carried out by Ciofini and coworkers.[20,211,221,336,353–360] Without referring to them as such, these authors introduce particle and hole densities (or attachment and detachment densities, which are equivalent within TD-DFT as discussed in Section 2.2). Because these quantities describe the parts of space that are characterized by positive ($\Delta\rho_{\text{elec}}$) and negative ($\Delta\rho_{\text{hole}}$) changes in the density, these density changes were called $\rho_{+}(\mathbf{r})$ and $\rho_{-}(\mathbf{r})$,[336,356] defined as

$$\Delta\rho_{+}(\mathbf{r}) = \begin{cases} \Delta\rho(\mathbf{r}), & \Delta\rho(\mathbf{r}) > 0 \\ 0, & \Delta\rho(\mathbf{r}) \leq 0 \end{cases} \tag{5.19a}$$

and

$$\Delta\rho_{-}(\mathbf{r}) = \begin{cases} 0 & \Delta\rho(\mathbf{r}) > 0 \\ \Delta\rho(\mathbf{r}), & \Delta\rho(\mathbf{r}) \leq 0 \end{cases} \ . \tag{5.19b}$$

Note that $\Delta\rho(\mathbf{r}) = \Delta\rho_+(\mathbf{r}) + \Delta\rho_-(\mathbf{r})$ [*cf.* Eq. (2.15)] and

$$\int \Delta\rho_+(\mathbf{r}) d\mathbf{r} = 1 = -\int \Delta\rho_-(\mathbf{r})\, d\mathbf{r} \,. \tag{5.20}$$

There is no new information here, beyond what is contained in $\Delta\rho_{\text{elec}}(\mathbf{r})$ and $\Delta\rho_{\text{hole}}(\mathbf{r})$. Since the latter quantities have names that invoke both their physical meaning and their connection to the particle/hole formalism of TD-DFT, we will use $\Delta\rho_{\text{elec}}(\mathbf{r})$ and $\Delta\rho_{\text{hole}}(\mathbf{r})$ rather than $\Delta\rho_+(\mathbf{r})$ and $\Delta\rho_-(\mathbf{r})$.

Ciofini *et al.*[336] introduced what is now a widely-used measure of charge separation, which they call D_{CT} and which is equal to the distance between the centroids of $\Delta\rho_{\text{elec}}(\mathbf{r})$ and $\Delta\rho_{\text{hole}}(\mathbf{r})$. However, this quantity is precisely equivalent to $d^-_{\text{e-h}}$ as defined in Eq. (5.13). A more detailed definition, for both $d^-_{\text{e-h}}$ and $d^+_{\text{e-h}}$, is

$$d^{\pm}_{\text{e-h}} = \left\| \int \left[\Delta\rho_{\text{elec}}(\mathbf{r}) \pm \Delta\rho_{\text{hole}}(\mathbf{r})\right] \mathbf{r}\, d\mathbf{r} \right\| \,. \tag{5.21}$$

Because the nomenclature $d^-_{\text{e-h}}$ more clearly identifies the physical meaning of this quantity, we prefer that notation over D_{CT}. In any case, this metric is increasingly being used to analyze TD-DFT calculations,[20,211,221,336,353–361] though most authors simply refer to it as "D_{CT}", "Ciofini's CT metric", or similar language that obscures its very straightforward physical interpretation as the distance between barycenters of the particle and the hole.[16] Although this fact has been noted elsewhere,[336,360] failure to introduce particle and hole densities *per se* obscures the conceptual origin of D_{CT} and its connection to quantities such as the attachment and detachment densities. For this reason, we suggest that this quantity be called $d^-_{\text{e-h}}$ rather than D_{CT}, as the physics is inherent in that nomenclature, namely, electron–hole separation as defined by the difference between centroids, rather than the more generic "CT". The definition of $d^-_{\text{e-h}}$ in Eq. (5.13) is more obvious and meaningful. Even more complicated variants of D_{CT} have been suggested,[359] though it is not clear what advantages these may have as compared to a simple moment analysis of the excitonic wave function, à la Eq. (5.11).

As noted in Section 5.2, $d^-_{\text{e-h}} \equiv 0$ for any centrosymmetric system.[18] To obtain a non-vanishing metric CT for systems with inversion symmetry, Ciofini *et al.* introduced alternative diagnostics that they call the "t index"[336,354] and the "H index".[211,221,336,354] The latter is essentially $(\sigma_{\text{elec}} + \sigma_{\text{hole}})/2$, which provides a measure of the spread of the excitation, while the former is defined as $t = D_{\text{CT}} - H$. We suggest replacing t with an alternative measure of essentially the same information, the *charge-displacement distance*[1]

$$d_{\text{CD}} = d^-_{\text{e-h}} - \frac{1}{2}\left(\sigma_{\text{elec}} + \sigma_{\text{hole}}\right) \,. \tag{5.22}$$

An alternative might be

$$\tilde{d}_{\text{CD}} = d^-_{\text{e-h}} + d_{\text{exc}} \,. \tag{5.23}$$

Both of these are similar to a different charge-separation metric ($\Delta\sigma$) introduced by Adamo *et al.*,[362] which will be discussed in Section 6.2. Essentially the same information that is encoded in D_{CT} and $\Delta\sigma$ is contained also in the quantities $d^-_{\text{e-h}}$ and d_{CD}, but the latter are defined in a manner that is more directly connected to properties of the particle and the hole. This analysis furthermore clarifies why the values of various charge-displacement metrics are found to be strongly correlated with one another.[22,191,229] In this author's view, the use of $d^-_{\text{e-h}}$ (distance between the centroids of the electron and the hole) and d_{CD} (center-to-center distance reduced by the average of the RMS size of the electron and the hole) are preferable ways to measure exciton size and electron–hole separation. These quantities provide a more intuitive and mutually self-consistent way to convey the same information as the D_{CT} and t indices.

One novel analysis tool contained in the work of Ciofini *et al.*[336] is the idea to use the the second moments σ^2_{elec} and σ^2_{hole} [Eq. (5.11)] to introduce Gaussian approximations to $\Delta\rho_{\text{elec}}(\mathbf{r})$ and $\Delta\rho_{\text{hole}}(\mathbf{r})$. These provide quantitative realizations of the cartoons in Fig. 16, free of the nodal structure of the particle and hole densities and perhaps slightly easier to conceptualize. Examples are depicted in Fig. 17 for a sequence of poly(*p*-phenyl)nitroaniline molecules. Due to the complex nodal structure along the conjugated backbone of these molecules, the barycenters of $\Delta\rho_{\text{elec}}(\mathbf{r})$ and $\Delta\rho_{\text{hole}}(\mathbf{r})$ are more clearly evident in their Gaussian

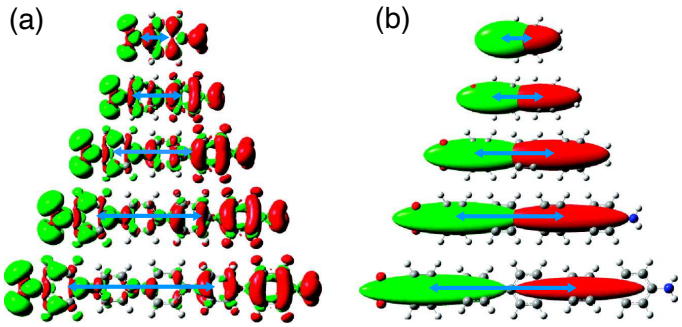

Figure 17: (a) Electron and hole densities (in green and red, respectively) and (b) Gaussian approximations to these quantities, for a sequence of poly(*p*-phenyl)nitroanilines, O_2N–$(C_6H_4)_n$–NH_2. Calculations were performed at the TD-PBE0/6-31+G* level using a solvent model.[336] Blue arrows connects centroids of the electron and hole densities in each case. Adapted from Ref. 336; copyright 2011 American Chemical Society.

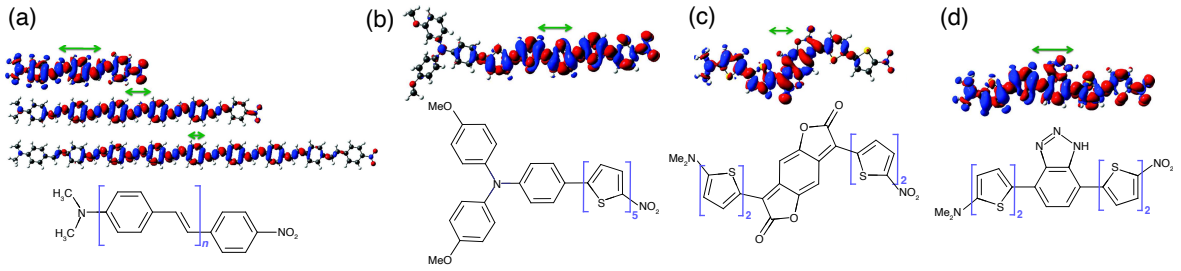

Figure 18: Particle densities $\Delta\rho_{\text{elec}}(\mathbf{r})$ (in red) and hole densities $\Delta\rho_{\text{hole}}(\mathbf{r})$ (in blue), for various push-pull chromophores that are indicated in the lower part of the figure. Each chromophore has the structure $(CH_3)_2N$–π–NO_2, where "π" indicates a large conjugated system. Examples include: (a) several oligomers of α,ω-dimethylamino-nitro-(*p*-phenylene vinylene)$_n$; (b) a tertiary amine of the form $N(PhOCH_3)_2(PhR)$, where Ph = phenyl and R is a pentathiophene side chain with a terminal nitro group; and finally, α,ω-dimethylaminonitro-(*p*-thiophene)$_5$ with the central thiophene unit replaced by either (c) benzodifuranone or else (d) benzotriazole. Green arrows indicate the charge-separation distance, $d^-_{\text{e-h}}$. These arrows have been displaced away from the molecules for clarity but their endpoints coincide with the centroids of the particle and hole densities. Adapted from Ref. 221; copyright 2012 American Chemical Society.

approximations (Fig. 17b). Note also that whereas the particle and hole densities extend to the very edges of the molecule, the charge separation distance $d^-_{\text{e-h}}$ (indicated by the blue arrows in Fig. 17) is noticeably shorter. This is even more clear in the examples of Fig. 18, where plots of the particle and hole densities appear to be considerably more delocalized than the quantitative measure afforded by $d^-_{\text{e-h}}$. The extent of spatial charge separation is therefore smaller than plots of $\Delta\rho_{\text{elec}}(\mathbf{r})$ and $\Delta\rho_{\text{hole}}(\mathbf{r})$ might lead one to imagine. The latter are susceptible to the choice of isocontour value, which can sometimes be used to make a density appear almost arbitrarily compact or diffuse. For that reason, the author recommends that such plots should always indicate the fraction of the indicated density that is encapsulated within the isosurface,[149] as in several of the figures presented elsewhere in this work.

The spatial overlap between particle and hole densities defines a region of space corresponding to a localized excitation. In contrast, charge separation suggests that the product $\Delta\rho_{\text{elec}}(\mathbf{r})\ \Delta\rho_{\text{hole}}(\mathbf{r}) \approx 0$, *i.e.*, there is little or no spatial overlap between the excited electron and the hole. This is depicted schematically in Fig. 19a using electron and hole densities that are drawn to resemble the Gaussian approximations in Fig. 17b. Based on this idea, Etienne *et al.*[12,13,363] suggest a charge-separation metric based on this product:

$$\phi = \int \left|\Delta\rho_{\text{elec}}(\mathbf{r})\ \Delta\rho_{\text{hole}}(\mathbf{r})\right|^{1/2} d\mathbf{r}\ . \tag{5.24}$$

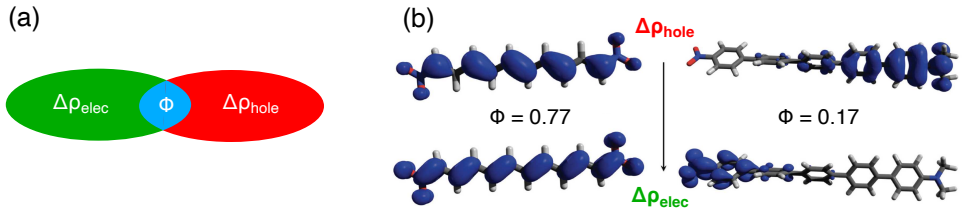

Figure 19: (a) Schematic view of the charge-separation metric ϕ defined in Eq. (5.24), using cartoon sketches of particle and hole densities made to resemble those in Fig. 17b. Roughly speaking, the integrand in Eq. (5.24) is non-zero in the blue region of overlap between $\Delta\rho_{\mathrm{elec}}(\mathbf{r})$ and $\Delta\rho_{\mathrm{hole}}(\mathbf{r})$. (b) Examples of a localized excitation (on the left) and a CT excitation (on the right) in the push-pull system $(H_2C)_2N$–$(C_6H_4)_5$–NO_2. In its planar geometry (on the left), there is significant overlap between $\Delta\rho_{\mathrm{elec}}(\mathbf{r})$ and $\Delta\rho_{\mathrm{hole}}(\mathbf{r})$, corresponding to a large value of ϕ, but when the molecule is twisted (on the right), these densities localize on opposite ends of the molecule and ϕ is small. Calculations in (b) were performed at the TD-PBE0/6-311++G(2d,p) level and the plots are adapted from Ref. 13.

Roughly speaking, this integrates over the blue region in Fig. 19a, corresponding to overlap of $\Delta\rho_{\mathrm{elec}}(\mathbf{r})$ and $\Delta\rho_{\mathrm{hole}}(\mathbf{r})$. In Eq. (5.24), we omit the normalizing denominator that is included in the definition of Ref. 12, as it equals unity for TD-DFT calculations where both $\Delta\rho_{\mathrm{elec}}(\mathbf{r})$ and $|\Delta\rho_{\mathrm{hole}}(\mathbf{r})|$ integrate to exactly one electron.

The metric ϕ is defined such that $0 \leq \phi \leq 1$. If $\phi = 0$ then there is no overlap between electron and hole, meaning that the excitation in question is entirely CT-like. An actual example that lies close to that limit is the end-to-end donor–acceptor electron-transfer excitation of the twisted push-pull chromophore $(H_3C)_2N$–$(C_6H_4)_5$–NO_2, whose particle and hole densities are plotted on the right of Fig. 19b. A twist in the geometry severs the conjugation of the π system, resulting in particle and hole densities that localize on opposite ends of the molecule and a much smaller value of ϕ as compared to when the molecule is planar. When planarity is restored (on the left in Fig. 19b), both $\Delta\rho_{\mathrm{elec}}(\mathbf{r})$ and $\Delta\rho_{\mathrm{hole}}(\mathbf{r})$ delocalize across the entire π system, leading to a value of ϕ that is closer to its upper limit.

6 Diagnosing the CT Problem

TD-DFT calculations are afflicted by severe underestimation of excitation energies for states having charge-separated character, as has been widely discussed.[1,9,19,24–32] In a sufficiently large system, this can manifest as "spurious" CT states,[1,24–28] whose energies are much lower than what one would estimate using Mulliken's formula,[9]

$$\omega_{\mathrm{CT}}(R) \approx \mathrm{IE} + \mathrm{EA} + \frac{1}{4\pi\epsilon_0 R} \,. \tag{6.1}$$

Equation (6.1) expresses the excitation energy ω_{CT} between well-separated donor and acceptor moieties in terms of the ionization energy (IE) of the donor and the electron affinity (EA) of the acceptor, along with a Coulomb penalty of $1/(4\pi\epsilon_0 R)$ for creating an ion pair. In conjugated polymers, problems with underestimated CT energies in TD-DFT lead to over-delocalization of the exciton wave functions.[318,325,327] The phenomenology of this problem is discussed next, in Section 6.1. We have already seen (in Section 5.3) that one can design metrics to measure the degree of CT in a given excited state. These and related metrics are discussed in the context of TD-DFT's CT problem in Section 6.2.

6.1 Overview of the problem

As discussed in Section 5, exciton size and delocalization can be characterized and quantified using properties of the transition density $T(\mathbf{r}_{\mathrm{elec}}, \mathbf{r}_{\mathrm{hole}})$, providing access to correlations between the electron and the hole quasiparticles that cannot always be inferred from the MOs and excitation amplitudes alone. This has a bearing on diagnosing anomalous CT in TD-DFT calculations, as shown schematically in Fig. 20 using

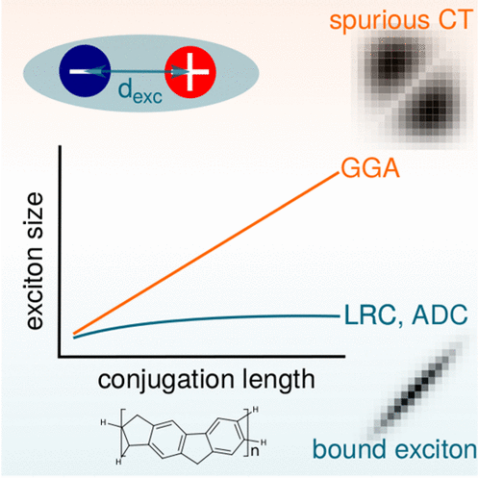

Figure 20: Cartoon depiction of exciton size versus conjugation length for ladder-type poly(*p*-phenylene). The quantity d_{exc} [eq. (5.12)] is the RMS exciton size, which increases without bound when GGA functionals are used in TD-DFT. Reprinted from Ref. 327; copyright 2017 American Chemical Society.

ladder-type poly(*p*-phenylene) polymers as an example.[320,364] Here, TD-DFT calculations using semilocal functionals (GGAs) predict a bound exciton that is delocalized across the entire polymer, regardless of oligomer length, which is the same problem that was documented for $(PPV)_{20}$ in Fig. 14. In the latter case, hybrid functionals with a large fraction of Hartree-Fock exchange significantly attenuate the charge separation (although not the FE delocalization).[318] As indicated in Fig. 20, LRC functionals also predict a finite size limit, in agreement with many-body calculations.[327] Such functionals include 100% Hartree-Fock exchange at long range only.[1,26,37–39,259]

The DMABN molecule that was introduced in Section 4.3 provides an interesting case study in TD-DFT's description of CT, and Fig. 21 characterizes the nature of its $S_0 \rightarrow S_1$ and $S_0 \rightarrow S_2$ transitions using particle and hole densities. These are the ^1L_a and ^1L_b states, and according to the lore one of them should be the $^1\pi\pi^*$ or "LE" state, while the other should exhibit nascent CT character that is enhanced upon twisting. At the planar ground-state geometry (on the left in Fig. 21), both transitions exhibit significant delocalization across the donor–π–acceptor framework, although the excited electron (attachment density) has slightly more density on the cyano group in S_2 than in S_1. Introducing a 90° twist of the amino group (on the right in Fig. 21), and in a dielectric medium characteristic of acetonitrile, detachment densities for both transitions localize on the $n(NH_2)$ lone pair. For the twisted geometry, S_1 is clearly the CT state and it is significantly stabilized by solvent polarization. In contrast, the excitation energy for the LE state is scarcely affected by the twist.

Historically, a point of some debate was the fact that the PBE and B3LYP functionals both predict reasonably accurate excitation energies for both the ^1L_a and ^1L_b states, with comparable errors in each, for DMABN and other small donor–π–acceptor molecules.[19,365,366] A resolution to this apparent paradox comes in the form of metric for quantifying CT character, that will be introduced below but which ultimately suggests that the extent of CT in the planar geometry of DMABN is not very large.[19] Only in hindsight can this be inferred from the densities in Fig. 21a, which do not suggest any dramatic difference between S_1 and S_2 at the ground-state geometry. (The difference is much more pronounced at the twisted geometry.) As such, DMABN serves as a cautionary tale to indicate that one must be careful with blanket statements that TD-DFT fails categorically for CT excitations,[19] or at least one must be careful about what gets called a CT excitation. Energies for truly long-range CT excitations will indeed be systematically (and catastrophically) underestimated using GGA functionals, but errors may be small if the donor and acceptor orbitals are not completely separated in space. In the planar geometry of ground-state DMABN, these orbitals are clearly *not* well-separated in space.

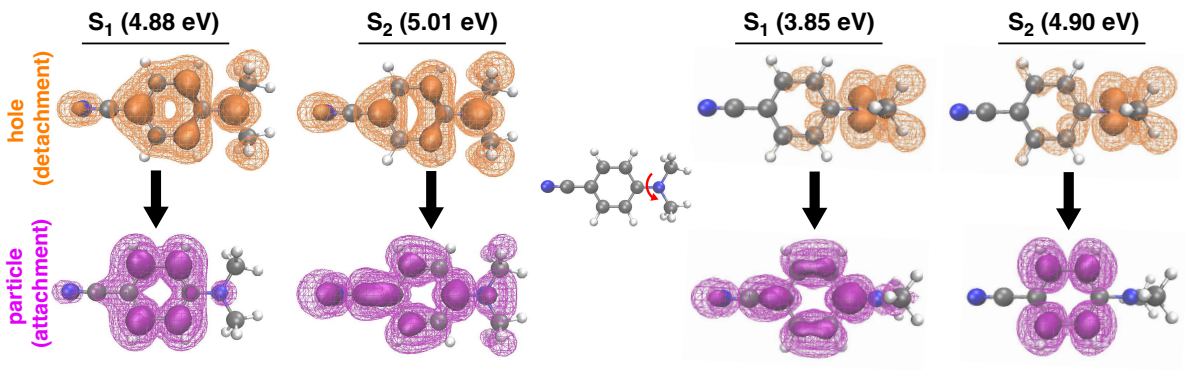

Figure 21: Particle (attachment) and hole (detachment) densities for the $S_0 \rightarrow S_1$ and $S_0 \rightarrow S_2$ transitions in DMABN, in both its planar, ground-state geometry (on the left) and upon introducing a 90° twist of the dimethylamino moiety (on the right). Opaque and wire mesh surfaces encapsulate 50% and 90% of each density, respectively. TD-DFT/TDA calculations were performed using LRC-ωPBE/6-31G* with a dielectric constant of 37.5 (representing acetonitrile).

6.2 Diagnostics

The resolution to the DMABN paradox described above was made possible through the use of the first CT metric to be introduced for CT calculations, by Tozer and co-workers.[19] Their proposed metric, denoted by Λ, is defined as

$$\Lambda = \frac{\sum_{ia} \kappa_{ia}^2 O_{ia}}{\sum_{jb} \kappa_{jb}^2} \tag{6.2}$$

where

$$\kappa_{ia} = x_{ia} + y_{ia} \tag{6.3}$$

and

$$O_{ia} = \int |\psi_i(\mathbf{r})| \, |\psi_a(\mathbf{r})| \, d\mathbf{r} \, . \tag{6.4}$$

Note the absolute value signs in the integrand of Eq. (6.4), which are necessary because occupied and virtual MOs are orthogonal. For this reason, we resist using the term "overlap" when it comes to MOs, in favor of "spatial proximity" versus "spatial separation", although we might call O_{ia} the "spatial overlap". This and similar metrics are sometimes used to quantify the spatial proximity of HOMO and LUMO in donor–acceptor materials.[367]

In view of the normalization condition for $\mathbf{x}$ and $\mathbf{y}$ [Eq. (2.4)], it is unclear why the definition of Λ in Eq. (6.2) does not involve both $\mathbf{x}+\mathbf{y}$ and $\mathbf{x}-\mathbf{y}$. Perhaps it is in loose analogy to the expressions for the particle and hole density matrices [Eq. (2.11)], which contain terms like $(\mathbf{x}+\mathbf{y})^\dagger(\mathbf{x}+\mathbf{y})$ and $(\mathbf{x}+\mathbf{y})(\mathbf{x}+\mathbf{y})^\dagger$, although these expressions also contain $(\mathbf{x}-\mathbf{y})^\dagger(\mathbf{x}-\mathbf{y})$ and $(\mathbf{x}-\mathbf{y})(\mathbf{x}-\mathbf{y})^\dagger$. (The latter have sometimes been erroneously omitted in our own work as well.[98]) Whatever the reason, the definition of Λ in Eq. (6.2) is the one that has been used in practice,[19,21,98,368–370] yet the decision to abdicate the proper normalization seems questionable, and has implications for other CT metrics that are discussed below. Within the TDA (where $\mathbf{y} = \mathbf{0}$) there is no issue, as the denominator in Eq. (6.2) has a well-defined normalization, namely, $\sum_{ia} x_{ia}^2 = 1$. The implies that $0 \leq \Lambda \leq 1$ within the TDA, however this need not be the case in full TD-DFT. In practice, Tozer *et al.* find that $0.45 \leq \Lambda \leq 0.89$ for localized valence excitations whereas Rydberg excitations lie in the range $0.08 \leq \Lambda \leq 0.27$.[19]

Examining excitation energy errors as a function of Λ, it becomes clear that there are approximate (albeit functional-dependent) thresholds below which TD-DFT results should not be trusted. For example, when $\Lambda < 0.4$ (for B3LYP) or $\Lambda < 0.3$ (for PBE), the excitation energies are "likely to be in very significant error".[19] Values of Λ are also found to correlate well with excitation energy errors along the torsional coordinate of a hydroxynaphthalene bichromophore that has the potential for intramolecular CT.[371] The Λ

metric has been successfully used to explain other trends in TD-DFT errors,[33] although other metrics can be used in that capacity as well.[131] Resolution of the DMABN paradox comes in noting that its intramolecular CT excitation at the PBE level exhibits $\Lambda = 0.72$ in the planar geometry,[19] which is not very CT-like in real space. For the LRC-ωPBE/6-31G* calculations in Fig. 21, the corresponding values are $\Lambda(S_1) = 0.53$ and $\Lambda(S_2) = 0.67$ in the planar geometry, indicating that the nominal CT state actually has somewhat larger spatial proximity between particle and hole. This is actually true in the twisted geometry as well, although the values are much smaller and lie in the "danger zone": $\Lambda(S_1) = 0.20$ and $\Lambda(S_2) = 0.22$. Results at the TD-B3LYP/6-31G* level are similar.

Thus, while Λ has proven to be successful as a diagnostic for TD-DFT errors, its numerical value does not provide much physical insight. Moreover, this metric may fail to detect problems when the excited state involves excitation from a relatively compact occupied MO into a much more delocalized virtual MO,[368] since these two orbitals may share significant spatial proximity (in the sense of O_{ia}) yet the delocalized nature of the final state might still engender an erroneously low TD-DFT excitation energy. One relevant class of examples is that large density rearrangements upon excitation of certain PAH molecules can lead to anomalously low TD-DFT excitation energies, especially in larger aromatic systems.[98,204,205,372] This problem can be rectified through the use of asymptotically-correct LRC functionals,[98,372] yet such states do not exhibit what might be understood as CT in intuitive chemical or functional-group terms, and values of Λ do not portend any problems in such cases.[98]

Other metrics that were introduced in Section 5.3 may do better job of providing physical insight, as they connect more directly on the physical separation between electron and hole. A straightforward measure is $d^-_{\text{e-h}}$ [Eq. (5.13)], which is the distance between the centroids of $\Delta\rho_{\text{elec}}(\mathbf{r})$ and hole density $\Delta\rho_{\text{hole}}(\mathbf{r})$. As discussed in Section 5.3, the quantity $d^-_{\text{e-h}}$ has sometimes been called simply a "CT metric", and denoted D_{CT} or d_{CT},[20,211,221,336,353–361] but this obscures its readily-interpretable physical origin. That $d^-_{\text{e-h}}$ is simply the electron–hole separation is evident both from the nomenclature and from the definition, either Eq. (5.13) or (5.21). On the other hand, $d^-_{\text{e-h}}$ measures center-to-center electron–hole distance but takes no account of the size of the distributions $\Delta\rho_{\text{elec}}(\mathbf{r})$ and $\Delta\rho_{\text{hole}}(\mathbf{r})$. That information is included in the charge-displacement distance, d_{CD} [Eq. (5.22)], which reduces $d^-_{\text{e-h}}$ by the average size of electron and hole as measured by their second moments.

Although $d^-_{\text{e-h}}$ and d_{CD} provide the most direct physical interpretation of the CT character, several alternatives have been proposed in the spirit of the Λ metric, as attempts to find a diagnostic that is also physically meaningful. One of these is a charge-separation metric Δr,[21,22] defined as

$$\Delta r = \frac{\sum_{ia} \kappa_{ia}^2 \|\mathbf{R}_{ia}\|}{\sum_{jb} \kappa_{jb}^2} \tag{6.5}$$

where

$$\mathbf{R}_{ia} = \langle\psi_i|\hat{\mathbf{r}}|\psi_i\rangle - \langle\psi_a|\hat{\mathbf{r}}|\psi_a\rangle \tag{6.6}$$

is the relative position vector of the centroids of orbitals $\psi_i(\mathbf{r})$ and $\psi_a(\mathbf{r})$. The quantity Δr measures the change in the orbital centroids upon $\psi_i \to \psi_a$ excitation, weighted by κ_{ia}^2.

Although the definition in Eq. (6.5) seems like an intuitive way to measure charge separation, the utility of Δr as a separate metric is questionable. Within the TDA, this quantity is precisely equal to the electron–hole separation $d^-_{\text{e-h}}$ defined in eq. (5.13), whereas for full TD-DFT the definition of Δr employs the same curious choice of normalization that was used to define Λ, namely, use of κ_{ia}^2 in the denominator of Eq. (6.5). Perhaps more damningly, Δr is not orbitally invariant so that its numerical value depends upon the choice of MOs that are used in Eq. (6.6).[22] It has been suggested to evaluate Δr in NTO basis, as this seems to afford good correlation between Δr and D_{CT},[22] but the need to make such a choice is a bothersome manifestation of having broken orbital invariance. Moreover, for a different data set of intramolecular CT energies,[373] reasonable correlations are found between Δr regardless of whether canonical MOs or NTOs are used, but those values also correlate well with d_{exc}.[191] The latter quantity, along with expectation values such as $\langle\mathbf{r}_{\text{elec}}\rangle$ and $\langle\mathbf{r}_{\text{hole}}\rangle$, and also $d^-_{\text{e-h}}$ that is defined from them, are invariant to unitary transformations of MOs. Quantities such as $d^-_{\text{e-h}}$, d_{exc}, and d_{CD} are thus fundamental properties of the exciton, independent of its representation, and should therefore be preferred as measures of its properties.

Note that $d_{\text{e-h}}^{-}$ vanishes in centrosymmetric systems, as does its doppelgänger, Δr. This is a significant drawback in some cases, but which is not shared by d_{CD}. Alternatively, to obtain a non-vanishing metric in the presence of inversion symmetry, an "effective electron displacement" measure has been suggested,[362] defined as

$$\Gamma = \Delta r + \Delta\sigma \; . \tag{6.7}$$

This combines Δr from Eq. (6.5) with

$$\Delta\sigma = \frac{\sum_{ia} \kappa_{ia}^2 |\sigma_i - \sigma_a|}{\sum_{jb} \kappa_{jb}^2} \tag{6.8}$$

where

$$\sigma_r = \left(\langle\psi_r|\hat{\mathbf{r}}\cdot\hat{\mathbf{r}}|\psi_r\rangle - \|\langle\psi_r|\hat{\mathbf{r}}|\psi_r\rangle\|^2 \right)^{1/2} \; . \tag{6.9}$$

The quantity σ_r^2 is the second moment of orbital ψ_r. In a sense, $\Delta\sigma$ is conceptually similar to d_{exc} in eqn. (5.12) in the same way that Δr is conceptually similar to $d_{\text{e-h}}^{-}$, with the important distinction that both Δr and $\Delta\sigma$ mangle the normalization when $\mathbf{y}$ is nonzero, and that the numerical values of both Δr and $\Delta\sigma$ depend upon the choice of representation.

In any case, these quantities correlate well enough with the largest errors in TD-DFT excitation energies so that one may define a "trust radius".[21] It is suggested that states with $\Gamma \leq 1.8$ Å for GGA functionals, or $\Gamma \leq 2.0$ Å for global hybrids, are "safe" in the sense that the excitation energy in question is is unlikely to be seriously affected by long-range CT effects in TD-DFT. Since $\Gamma \approx d_{\text{e-h}}^{-} + d_{\text{exc}}$ (insofar as the y_{ia} amplitudes are small), this quantity provides not only a reliability metric for TD-DFT excitation energies but also a physically-interpretable numerical value for how charge moves ($d_{\text{e-h}}^{-}$) and spreads (d_{exc}) upon excitation. For long-range excitations beyond 2.0 Å, it is suggested that the use of LRC functionals, or else global hybrids with at least 33% Hartree-Fock exchange, is mandatory.[21]

Finally, a "Mulliken-averaged configuration index" (MAC) has been suggested for detecting spurious low-energy CT states.[360,374] Using a crude Koopmans-style approximation for long-range electron transfer from ψ_i to ψ_a,

$$\text{IE} + \text{EA} \approx -(\varepsilon_i + \varepsilon_a) \; , \tag{6.10}$$

in conjunction with Mulliken's asymptotic CT formula [Eq. (6.1)], suggests a definition

$$\omega_{\text{MAC}} = \frac{-\sum_{ia} x_{ia}(\varepsilon_i + \varepsilon_a)}{\sum_{jb} x_{jb}^2} - \frac{1}{d_{\text{e-h}}^{-}} \; . \tag{6.11}$$

(This is a slightly modified version of the metric called M_{AC} that was proposed in Ref. 374, correcting what this author believes to be a typographical error.) The idea is that if $\omega < \omega_{\text{MAC}}$, where ω is the excitation energy computed using TD-DFT, then the excited state in question is likely a "ghost" CT state, which should not be taken at face value.[374] However, this metric should only be used for large values of $d_{\text{e-h}}^{-}$, because Mulliken's formula (on which it is based) makes sense only for large donor–acceptor separation. Moreover, given the crudeness of the approximation in Eq. (6.10), it is unclear how reliable this metric will be. As such, proper statistical measures of electron–hole correlation seem preferable.

7 Summary

Visualizing TD-DFT excitations in terms of NTOs, as a conceptually superior alternative to canonical MOs, has become standard practice. The present work provides a theoretical foundation to understand how the NTOs relate to other common visualization tools including attachment and detachment densities, which are equivalent (within the TD-DFT formalism) to separate densities for the excited electron and for the hole. Atomic (or fragment) partitions of the density change $\Delta\rho(\mathbf{r})$ have been surveyed and related to one another. Previous literature has not always been clear regarding these connections.

CT numbers $\Omega_{A\to B}$, which quantify electron flow from A to B upon excitation, are one such atomic partition. Arranged in the form of a matrix $\mathbf{\Omega}$, these quantities provides a simple visual representation of the

transition density $T(\mathbf{r}_{\text{hole}}, \mathbf{r}_{\text{elec}})$, a quantity that has occassionally been described as an "exciton wave function". Heat maps of the matrix $\mathbf{\Omega}$ provide an easy way to distinguish localized versus delocalized excited states. This method can distinguish between delocalization caused by excitonic coupling between chromophores, versus delocalization due to charge separation; these possibilities are not mutually exclusive but also not equivalent. In multichromophore systems including conjugated polymers and crystalline acenes, this analysis exposes qualitative differences in the low-energy states obtained using different exchange-correlation functionals.

Atomic partitions of $\Delta\rho(\mathbf{r})$ also lend themselves to construction of various metrics intended to quantify the CT character in a given excitation. This is an important descriptor in view of TD-DFT's well known tendency to underestimate long-range CT excitation energies, sometimes to the point of predicting spurious low-lying states in large systems.[25] Some of these CT metrics have more desirable properties than others, such as correct normalization and invariance to unitary transformations of the MOs. The present work advocates for the use of direct measures of exciton size that correspond to well-defined statistical quantities, rather than *ad hoc* constructions. The former include the RMS electron–hole separation (d_{exc}), which is expressed in terms of the particle and hole densities $\Delta\rho_{\text{elec}}(\mathbf{r})$ and $\Delta\rho_{\text{hole}}(\mathbf{r})$. The mean separation between the centroids of these quantities ($d^{-}_{\text{e-h}}$) can also be used, although it vanishes in centrosymmetric systems, but in such cases a charge-displacement metric (d_{CD}) can be used instead. These quantities are directly interpretable and readily computable using third-party software,[150,195,375,376] based on formatted output from various electronic structure programs. The TheoDORE program is especially recommended,[195] as it implements various measures of exciton size that are grounded in proper expectation values, as well as CT numbers $\Omega_{A\to B}$ that properly account for non-orthogonality of the AO basis functions. Much of this functionality exists in the Q-Chem program also,[378] without the need for third-party software. The author hopes that this Perspective will lead to better understanding and more erudite discussion of precisely what is being visualized or quantified when discussing the output of TD-DFT calculations.

Conflicts of interest

J.M.H. serves on the board of directors of Q-Chem Inc.

Acknowledgements

This work was supported by National Science Foundation grants CHE-1665322 and CHE-1955282. Some calculations were performed at the Ohio Supercomputer Center[377] using the Q-Chem program.[378]

References

[1] J. M. Herbert, "Density-functional theory for electronic excited states", in *Theoretical and Computational Photochemistry: Fundamentals, Methods, Applications and Synergy with Experimental Approaches*, C. García-Iriepa and M. Marazzi, Eds.; Elsevier, 2023; chapter 3, pages 69–118.

[2] M. E. Casida, "Time-dependent density functional response theory for molecules", in *Recent Advances in Density Functional Methods, Part I*, D. P. Chong, Ed., Vol. I of *Recent Advances in Computational Chemistry;* World Scientific: River Edge, NJ, 1995; chapter 5, pages 155–192.

[3] S. Hirata and M. Head-Gordon, "Time-dependent density functional theory within the Tamm-Dancoff approximation", *Chem. Phys. Lett.*, **314**, 291–299 (1999).

[4] F. Furche, "On the density matrix based approach to time-dependent density functional response theory", *J. Chem. Phys.*, **114**, 5982–5992 (2001).

[5] C. Ullrich, *Time-Dependent Density-Functional Theory: Concepts and Applications*, Oxford University Press: New York, 2012.

[6] M. E. Casida, "Time-dependent density-functional theory for molecules and molecular solids", *J. Mol. Struct. (Theochem)*, **914**, 3–18 (2009).

[7] F. Furche and D. Rappoport, "Density functional methods for excited states: Equilibrium structure and electronic spectra", in *Computational Photochemistry*, M. Olivucci, Ed., Vol. 16 of *Theoretical and Computational Chemistry;* Elsevier: Amsterdam, 2005; chapter 3, pages 93–128.

[8] P. Elliott, F. Furche, and K. Burke, "Excited states from time-dependent density functional theory", in *Reviews in Computational Chemistry*, K. B. Lipkowitz and T. R. Cundari, Eds., Vol. 26; Wiley-VCH: New York, 2009; chapter 3, pages 91–165.

[9] A. Dreuw and M. Head-Gordon, "Single-reference ab initio methods for the calculation of excited states of large molecules", *Chem. Rev.*, **105**, 4009–4037 (2005).

[10] A. D. Laurent and D. Jacquemin, "TD-DFT benchmarks: A review", *Int. J. Quantum Chem.*, **113**, 2019–2039 (2013).

[11] J. M. Herbert, Y. Zhu, B. Alam, and A. K. Kumar, "Time-dependent density functional theory for x-ray absorption spectra: Comparing the real-time approach to linear response", *J. Chem. Theory Comput.*, **19**, 6745–6760 (2023).

[12] T. Etienne, X. Assfeld, and A. Monari, "Toward a quantitative assessment of electron transitions' charge-transfer character", *J. Chem. Theory Comput.*, **10**, 3896–3905 (2014).

[13] T. Etienne, "Theoretical insights into the topology of molecular excitons from single-reference excited states calculation methods", in *Excitons*, S. L. Pyshkin, Ed.; IntechOpen, 2018; chapter 3, pages 31–54.

[14] F. Plasser, M. Wormit, and A. Dreuw, "New tools for the systematic analysis and visualization of electronic excitations. I. Formalism", *J. Chem. Phys.*, **140**, 024106:1–13 (2014).

[15] F. Plasser, S. A. Bäppler, M. Wormit, and A. Dreuw, "New tools for the systematic analysis and visualization of electronic excitations. II. Applications", *J. Chem. Phys.*, **141**, 024107:1–12 (2014).

[16] S. A. Mewes and A. Dreuw, "Density-based descriptors and exciton analyses for visualizing and understanding the electronic structure of excited states", *Phys. Chem. Chem. Phys.*, **21**, 2843–2856 (2019).

[17] P. Kimber and F. Plasser, "Classification and analysis of molecular excited states", in *Comprehensive Computational Chemistry* volume 4; M. Yáñeez and R. J. Boyd, Eds.; Elsevier, 2023, pages 55–83.

[18] F. Plasser, B. Thomitzni, S. A. Bäppler, J. Wenzel, D. R. Rehn, M. Wormit, and A. Dreuw, "Statistical analysis of electronic excitation processes: Spatial location, compactness, charge transfer, and electron-hole correlation", *J. Comput. Chem.*, **36**, 1609–1620 (2015).

[19] M. J. G. Peach, P. Benfield, T. Helgaker, and D. J. Tozer, "Excitation energies in density functional theory: An evaluation and a diagnostic test", *J. Chem. Phys.*, **128**, 044118:1–18 (2008).

[20] D. Jacquemin, T. Le Bahers, C. Adamo, and I. Ciofini, "What is the "best" atomic charge model to describe through-space charge-transfer excitations?", *Phys. Chem. Chem. Phys.*, **14**, 5383–5388 (2012).

[21] C. A. Guido, P. Cortona, B. Mennucci, and C. Adamo, "On the metric of charge transfer molecular excitations: A simple chemical descriptor", *J. Chem. Theory Comput.*, **9**, 3118–3126 (2013).

[22] M. Savarese, C. A. Guido, E. Brémond, I. Ciofini, and C. Adamo, "Metrics for molecular electronic excitations: A comparison between orbital- and density-based descriptors", *J. Phys. Chem. A*, **121**, 7543–7549 (2017).

[23] S. Mai, F. Plasser, J. Dorn, M. Fumanal, C. Daniel, and L. González, "Quantitative wave function analysis for excited states of transition metal complexes", *Coord. Chem. Rev.*, **361**, 74–97 (2018).

[24] R. J. Magyar and S. Tretiak, "Dependence of spurious charge-transfer excited states on orbital exchange in TDDFT: Large molecules and clusters", *J. Chem. Theory Comput.*, **3**, 976–987 (2007).

[25] A. Lange and J. M. Herbert, "Simple methods to reduce charge-transfer contamination in time-dependent density-functional calculations of clusters and liquids", *J. Chem. Theory Comput.*, **3**, 1680–1690 (2007).

[26] A. W. Lange, M. A. Rohrdanz, and J. M. Herbert, "Charge-transfer excited states in a π-stacked adenine dimer, as predicted using long-range-corrected time-dependent density functional theory", *J. Phys. Chem. B*, **112**, 6304–6308 (2008).

[27] A. W. Lange and J. M. Herbert, "Both intra- and interstrand charge-transfer excited states in B-DNA are present at energies comparable to, or just above, the $^1\pi\pi^*$ excitonic bright states", *J. Am. Chem. Soc.*, **131**, 3913–3922 (2009).

[28] C. M. Isborn, B. D. Mar, B. F. E. Curchod, I. Tavernelli, and T. J. Martínez, "The charge transfer problem in density functional theory calculations of aqueously solvated molecules", *J. Phys. Chem. B*, **117**, 12189–12201 (2013).

[29] N. T. Maitra, "Charge-transfer in time-dependent density functional theory", *J. Phys.: Condens. Matt.*, **29**, 423001:1–17 (2017).

[30] D. J. Tozer, R. D. Amos, N. C. Handy, B. O. Roos, and L. Serrano-Andrés, "Does density functional theory contribute to the understanding of excited states of unsaturated organic compounds?", *Mol. Phys.*, **97**, 859–868 (1999).

[31] A. Dreuw, J. L. Weisman, and M. Head-Gordon, "Long-range charge-transfer excited states in time-dependent density functional theory require non-local exchange", *J. Chem. Phys.*, **119**, 2943–2946 (2003).

[32] O. Gritsenko and E. J. Baerends, "Asymptotic correction of the exchange–correlation kernel of time-dependent density functional theory for long-range charge-transfer excitations", *J. Chem. Phys.*, **121**, 655–660 (2004).

[33] S. S. Leang, F. Zahariev, and M. S. Gordon, "Benchmarking the performance of time-dependent density functional methods", *J. Chem. Phys.*, **136**, 104101:1–13 (2012).

[34] T. Stein, L. Kronik, and R. Baer, "Reliable prediction of charge transfer excitations in molecular complexes using time-dependent density functional theory", *J. Am. Chem. Soc.*, **131**, 2818–2820 (2009).

[35] R. Baer, E. Livshits, and U. Salzner, "Tuned range-separated hybrids in density functional theory", *Annu. Rev. Phys. Chem.*, **61**, 85–109 (2010).

[36] S. Kümmel, "Charge-transfer excitations: A challenge for time-dependent density functional theory that has been met", *Adv. Energy Mater.*, **7**, 1700440:1–6 (2017).

[37] Y. Tawada, T. Tsuneda, S. Yanagisawa, T. Yanai, and K. Hirao, "A long-range corrected time-dependent density functional theory", *J. Chem. Phys.*, **120**, 8425–8433 (2004).

[38] M. A. Rohrdanz and J. M. Herbert, "Simultaneous benchmarking of ground- and excited-state properties with long-range-corrected density functional theory", *J. Chem. Phys.*, **129**, 034107:1–9 (2008).

[39] M. A. Rohrdanz, K. M. Martins, and J. M. Herbert, "A long-range-corrected density functional that performs well for both ground-state properties and time-dependent density functional theory excitation energies, including charge-transfer excited states", *J. Chem. Phys.*, **130**, 054112:1–8 (2009).

[40] M. Head-Gordon, A. M. Graña, D. Maurice, and C. A. White, "Analysis of electronic transitions as the difference of electron attachment and detachment densities", *J. Phys. Chem.*, **99**, 14261–14270 (1995).

[41] K. Yabana, T. Nakatsukasa, J.-I. Iwata, and G. F. Bertsch, "Real-time, real-space implementation of the linear response time-dependent density functional theory", *Phys. Stat. Sol. B*, **243**, 1121–1138 (2006).

[42] M. R. Provorse and C. M. Isborn, "Electron dynamics with real-time time-dependent density functional theory", *Int. J. Quantum Chem.*, **116**, 739–749 (2016).

[43] X. Li, N. Govind, C. Isborn, A. E. DePrince III, and K. Lopata, "Real-time time-dependent electronic structure theory", *Chem. Rev.*, **120**, 9951–9993 (2020).

[44] Y. Kawashita, T. Nakatsukasa, and K. Yabana, "Time-dependent density-functional theory simulation for electron-ion dynamics in molecules under intense laser pulses", *J. Phys.: Condens. Matt.*, **21**, 064222:1–5 (2009).

[45] K. Yabana, T. Sugiyama, Y. Shinohara, T. Otobe, and G. F. Bertsch, "Time-dependent density functional theory for strong electromagnetic fields in crystalline solids", *Phys. Rev. B*, **85**, 045134:1–11 (2012).

[46] C. A. Ullrich and A. D. Bandrauk, "Atoms and molecules in strong laser fields", in *Fundamentals of Time-Dependent Density Functional Theory*, M. A. L. Marques, N. T. Maitra, F. M. S. Nogueira, E. K. U. Gross, and A. Rubio, Eds., Vol. 837 of *Lecture Notes in Physics;* Springer-Verlag: Berlin, 2012; chapter 18, pages 351–371.

[47] U. De Giovannini, G. Brunetto, A. Castro, J. Walkenhorst, and A. Rubio, "Simulating pump–probe photoelectron and absorption spectroscopy on the attosecond timescale with time-dependent density functional theory", *ChemPhysChem*, **14**, 1363–1376 (2013).

[48] Y. Miyamoto, H. Zhang, X. L. Cheng, and A. Rubio, "Modeling of laser-pulse induced water decomposition on two-dimensional materials by simulations based on time-dependent density functional theory", *Phys. Rev. B*, **96**, 115451:1–7 (2017).

[49] F. Bedurke, T. Klamroth, and P. Saalfrank, "Many-electron dynamics in laser-driven molecules: Wavefunction theory *vs.* density functional theory", *Phys. Chem. Chem. Phys.*, **23**, 13544–13560 (2021).

[50] Y. Zhu and J. M. Herbert, "High harmonic spectra computed using time-dependent Kohn-Sham theory with Gaussian orbitals and a complex absorbing potential", *J. Chem. Phys.*, **156**, 204123:1–16 (2022).

[51] E. Coccia and E. Luppi, "Time-dependent *ab initio* approaches for high-harmonic generation spectroscopy", *J. Phys.: Condens. Matt.*, **34**, 073001:1–17 (2022).

[52] Y. H. Li and C. A. Ullrich, "The particle-hole map: A computational tool to visualize electronic excitations", *J. Chem. Theory Comput.*, **11**, 5838–5852 (2015).

[53] M. Repisky, L. Konecny, M. Kadek, S. Komorovsky, O. L. Malkin, V. G. Malkin, and K. Ruud, "Excitation energies from real-time propagation of the four-component Dirac-Kohn-Sham equation", *J. Chem. Theory Comput.*, **11**, 980–991 (2015).

[54] A. Bruner, D. LaMaster, and K. Lopata, "Accelerated broadband spectra using transition dipole decomposition and Padé approximants", *J. Chem. Theory Comput.*, **12**, 3741–3750 (2016).

[55] T. P. Rossi, M. Kuisma, M. J. Puska, R. M. Nieminen, and P. Erhart, "Kohn-Sham decomposition in real-time time-dependent density-functional theory: An efficient tool for analyzing plasmonic excitations", *J. Chem. Theory Comput.*, **13**, 4779–4790 (2017).

[56] R. Sinha-Roy, P. García-González, X. L. Lozano, R. L. Whetten, and H.-C. Weissker, "Identifying electronic modes by Fourier transform from δ-kick time-evolution TDDFT calculations", *J. Chem. Theory Comput.*, **14**, 6417–6426 (2018).

[57] A. Parise, A. Alvarez-Ibarra, X. Wu, X. Zhao, J. Pilmé, and A. de la Lande, "Quantum chemical topology of the electron localization function in the field of attosecond electron dynamics", *J. Phys. Chem. Lett.*, **9**, 844–850 (2018).

[58] W. Koch and M. C. Holthausen, *A Chemist's Guide to Density Functional Theory*, Wiley-VCH: New York, 2nd ed., 2001.

[59] H. Weiss, R. Ahlrichs, and M. Häser, "A direct algorithm for self-consistent-field linear response theory and application to C_{60}: Excitation energies, oscillator strengths, and frequency-dependent polarizabilities", *J. Chem. Phys.*, **99**, 1262–1270 (1993).

[60] A. V. Luzanov and O. A. Zhikol, "Electron invariants and excited state structural analysis for electronic transitions within CIS, RPA, and TDDFT models", *Int. J. Quantum Chem.*, **110**, 902–924 (2010).

[61] T. Etienne, "Transition matrices and orbitals from reduced density matrix theory", *J. Chem. Phys.*, **142**, 244103:1–17 (2015).

[62] T. Etienne, "A comprehensive, self-contained derivation of the one-body density matrices from single-reference excited-state calculation methods using the equation-of-motion formalism", *Int. J. Quantum Chem.*, **120**, e26110:1–30 (2020).

[63] N. Ullah and D. J. Rowe, "Properties of real RPA matrices and a simple diagonalization procedure", *Nucl. Phys. A*, **A163**, 257–264 (1971).

[64] M. Grüning, A. Marini, and X. Gonze, "Exciton-plasmon states in nanoscale materials: Breakdown of the Tamm–Dancoff approximation", *Nano Lett.*, **9**, 2820–2824 (2009).

[65] Y.-M. Byun and C. A. Ullrich, "Excitons in solids from time-dependent density-functional theory: Assessing the Tamm-Dancoff approximation", *Computation*, **5**, 9:1–11 (2017).

[66] H. Eshuis, J. E. Bates, and F. Furche, "Electron correlation methods based on the random phase approximation", *Theor. Chem. Acc.*, **131**, 1084:1–18 (2012).

[67] A. Heßelmann and A. Görling, "Random-phase approximation correlation methods for molecules and solids", *Mol. Phys.*, **109**, 2473–2500 (2011).

[68] X. Ren, P. Rinke, C. Joas, and M. Scheffler, "Random-phase approximation and its applications in computational chemistry and materials science", *J. Mater. Sci.*, **47**, 7447–7471 (2012).

[69] G. P. Chen, V. K. Voora, M. M. Agee, S. G. Balasubramani, and F. Furche, "Random-phase approximation methods", *Annu. Rev. Phys. Chem.*, **68**, 421–445 (2017).

[70] M. J. G. Peach, M. J. Williamson, and D. J. Tozer, "Influence of triplet instabilities in TDDFT", *J. Chem. Theory Comput.*, **7**, 3578–3585 (2011).

[71] M. J. G. Peach and D. J. Tozer, "Overcoming low orbital overlap and triplet instability problems in TDDFT", *J. Phys. Chem. A*, **116**, 9783–9789 (2012).

[72] M. J. G. Peach, N. Warner, and D. J. Tozer, "On the triplet instability in TDDFT", *Mol. Phys.*, **111**, 1271–1274 (2013).

[73] C. Y. Cheng, M. S. Ryley, M. J. G. Peach, D. J. Tozer, T. Helgaker, and A. M. Teale, "Molecular properties in the Tamm–Dancoff approximation: Indirect nuclear spin–spin coupling constants", *Mol. Phys.*, **113**, 1937–1951 (2015).

[74] R. Bauernschmitt and R. Ahlrichs, "Stability analysis for solutions of the closed shell Kohn–Sham equation", *J. Chem. Phys.*, **104**, 9047–9052 (1996).

[75] M. E. Casida, A. Ipatov, and F. Cordova, "Linear-response time-dependent density functional theory for open-shell molecules", in *Time-Dependent Density Functional Theory*, M. A. L. Marques, C. A. Ullrich, F. Nogueira, A. Rubio, K. Burke, and E. K. U. Gross, Eds., Vol. 706 of *Lecture Notes in Physics;* Springer-Verlag: Berlin, 2006; chapter 16, pages 243–257.

[76] F. Cordova, L. J. Doriol, A. Ipatov, M. E. Casida, C. Filippi, and A. Vela, "Troubleshooting time-dependent density-functional theory for photochemical applications: Oxirane", *J. Chem. Phys.*, **127**, 164111:1–18 (2007).

[77] E. Tapavicza, I. Tavernelli, U. Rothlisberger, C. Filippi, and M. E. Casida, "Mixed time-dependent density-functional theory/classical trajectory surface hopping study of oxirane photochemistry", *J. Chem. Phys.*, **129**, 124108:1–19 (2008).

[78] J. D. Goddard and G. Orlova, "Density functional theory with fractionally occupied frontier orbitals and the instabilities of the Kohn–Sham solutions for defining radical transition states: Ring-opening reactions", *J. Chem. Phys.*, **111**, 7705–7712 (1999).

[79] G. Orlova and J. D. Goddard, "Singularities in the behavior of density functionals in predictions of singlet biradicals: The 1,2-dichalcogenins", *J. Chem. Phys.*, **112**, 10085–10094 (2000).

[80] G. Orlova and J. D. Goddard, "Is density functional theory free of spatial symmetry breaking? The case of the linear carbon radical cations: C_3^+, C_5^+, C_7^+, and C_9^+", *Chem. Phys. Lett.*, **363**, 486–491 (2002).

[81] G. Orlova and J. D. Goddard, "Practical failures from the inclusion of exact exchange: How much exact exchange is appropriate?", *Mol. Phys.*, **100**, 483–497 (2002).

[82] F. Furche and R. Ahlrichs, "Adiabatic time-dependent density functional methods for excited state properties", *J. Chem. Phys.*, **117**, 7433–7447 (2002).

[83] O. B. Lutnæs, T. Helgaker, and M. Jaszuński, "Spin–spin coupling constants and triplet instabilities in Kohn–Sham theory", *Mol. Phys.*, **108**, 2579–2590 (2010).

[84] G. Cui and W. Yang, "Challenges with range-separated exchange-correlation functionals in time-dependent density functional theory calculations", *Mol. Phys.*, **108**, 2745–2750 (2010).

[85] J. S. Sears, T. Koerzdoerfer, C.-R. Zhang, and J.-L. Brédas, "Communication: Orbital instabilities and triplet states from time-dependent density functional theory and long-range corrected functionals", *J. Chem. Phys.*, **135**, 151103:1–4 (2011).

[86] O. S. Bokareva, G. Grell, S. I. Bokarev, and O. Kühn, "Tuning range-separated density functional theory for photocatalytic water splitting systems", *J. Chem. Theory Comput.*, **11**, 1700–1709 (2015).

[87] A. Savin, C. J. Umrigar, and X. Gonze, "Relationship of Kohn–Sham eigenvalues to excitation energies", *Chem. Phys. Lett.*, **288**, 391–395 (1998).

[88] M. Petersilka, E. K. U. Gross, and K. Burke, "Excitation energies from time-dependent density functional theory using exact and approximate potentials", *Int. J. Quantum Chem.*, **80**, 534–554 (2000).

[89] E. J. Baerends, O. V. Gritsenko, and R. van Meer, "The Kohn–Sham gap, the fundamental gap and the optical gap: The physical meaning of occupied and virtual Kohn–Sham orbital energies", *Phys. Chem. Chem. Phys.*, **15**, 16408–16425 (2013).

[90] R. van Meer, O. V. Gritsenko, and E. J. Baerends, "Physical meaning of virtual Kohn–Sham orbitals and orbital energies: An ideal basis for the description of molecular excitations", *J. Chem. Theory Comput.*, **10**, 4432–4441 (2014).

[91] J. Kim, K. Hong, S. Choi, S.-Y. Hwang, and W. Y. Kim, "Configuration interaction singles based on the real-space numerical grid method: Kohn–Sham *versus* Hartree–Fock orbitals", *Phys. Chem. Chem. Phys.*, **17**, 31434–31443 (2015).

[92] S. Kang, J. Woo, J. Kim, H. Kim, Y. Kim, J. Lim, S. Choi, and W. Y. Kim, "ACE-Molecule: An open-source real-space quantum chemistry package", *J. Chem. Phys.*, **152**, 124110:1–14 (2020).

[93] A. Szabo and N. S. Ostlund, *Modern Quantum Chemistry*, Macmillan: New York, 1982.

[94] J. M. Herbert, "The quantum chemistry of loosely-bound electrons", in *Reviews in Computational Chemistry*, A. L. Parill and K. Lipkowitz, Eds., Vol. 28; Wiley-VCH: Hoboken, 2015; chapter 8, pages 391–517.

[95] F. Maschietto, M. Campetella, M. J. Frisch, G. Scalmani, C. Adamo, and I. Ciofini, "How are the charge transfer descriptors affected by the quality of the underpinning electronic density?", *J. Comput. Chem.*, **39**, 735–742 (2018).

[96] A. Ipatov, F. Cordova, L. J. Doriol, and M. E. Casida, "Excited-state spin-contamination in time-dependent density-functional theory for molecules with open-shell ground states", *J. Mol. Struct. (Theochem)*, **914**, 60–73 (2009).

[97] D. Rappoport and J. Hutter, "Excited-state properties and dynamics", in *Fundamentals of Time-Dependent Density Functional Theory*, M. A. L. Marques, N. T. Maitra, F. M. S. Nogueira, E. K. U. Gross, and A. Rubio, Eds., Vol. 837 of *Lecture Notes in Physics;* Springer-Verlag: Berlin, 2012; chapter 16, pages 317–336.

[98] R. M. Richard and J. M. Herbert, "Time-dependent density-functional description of the $^1\mathrm{L}_a$ state in polycyclic aromatic hydrocarbons: Charge-transfer character in disguise?", *J. Chem. Theory Comput.*, **7**, 1296–1306 (2011).

[99] I. Franco and S. Tretiak, "Electron-vibrational dynamics of photoexcited polyfluorenes", *J. Am. Chem. Soc.*, **126**, 12130–12140 (2004).

[100] P. R. Surján, "Natural orbitals in CIS and singular-value decomposition", *Chem. Phys. Lett.*, **439**, 393–394 (2007).

[101] E. Ronca, C. Angeli, L. Belpassi, F. De Angelis, F. Tarantelli, and M. Pastore, "Density relaxation in time-dependent density functional theory: Combining relaxed density natural orbitals and multireference perturbation theories for an improved description of excited states", *J. Chem. Theory Comput.*, **10**, 4014–4024 (2014).

[102] K. N. Walzl, C. F. Koerting, and A. Kuppermann, "Electron-impact spectroscopy of acetaldehyde", *J. Chem. Phys.*, **87**, 3796–3803 (1987).

[103] D. E. Freeman, J. R. Lombardi, and W. Klemperer, "Electric dipole moment of the lowest singlet π^* state of propynal", *J. Chem. Phys.*, **45**, 58–60 (1966).

[104] S. Millefiori, G. Favini, A. Millefiori, and D. Grasso, "Electronic spectra and structure of nitroanilines", *Spectrochim. Acta A*, **33**, 21–27 (1977).

[105] B. H. Smith, A. Buonaugurio, J. Chen, E. Collins, K. H. Bowen, R. N. Compton, and T. Sommerfeld, "Negative ions of p-nitroaniline: Photodetachment, collisions, and *ab initio* calculations", *J. Chem. Phys.*, **138**, 234304:1–8 (2013).

[106] J. B. Foresman, M. Head-Gordon, J. A. Pople, and M. J. Frisch, "Toward a systematic molecular orbital theory for excited states", *J. Phys. Chem.*, **96**, 135–149 (1992).

[107] H. K. Sinha and K. Yates, "On the ground and excited state dipole moments of planar vs. twisted nitroaniline analogues", *Can. J. Chem.*, **69**, 550–557 (1991).

[108] R. L. Martin, "Natural transition orbitals", *J. Chem. Phys.*, **118**, 4775–4777 (2003).

[109] A. V. Luzanov, A. A. Sukhorukov, and V. E. Umanskii, "Application of transition density matrix for analysis of excited states", *Theor. Exp. Chem.*, **10**, 354–361 (1974).

[110] A. V. Luzanov and V. F. Pedash, "Interpretation of excited states using charge-transfer numbers", *Theor. Exp. Chem.*, **15**, 338–341 (1980).

[111] I. Mayer, "Using singular value decomposition for a compact presentation and improved interpretation of the CIS wave functions", *Chem. Phys. Lett.*, **437**, 284–286 (2007).

[112] P.-O. Löwdin, "Quantum theory of many-particle systems. I. Physical interpretation by means of density matrices, natural spin-orbitals, and convergence problems in the method of configuration interaction", *Phys. Rev.*, **97**, 1474–1489 (1955).

[113] P.-O. Löwdin and H. Shull, "Natural orbitals in the quantum theory of two-electron systems", *Phys. Rev.*, **101**, 1730–1739 (1956).

[114] V. I. Minkin, "Glossary of terms used in theoretical organic chemistry", *Pure Appl. Chem.*, **71**, 1919–1981 (1999).

[115] L. M. Thompson, H. Harb, and H. P. Hratchian, "Natural ionization orbitals for interpreting electron detachment processes", *J. Chem. Phys.*, **144**, 204117:1–7 (2016).

[116] F. Weinhold, "Natural bond orbital methods", in *Encyclopedia of Computational Chemistry*, P. v. R. Schleyer, P. R. Schreiner, N. L. Allinger, T. Clark, J. Gasteiger, P. Kollman, and H. F. Schaefer III, Eds., Vol. 3; Wiley, 1998; pages 1792–1811.

[117] F. Weinhold and C. R. Landis, *Valency and Bonding*, Cambridge University Press: Cambridge, UK, 2005.

[118] E. D. Glendening, C. R. Landis, and F. Weinhold, "Natural bond orbital methods", *WIREs Comput. Mol. Sci.*, **2**, 1–42 (2012).

[119] A. T. Amos and G. G. Hall, "Single determinant wave functions", *Proc. R. Soc. Lond. A*, **263**, 483–493 (1961).

[120] H. F. King, R. E. Stanton, H. Kim, R. E. Wyatt, and R. G. Parr, "Corresponding orbitals and the nonorthogonality problem in molecular quantum mechanics", *J. Chem. Phys.*, **47**, 1936–1941 (1967).

[121] A. F. Morrison, Z.-Q. You, and J. M. Herbert, "Ab initio implementation of the Frenkel-Davydov exciton model: A naturally parallelizable approach to computing collective excitations in crystals and aggregates", *J. Chem. Theory Comput.*, **10**, 5366–5376 (2014).

[122] I.-M. Høyvik, R. H. Myhre, and H. Koch, "Correlated natural transition orbitals for core excitation energies in multilevel coupled cluster models", *J. Chem. Phys.*, **146**, 144109:1–6 (2017).

[123] C.-N. Tsai, M. M. Allard, R. L. Lord, D.-W. Luo, Y.-J. Chen, H. B. Schlegel, and J. F. Endicott, "Characterization of low energy charge transfer transitions in (terpyridine)(bipyridine)ruthenium(II) complexes and their cyanide-bridged bi- and tri-metallic analogues", *Inorg. Chem.*, **50**, 11965–11977 (2011).

[124] S. Ling, S. Schumacher, I. Galbraith, and M. J. Paterson, "Excited-state absorption of conjugated polymers in the near-infrared and visible: A computational study of oligofluorenes", *J. Phys. Chem. A*, **117**, 6889–6895 (2013).

[125] S. Prager, A. Zech, T. A. Wesolowski, and A. Dreuw, "Implementation and application of the frozen density embedding theory with the algebraic diagrammatic construction scheme for the polarization propagator up to third order", *J. Chem. Theory Comput.*, **13**, 4711–4725 (2017).

[126] Z. Lin and T. Van Voorhis, "Triplet tuning: A novel family of non-empirical exchange–correlation functionals", *J. Chem. Theory Comput.*, **15**, 1226–1241 (2019).

[127] T. Zhang, F. Meng, L. Lin, J. Luo, H. Wu, X. S. and C.-Z. Wang, H. Lin, Z. Wang, and S. Zhuo, "Theoretical study and experimental validation on the optical emission processes in "free" and "locked" pyrazine derivatives", *Spectrochim. Acta A*, **223**, 117296:1–7 (2019).

[128] X. Wen, D. S. Graham, D. V. Chulhai, and J. D. Goodpaster, "Absolutely localized projection-based embedding for excited states", *J. Chem. Theory Comput.*, **16**, 385–398 (2020).

[129] P. Kang, B.-L. Lin, T. A. G. Large, J. Ainsworth, E. C. Wasinger, and T. D. P. Stack, "Phenolate-bonded bis(μ-oxido)-bis-copper(II) intermediates: Hydroxylation and dehalogenation reactivities", *Faraday Discuss.*, **234**, 86–108 (2022).

[130] M. Hédouin, E. Luppi, O. W. and D. Harrowven, C. Fressigné, and I. Chataigner, "Predictive TDDFT methodology for aromatic molecules UV-vis properties: From benchmark to applications", *ChemistrySelect*, **8**, e202301943:1–8 (2023).

[131] Z. Wang, J. Liang, and M. Head-Gordon, "Earth mover's distance as a metric to evaluate the extent of charge transfer in excitations using discretized real-space densities", *J. Chem. Theory Comput.*, **19**, 7704–7714 (2023).

[132] L. Mei, J. Hu, X. Cao, F. Wang, C. Zheng, Y. Tao, X. Zhang, and W. Huang, "The inductive-effect of electron withdrawing trifluoromethyl for thermally activated delayed fluorescence: Tunable emission from tetra- to penta-carbazole in solution processed blue OLEDs", *Chem. Commun.*, **51**, 13024–13027 (2015).

[133] T. Chen, L. Zheng, J. Yuan, Z. An, R. Chen, Y. Tao, H. Li, X. Xie, and W. Huang, "Understanding the control of singlet-triplet splitting for organic exciton manipulating: A combined theoretical and experimental approach", *Sci. Rep.*, **5**, 10923:1–11 (2015).

[134] X. Cai, X. Li, G. Xie, Z. He, K. Gao, K. Liu, D. Chen, Y. Cao, and S.-J. Su, ""Rate-limited effect" of reverse intersystem crossing process: The key for tuning thermally activated delayed fluorescence lifetime and efficiency roll-off of organic light emitting diodes", *Chem. Sci.*, **7**, 4264–4275 (2016).

[135] R. Chen, Y. Tang, Y. Wan, T. Chen, C. Zheng, Y. Qi, Y. Cheng, and W. Huang, "Promoting singlet/triplet exciton transformation in organic optoelectronic molecules: Role of excited state transition configuration", *Sci. Rep.*, **7**, 6225:1–11 (2017).

[136] Y. Olivier, M. Moral, L. Muccioli, and J.-C. Sancho-García, "Dynamic nature of excited states of donor–acceptor TADF materials for OLEDs: How theory can reveal structure–property relationships", *J. Mater. Chem. C*, **5**, 5718–5729 (2017).

[137] X. Kong, L. Cai, J. Fan, and L. Lin, "Structure-property relationship of phosphine oxide based thermally activated delayed fluorescence molecules: First-principles study", *Org. Electron.*, **59**, 7–14 (2018).

[138] R. Ansari, W. Shao, S.-J. Yoon, J. Kim, and J. Kieffer, "Charge transfer as the key parameter affecting the color purity of thermally activated delayed fluorescence emitters", *ACS Appl. Mater. Interf.*, **13**, 28529–28537 (2021).

[139] S. Xu, Q. Yang, Y. Wan, R. Chen, S. Wang, Y. Si, B. Yang, D. Liu, C. Zheng, and W. Huang, "Predicting intersystem crossing efficiencies of organic molecules for efficient thermally activated delayed fluorescence", *J. Mater. Chem. C*, **7**, 95223–9530 (2019).

[140] J. Guo, J. Fan, L. Lin, J. Z. and H. Liu, C.-K. Wang, Z. Zhao, and B. Z. Tang, "Mechanical insights into aggregation-induced delayed fluorescence materials with anti-Kasha behavior", *Adv. Sci.*, **6**, 1801629:1–9 (2019).

[141] R. Dhali, D. K. A. P. Huu, F. Terenziani, C. Sissa, and A. Painelli, "Thermally activated delayed fluorescence: A critical assessment of environmental effects on the singlet–triplet energy gap", *J. Chem. Phys.*, **154**, 134112:1–9 (2021).

[142] C. Leng, S. You, Y. Si, H.-M. Qin, J. Liu, W.-Q. Huang, and K. Li, "Unraveling the mechanism of near-infrared thermally activated delayed fluorescence of TPA-based molecules: Effect of hydrogen bond steric hindrance", *J. Phys. Chem. A*, **125**, 2905–2912 (2021).

[143] H. Miranda-Salinas, Y.-T. Hung, Y.-S. Chen, D. Luo, H.-C. Kao, C.-H. Chang, K.-T. Wong, and A. Monkman, "Controlling through-space charge transfer in bridged D–D′–A TADF emitters", *J. Mater. Chem. C*, **9**, 8819–8833 (2021).

[144] C.-Y. Lin, C.-H. L. and K.-H. Kuo, M. Wang, Y. Tang, Y. Dou, B. Hu, C.-C. Wu, and K.-T. Wong, "Highly efficient blue thermally activated fluorescence emitters with a triphenylamine-based macrocyclic donor", *Adv. Opt. Mater.*, **11**, 2202292:1–10 (2022).

[145] R. Keruckiene, E. Vijaikis, C.-H. Chen, B.-Y. Lin, J.-X. Huang, C.-C. Chu, Y.-C. Dzeng, C. Chen, J.-H. Lee, T.-L. Chiu, S. M. and J. Keruckas, R. Butkute, and J. V. Grazulevicius, "Power efficiency enhancement of organic light-emitting diodes due to the favorable horizontal orientation of a naphthyridine-based thermally activated delayed fluorescence luminophore", *ACS Appl. Electron. Mater.*, **5**, 1013–1023 (2023).

[146] E. Badaeva, V. V. Albert, S. Kilina, A. K. M. Sykora, and S. Tretiak, "Effect of deprotonation on absorption and emission spectra of Ru(II)-bpy complexes functionalized with carboxyl groups", *Phys. Chem. Chem. Phys.*, **12**, 8902–8913 (2010).

[147] M. Gray and J. M. Herbert, "Comprehensive basis-set testing of extended symmetry-adapted perturbation theory and assessment of mixed-basis combinations to reduce cost", *J. Chem. Theory Comput.*, **18**, 2308–2330 (2022).

[148] M. Stener, G. Fronzoni, and M. de Simone, "Time dependent density functional theory of core electrons excitations", *Chem. Phys. Lett.*, **373**, 115–123 (2003).

[149] M. Haranczyk and M. Gutowski, "Visualization of molecular orbitals and the related electron densities", *J. Chem. Theory Comput.*, **4**, 689–693 (2008).

[150] IQmol (www.iqmol.org), accessed 2023-08-31.

[151] H. Ma, T. Qin, and A. Troisi, "Electronic excited states in amorphous MEH-PPV polymers from large-scale first principles calculations", *J. Chem. Theory Comput.*, **10**, 1272–1282 (2014).

[152] Y. Li, J. Wan, and X. Xu, "Theoretical study of the vertical excited states of benzene, pyrimidine, and pyrazine by the symmetry adapted cluster–configuration interaction method", *J. Comput. Chem.*, **28**, 1658–1667 (2007).

[153] M. Leclerc, "Polyfluorenes: Twenty years of progress", *J. Polym. Sci. A Pol. Chem.*, **39**, 2867–2873 (2001).

[154] D. Neher, "Polyfluorene homopolymers: Conjugated liquid-crystalline polymers for bright blue emission and polarized electroluminescence", *Macromol. Rapid Commun.*, **22**, 1365–1385 (2001).

[155] U. Scherf and E. J. W. List, "Semiconducting polyfluorenes—towards reliable structure–property relationships", *Adv. Mater.*, **14**, 477–487 (2002).

[156] C. D. Müller, A. Falcou, N. Reckefuss, M. Rojahn, V. Widerhirn, P. Rudati, H. Frohne, O. Nuyken, H. Becker, and K. Meerholz, "Multi-colour organic light-emitting displays by solution processing", *Nature*, **421**, 829–833 (2003).

[157] U. Scherf and D. Neher, Eds., *Polyfluorenes*, Vol. 212 of *Advances in Polymer Science*, Springer-Verlag: Berlin, 2008.

[158] L.-H. Xie, S.-H. Yang, J.-Y. Lin, M.-D. Yi, and W. Huang, "Fluorene-based macromolecular nanostructures and nanomaterials for organic (opto)electronics", *Phil. Trans. R. Soc. A*, **371**, 20120337:1–34 (2012).

[159] D. Pugh and J. O. Morley, "Molecular hyperpolarizabilities of organic materials", in *Nonlinear Optical Properties of Organic Molecules and Crystals*, D. S. Chemla and J. Zyss, Eds., Vol. 1; Academic Press, 1987; chapter II-2, pages 193–225.

[160] I. Mayer, "Identifying a pair of interacting chromophores by using SVD transformed CIS wave functions", *Chem. Phys. Lett.*, **443**, 420–425 (2007).

[161] H. Uoyama, K. Goushi, K. Shizu, H. Nomura, and C. Adachi, "Highly efficient organic light-emitting diodes from delayed fluorescence", *Nature*, **492**, 234–240 (2012).

[162] Y. Tao, K. Yuan, T. Chen, P. Xu, H. Li, R. Chen, C. Zheng, L. Zhang, and W. Huang, "Thermally activated delayed fluorescence materials towards the breakthrough of organoelectronics", *Adv. Mater.*, **26**, 7931–7958 (2014).

[163] P.-Y. Chou, H.-H. Chou, Y.-H. Chen, T.-H. Su, C.-Y. Liao, H.-W. Lin, W.-C. Lin, H.-Y. Yen, I.-C. Chen, and C.-H. Cheng, "Efficient delayed fluorescence *via* triplet–triplet annihilation for deep-blue electroluminescence", *Chem. Commun.*, **50**, 6869–6871 (2014).

[164] O. Ostroverkhova, "Organic optoelectronic materials: Mechanisms and applications", *Chem. Rev.*, **116**, 13279–13412 (2016).

[165] T. J. Penfold, F. B. Dias, and A. P. Monkman, "The theory of thermally activated delayed fluorescence for organic light emitting diodes", *Chem. Commun.*, **54**, 3926–3935 (2018).

[166] J.-H. Li, T. J. Zuehlsdorff, M. C. Payne, and N. D. M. Hine, "Identifying and tracing potential energy surfaces of electronic excitations with specific character *via* their transition origins: Application to oxirane", *Phys. Chem. Chem. Phys.*, **17**, 12065–12079 (2015).

[167] A. V. Luzanov and O. A. Zhikol, "Collectivity, shell openness indices, and complexity measures of multiconfigurational states: Computations within full CI scheme", *Int. J. Quantum Chem.*, **104**, 167–180 (2005).

[168] R. B. Woodward and R. Hoffmann, "The conservation of orbital symmetry", *Angew. Chem. Int. Ed. Engl.*, **8**, 781–853 (1969).

[169] J. Friedrichs and I. Frank, "Mechanism of electrocyclic ring-opening of diphenyloxirane: 40 years after Woodward and Hoffmann", *Angew. Chem. Int. Ed. Engl.*, **15**, 10825–10829 (2009).

[170] R. S. Mulliken, "Electronic population analysis on LCAO-MO molecular wave functions. I", *J. Chem. Phys.*, **23**, 1833–1840 (1955).

[171] S. Huzinaga and S. Narita, "Mulliken population analysis and point charge model of molecules", *Isr. J. Chem.*, **19**, 242–254 (1980).

[172] S. M. Bachrach, "Population analysis and electron densities from quantum mechanics", in *Reviews in Computational Chemistry*, K. Lipkowitz and D. B. Boyd, Eds., Vol. 5; Wiley-VCH: Hoboken, 1994; chapter 3, pages 171–228.

[173] A. V. Luzanov, "The structure of the electronic excitation of molecules in quantum-chemical models", *Russ. Chem. Rev.*, **49**, 1033–1048 (1980).

[174] A. V. Luzanov, "Analysis of the exciton states of polyconjugated systems by the transition density matrix method", *J. Struct. Chem.*, **43**, 711–720 (2002).

[175] A. V. Luzanov and O. A. Zhikol, "Excited state structural analysis: TDDFT and related models", in *Practical Aspects of Computational Chemistry I: An Overview of the Last Two Decades of Current Trends*, J. Leszczynski and M. K. Shukla, Eds.; Springer Science + Business Media, 2012; chapter 14, pages 415–449.

[176] D. R. Maurice, *Single Electron Theories of Excited States*, PhD thesis, University of California, Berkeley, CA (1998).

[177] A. F. Morrison, E. Epifanovsky, and J. M. Herbert, "Double-buffered, heterogeneous CPU + GPU integral digestion algorithm for single-excitation calculations involving a large number of excited states", *J. Comput. Chem.*, **39**, 2173–2182 (2018).

[178] L. Czuchajowski and A. K. Wisor, "Electronic effects in multibridged cyclophanes as viewed by the indices of excitation", *J. Electron Spectrosc.*, **43**, 169–181 (1987).

[179] L. Czuchajowski and A. K. Wisor, "Electronic structure of multilayered and multistepped cyclophanes", *J. Mol. Struct. (Theochem)*, **165**, 163–174 (1988).

[180] M. Reinhardt, K. Kirschke, and H. Baumann, "UV-VIS spectra of some 3-arylazopropenoic acid esters", *J. Mol. Spectrosc.*, **348**, 417–420 (1995).

[181] V. G. Mitina, V. V. Ivanov, O. A. Ponomarev, L. A. Sieta, and V. M. Shershukov, "Nature of electronic transitions in *N*-phenyl-1,8-naphthalimide and some of its derivatives", *Mol. Eng.*, **6**, 249–259 (1996).

[182] A. O. Doroshenko, A. V. Kirichenko, V. G. Mitina, and O. A. Ponomaryov, "Spectral properties and dynamics of the excited state structural relaxation of the ortho analogues of POPOP—Effective abnormally large Stokes shift luminophores", *J. Photochem. Photobiol. A*, **94**, 15–26.

[183] A. O. Doroshenko, E. A. Posokhov, A. A. Verezubova, and L. M. Ptyagina, "Excited state intramolecular proton transfer reaction and luminescent properties of the *ortho*-hydroxy derivatives of 2,5-diphenyl-1,3,4-oxadiazole", *J. Phys. Org. Chem.*, **13**, 253–265 (2000).

[184] A. O. Doroshenko, E. A. Posokhov, A. A. Verezubova, L. M. Ptyagina, V. T. Skripkina, and V. M. Shershukov, "Radiationless deactivation of the excited phototautomer form and molecular structure of ESIPT-compounds", *Photochem. Photobiol. Sci.*, **1**, 92–99 (2002).

[185] E. Titov, "On the low-lying electronically excited states of azobenzene dimers: Transition density matrix analysis", *Molecules*, **26**, 4245:1–24 (2021). Erratum: *ibid.* **28**, 1370 (2023).

[186] F. Plasser and H. Lischka, "Analysis of excitonic and charge transfer interactions from quantum chemical calculations", *J. Chem. Theory Comput.*, **8**, 2777–2789 (2012).

[187] I. Mayer, "Charge, bond order and valence in the ab initio SCF theory", *Chem. Phys. Lett.*, **97**, 270–274 (1983).

[188] I. Mayer, "Bond orders and valences from ab initio wave functions", *Int. J. Quantum Chem.*, **29**, 477–483 (1986).

[189] A. A. Voityuk, "Fragment transition density method to calculate electronic coupling for excitattion energy transfer", *J. Chem. Phys.*, **140**, 244117:1–7 (2014).

[190] L. Blancafort and A. A. Voityuk, "Exciton delocalization, charge transfer, and electronic coupling for singlet excitation energy transfer between stacked nucleobases in DNA: An MS-CASPT2 study", *J. Chem. Phys.*, **140**, 095102:1–8 (2014).

[191] D. Mester and M. Kállay, "Charge-transfer excitations within density functional theory: How accurate are the most recommended approaches?", *J. Chem. Theory Comput.*, **18**, 1646–1662 (2022).

[192] P.-O. Löwdin, "Quantum theory of cohesive properties of solids", *Adv. Phys.*, **5**, 1–171 (1956).

[193] B. C. Carlson and J. M. Keller, "Orthogonalization procedures and the localization of Wannier functions", *Phys. Rev.*, **105**, 102–103 (1957).

[194] I. Mayer, "On Löwdin's method of symmetric orthogonalization", *Int. J. Quantum Chem.*, **90**, 63–65 (2002).

[195] F. Plasser, "TheoDORE: A toolbox for a detailed and automated analysis of electronic excited state computations", *J. Chem. Phys.*, **152**, 084108:1–14 (2020).

[196] M. Orchin and H. H. Jaffé, *Symmetry, Orbitals, and Spectra*, Wiley, 1971.

[197] K. Rotkiewicz, K. H. Grellmann, and Z. R. Grabowski, "Reinterpretation of the anomalous fluorescence of *p*-N,N-dimethylamino-benzonitrile", *Chem. Phys. Lett.*, **19**, 315–318 (1973).

[198] W. Rettig, G. Wermuth, and E. Lippert, "Photophysical primary processes in solutions of p-substituted dialkylanilines", *Ber. Bunsenges. Phys. Chem.*, **83**, 692–697 (1979).

[199] J. R. Platt, "Classification of spectra of cata-condensed hydrocarbons", *J. Chem. Phys.*, **17**, 484–495 (1949).

[200] W. Moffitt, "The electronic spectra of cata-condensed hydrocarbons", *J. Chem. Phys.*, **22**, 320–333 (1954).

[201] W. Moffitt, "Configurational interaction in simple molecular orbital theory", *J. Chem. Phys.*, **22**, 1820–1829 (1954).

[202] T. Handa, "The interpretation of absorption spectra of condensed polycyclic aromatic hydrocarbons by using a simple resonance theory. I. The resonance structure of the excited state in correlation with Platt's theory", *Bull. Chem. Soc. Jpn.*, **36**, 235–247 (1963).

[203] P. R. Callis, "Transition density topology of the L_a and L_b states in indoles and purines", *Int. J. Quantum Chem. Symp.*, **18**, 579–588 (1984).

[204] M. Parac and S. Grimme, "A TDDFT study of the lowest excitation energies of polycyclic aromatic hydrocarbons", *Chem. Phys.*, **292**, 11–21 (2003).

[205] S. Grimme and M. Parac, "Substantial errors from time-dependent density functional theory for the calculation of excited states of large π systems", *ChemPhysChem*, **4**, 292–295 (2003).

[206] D. Rappoport and F. Furche, "Photoinduced intramolecular charge transfer in 4-(dimethyl)aminobenzonitrile—a theoretical perspective", *J. Am. Chem. Soc.*, **126**, 1277–1284 (2004).

[207] Z. R. Grabowski, K. Rotkiewicz, and W. Rettig, "Structural changes accompanying intramolecular electron transfer: Focus on twisted intramolecular charge-transfer states and structures", *Chem. Rev.*, **103**, 3899–4032 (2003).

[208] T. Atsbeha, A. M. Mohammed, and M. Redi-Abshiro, "Excitation wavelength dependence of dual fluorescence of DMABN in polar solvents", *J. Fluoresc.*, **20**, 1241–1248 (2010).

[209] J. Catalán, "On the dual emission of *p*-dimethylaminobenzonitrile and its photophysical implications", *Phys. Chem. Chem. Phys.*, **15**, 8811–8820 (2013).

[210] D. R. Kanis, M. A. Ratner, and T. J. Marks, "Design and construction of molecular assemblies with large second-order optical nonlinearities. Quantum chemical aspects", *Chem. Rev.*, **94**, 195–242 (1994).

[211] G. García, C. Adamo, and I. Ciofini, "Evaluating push–pull dye efficiciency using TD-DFT and charge transfer indices", *Phys. Chem. Chem. Phys.*, **15**, 20210–20219 (2013).

[212] D. Pines, E. Pines, T. W. J. Steele, and V. Papper, "Dual fluorescence phenomenon in 'push-pull' stilbenes", in *Reviews in Fluorescence 2015*, C. D. Geddes, Ed.; Springer, 2016; chapter 13, pages 337–352.

[213] H. Imahori, T. Umeyama, and S. Ito, "Large π-aromatic molecules as potential sensitizers for highly efficient dye-sensitized solar cells", *Acc. Chem. Res.*, **42**, 1809–1818 (2009).

[214] C. Duan, F. Huang, and Y. Cao, "Recent development of push-pull conjugated polymers for bulk-heterojunction photovoltaics: Rational design and fine tailoring of molecular structure", *J. Mater. Chem.*, **22**, 10416–10434 (2012).

[215] L.-L. Li and E. W.-G. Diau, "Porphyrin-sensitized solar cells", *Chem. Soc. Rev.*, **42**, 291–304 (2013).

[216] R. C. Jemison and R. D. McCullough, "Techniques for the molecular design of push-pull polymers towards enhanced organic photovoltaic performance", in *Polymer Composites for Energy Harvesting, Conversion, and Storage*, L. Li, W. Wong-Ng, and J. Sharp, Eds., Vol. 1161 of *ACS Symposium Series;* American Chemical Society, 2014; chapter 4, pages 71–109.

[217] L. Beverina and G. A. Pagani, "π-conjugated zwitterions as paradigm of donor-acceptor building blocks in organic-based materials", *Acc. Chem. Res.*, **47**, 319–329 (2014).

[218] V. Malytskyi, J.-J. Simon, L. Patrone, and J.-M. Raimundo, "Thiophene-based push-pull chromophores for small molecule organic solar cells (SMOSCs)", *RSC Adv.*, **5**, 354–397 (2015).

[219] Z. Parsa, S. S. Naghavi, and S. N. Shahab, "Designing push-pull porphyrins for efficient dye-sensitized solar cells", *J. Phys. Chem. A*, **122**, 5870–5877 (2018).

[220] A. Torres, L. R. Prado, G. Bortolini, and L. G. C. Rego, "Charge transfer driven structural relaxation in a push–pull azobenzene dye–semiconductor complex", *J. Phys. Chem. Lett.*, **9**, 5926–5933 (2018).

[221] I. Ciofini, T. Le Bahers, C. Adamo, F. Odobel, and D. Jacquemin, "Through-space charge transfer in rod-like molecules: Lessons from theory", *J. Phys. Chem. C*, **116**, 11946–11955 (2012).

[222] M. P. Balanay and D. H. Kim, "Strategic design of bacteriochlorins as possible dyes for photovoltaic applications", *J. Phys. Chem. A*, **121**, 6660–6669 (2017).

[223] S. Hadsadee, R. Rattanawan, R. Tarsang, N. Kungwan, and S. Jungsuttiwong, "Push-pull *N*-annulated perylene-based sensitizers for dye-sensitized solar cells: Theoretical property tuning by DFT/TDDFT", *ChemistrySelect*, **2**, 9829–9837 (2017).

[224] S. S. Madugula and S. Yarasi, "Molecular design of porphyrin dyes for dye sensitized solar cells: A quantitative structure property relationship study", *Int. J. Quantum Chem.*, **117**, e25385:1–13 (2017).

[225] B. Basheer, T. M. Robert, K. P. Vijayalakshmi, and D. Mathew, "Solar cells sensitized by push-pull azo dyes: Dependence of photovoltaic performance on electronic structure, geometry and conformation of the sensitizer", *Int. J. Amb. Energy*, **39**, 433–440 (2018).

[226] F. Castet, V. Rodriguez, J.-L. Pozzo, L. Ducasse, A. Plaquet, and B. Champagne, "Design and characterization of molecular nonlinear optical switches", *Acc. Chem. Res.*, **46**, 2656–2665 (2013).

[227] M. Kivala and F. Diedrich, "Acetylene-derived strong organic acceptors for planar and nonplanar push–pull chromophores", *Acc. Chem. Res.*, **42**, 235–248 (2009).

[228] G. N. Lipunova, E. V. Nosova, V. N. Charushin, and O. N. Chupakhin, "Functionalized quinazolines and pyrimidines for optoelectronic materials", *Curr. Org. Synth.*, **15**, 793–814 (2018).

[229] Y. Olivier, J.-C. Sancho-García, L. Muccioli, G. D'Avino, and D. Beljonne, "Computational design of thermally activated delayed fluorescence materials: The challenges ahead", *J. Phys. Chem. Lett.*, **9**, 6149–6163 (2018).

[230] M. Kasha, "Characterization of electronic transitions in complex molecules", *Discuss. Faraday Soc.*, **9**, 14–19 (1950).

[231] G. Brancato, G. Signore, P. Neyroz, D. Polli, G. Cerullo, G. Abbandonato, L. Nucara, V. Barone, F. Beltram, and R. Bizzarri, "Dual fluorescence through Kasha's rule breaking: An unconventional photomechanism for intracellular probe design", *J. Phys. Chem. B*, **119**, 6144–6154 (2015).

[232] A. P. Demchenko, V. I. Tomin, and P.-T. Chou, "Breaking the Kasha rule for more efficient photochemistry", *Chem. Rev.*, **117**, 13353–13381 (2017).

[233] Z. R. Grabowski and J. Dobkowski, "Twisted intramolecular charge transfer (TICT) states: Energy and molecular structure", *Pure Appl. Chem.*, **55**, 245–252 (1983).

[234] Z. R. Grabowski, "Electron transfer and the structural changes in the excited state", *Pure Appl. Chem.*, **64**, 1249–1255 (1992).

[235] N. Ghoneim and P. Suppan, "Solvation of TICT* states in solvent mixtures", *Pure Appl. Chem.*, **65**, 1739–1743 (1993).

[236] M. Hashimoto and H. Hamaguchi, "Structure of the twisted-intramolecular-charge-transfer excited singlet and triplet states of 4-(dimethylamino)benzonitrile as studied by nanosecond time-resolved infrared spectroscopy", *J. Phys. Chem.*, **99**, 7875–7877 (1995).

[237] L. Serrano-Andrés, M. Merchán, B. O. Roos, and R. Lindh, "Theoretical study of the internal charge transfer in aminobenzonitriles", *J. Am. Chem. Soc.*, **117**, 3189–3204 (1995).

[238] J. Dobkowski, J. Wójcik, W. Koźmiński, R. Kołos, J. Waluk, and J. Michl, "An experimental test of C–N bond twisting in the TICT state: Syn–anti photoisomerization in 2-(*N*-methyl-*N*-isopropylamino)-5-cyanopyridine", *J. Am. Chem. Soc.*, **124**, 2406–2407 (2002).

[239] W. Zhang, Z. Lan, Z. Sun, and K. J. Gaffney, "Resolving photo-induced twisted intramolecular charge transfer with vibrational anisotropy and TDDFT", *J. Phys. Chem. B*, **116**, 11527–11536 (2012).

[240] H. Li, J. Han, H. Zhao, X. Liu, Y. Luo, Y. Shi, C. Liu, M. Jin, and D. Ding, "Lighting up the invisible twisted intramolecular charge transfer state by high pressure", *J. Phys. Chem. Lett.*, **10**, 748–753 (2019).

[241] M. A. Kochman and B. Durbeej, "Simulating the nonadiabatic relaxation dynamics of 4-(*N*,*N*-dimethylamino)benzonitrile (DMABN) in polar solution", *J. Phys. Chem. A*, **124**, 2193–2206 (2020).

[242] K. A. Zachariasse, T. von der Haar, A. Hebecker, U. Leinhos, and W. Kühnle, "Intramolecular charge transfer in amino-benzonitriles: Requirements for dual fluorescence", *Pure Appl. Chem.*, **65**, 1745–1750 (1993).

[243] K. A. Zachariasse, M. Grobys, T. von der Haar, A. Hebecker, Y. V. Il'ichev, Y.-B. Jiang, O. Morawski, and W. Kühnle, "Intramolecular charge transfer in the excited state. Kinetics and configurational changes", *J. Photochem. Photobiol. A*, **102**, 59–70 (1996).

[244] K. A. Zachariasse, M. Grobys, T. von der Haar, A. Hebecker, Y. V. Il'ichev, O. Morawski, I. Rückert, and W. Kühnle, "Photoinduced intramolecular charge transfer and internal conversion in molecules with a small energy gap between S_1 and S_2. Dynamics and structure", *J. Photochem. Photobiol. A*, **105**, 373–383 (1997).

[245] M. Z. Zgierski, T. Fujiwara, and E. C. Lim, "Non-adiabatic photoprocesses of fundamental importance to chemistry: From electronic relaxation of DNA bases to intramolecular charge transfer in electron donor-acceptor molecules", in *Radiation Induced Molecular Phenomena in Nucleic Acids*, M. K. Shukla and J. Leszczynski, Eds., Vol. 5 of *Challenges and Advances in Computational Chemistry and Physics;* Springer Science+Business Media, 2008; chapter 15, pages 395–433.

[246] T. Gustavsson, P. B. Coto, L. Serrano-Andrés, T. Fujiwara, and E. C. Lim, "Do fluorescence and transient absorption probe the same intramolecular charge transfer state of 4-(dimethylamino)benzonitrile?", *J. Chem. Phys.*, **131**, 031101:1–4 (2009).

[247] T. Fujiwara, M. Z. Zgierski, and E. C. Lim, "The role of the $\pi\sigma^*$ state in intramolecular charge transfer of 4-(dimethylamino)benzonitrile", *Phys. Chem. Chem. Phys.*, **13**, 6779–6783 (2011).

[248] A. Perveaux, P. J. Castro, D. Lauvergnat, M. Reguero, and B. Lasorne, "Intramolecular charge transfer in 4-aminobenzonitrile does not need the twist and may not need the bend", *J. Phys. Chem. Lett.*, **6**, 1316–1320 (2015).

[249] B. F. E. Curchod, A. Sisto, and T. J. Martínez, "Ab initio multiple spawning photochemical dynamics of DMABN using GPUs", *J. Phys. Chem. A*, **121**, 265–276 (2017).

[250] J.-S. Yang, K.-L. Liau, C.-M. Wang, and C.-Y. Hwang, "Substituent-dependent photoinduced intramolecular charge transfer in *N*-aryl-substituted *trans*-4-aminostilbenes", *J. Am. Chem. Soc.*, **126**, 12325–12335 (2004).

[251] T. Fujiwara, C. Reichardt, R. A. Vogt, C. E. Crespo-Hernández, M. Z. Zgierski, and E. C. Lim, "Electronic spectra and excited-state dynamics of 4-fluoro-*N*,*N*-dimethylaniline", *Chem. Phys. Lett.*, **586**, 70–75 (2013).

[252] K. A. Zachariasse, A. Demeter, and S. I. Druzhinin, "Absence of intramolecular charge transfer with 4-fluoro-*N*,*N*-dimethylaniline (DMA4F), contrary to an experimental report supported by computations", *J. Phys. Chem. A*, **121**, 1223–1232 (2017).

[253] M. V. Bohnwagner and A. Dreuw, "Regular fluorescence of 4-fluoro-*N*,*N*-dimethylaniline: No charge transfer and no twisting", *J. Phys. Chem. A*, **121**, 5834–5841 (2017).

[254] M. Kasha, H. R. Rawls, and M. A. El-Bayoumi, "The exciton model in molecular spectroscopy", *Pure Appl. Chem.*, **11**, 371–392 (1965).

[255] J. B. Birks, "Excimers", *Rep. Prog. Phys.*, **38**, 903–974 (1975).

[256] S. J. Jang and B. Mennucci, "Delocalized excitons in natural light harvesting complexes", *Rev. Mod. Phys.*, **90**, 035003:1–49 (2018).

[257] S. J. Jang, *Dynamics of Molecular Excitons*, Elsevier: Amsterdam, 2020.

[258] F. C. Spano and C. Silva, "H- and J-aggregate behavior in polymeric semiconductors", *Annu. Rev. Phys. Chem.*, **65**, 477–500 (2014).

[259] B. Alam, A. F. Morrison, and J. M. Herbert, "Charge separation and charge transfer in the low-lying excited states of pentacene", *J. Phys. Chem. C*, **124**, 24653–24666 (2020).

[260] B. Alam, H. Jiang, P. M. Zimmerman, and J. M. Herbert, "State-specific solvation for restricted active space spin-flip (RAS-SF) wave functions based on the polarizable continuum formalism", *J. Chem. Phys.*, **156**, 194110:1–13 (2022).

[261] A. K. Chandra and E. C. Lim, "Semiempirical theory of excimer luminescence", *J. Chem. Phys.*, **48**, 2589–2595 (1968).

[262] A. K. Chandra and E. C. Lim, "Semiempirical theory of excimer luminescence. II. Comparison with previous theories and consideration of the transition probability and the stability of the excimer triplet state", *J. Chem. Phys.*, **49**, 5066–5072 (1968).

[263] A. L. L. East and E. C. Lim, "Naphthalene dimer: Electronic states, excimers, and triplet decay", *J. Chem. Phys.*, **113**, 8981–8994 (2000).

[264] R. Improta and V. Barone, "Interplay between "neutral" and "charge-transfer" excimers rules the excited state decay in adenine-rich polynucleotides", *Angew. Chem. Int. Ed. Engl.*, **50**, 12016–12019 (2011).

[265] F. Plasser, A. J. A. Aquino, W. L. Hase, and H. Lischka, "UV absorption spectrum of alternating DNA duplexes. Analysis of excitonic and charge transfer interactions", *J. Phys. Chem. A*, **116**, 11151–11160 (2012).

[266] V. A. Spata, W. Lee, and S. Matsika, "Excimers and exciplexes in photoiniated processes of oligonucleotides", *J. Phys. Chem. Lett.*, **7**, 976–984 (2016).

[267] J. Eisinger, M. Guéron, R. G. Shulman, and T. Yamane, "Excimer fluorescence of dinucleotides, polynucleotides, and DNA", *Proc. Natl. Acad. Sci. USA*, **55**, 1015–1020 (1966).

[268] M. Guéron, R. G. Shulman, and J. Eisinger, "Energy transfer in dinucleotides", *Proc. Natl. Acad. Sci. USA*, **56**, 814–818 (1966).

[269] J. Eisinger and R. G. Shulman, "Excited electronic states of DNA", *Science*, **161**, 1311–1319 (1968).

[270] C. T. Middleton, K. de La Harpe, C. Su, Y. K. Law, C. E. Crespo-Hernández, and B. Kohler, "DNA excited-state dynamics: From single bases to the double helix", *Annu. Rev. Phys. Chem.*, **60**, 217–239 (2009).

[271] B. Kohler, "Nonradiative decay mechanisms in DNA model systems", *J. Phys. Chem. Lett.*, **1**, 2047–2053 (2010).

[272] J. Chen, Y. Zhang, and B. Kohler, "Excited states in DNA strands investigated by ultrafast laser spectroscopy", in *Photoinduced Phenomena in Nucleic Acids II*, Vol. 356 of *Topics in Current Chemistry;* Springer, 2015; pages 39–87.

[273] S. Sharifzadeh, P. Darancet, L. Kronik, and J. B. Neaton, "Low-energy charge-transfer excitons in organic solids from first-principles: The case of pentacene", *J. Phys. Chem. Lett.*, **4**, 2197–2201 (2013).

[274] S. Sharifzadeh, C. Y. Wong, H. Wu, B. L. Cotts, L. Kronik, N. S. Ginsberg, and J. B. Neaton, "Relating the physical structure and optoelectronic function of crystalline TIPS-pentacene", *Adv. Funct. Mater.*, **25**, 2038–2046 (2015).

[275] T. C. Berkelbach, M. S. Hybertsen, and D. R. Reichman, "Microscopic theory of singlet exciton fission. II. Application to pentacene dimers and the role of superexchange", *J. Chem. Phys.*, **138**, 114103:1–12 (2013).

[276] T. C. Berkelbach, M. S. Hybertsen, and D. R. Reichman, "Microscopic theory of singlet exciton fission. III. Crystalline pentacene", *J. Chem. Phys.*, **141**, 074705:1–12 (2014).

[277] N. Monahan and X.-Y. Zhu, "Charge transfer–mediated singlet fission", *Annu. Rev. Phys. Chem.*, **66**, 601–618 (2015).

[278] M. B. Smith and J. Michl, "Singlet fission", *Chem. Rev.*, **110**, 6891–6936 (2010).

[279] M. B. Smith and J. Michl, "Recent advances in singlet fission", *Annu. Rev. Phys. Chem.*, **64**, 361–386 (2013).

[280] T. C. Berkelbach, "Electronic structure and dynamics of singlet fission in organic molecules and crystals", *Adv. Chem. Phys.*, **162**, 1–38 (2017).

[281] A. Japahuge and T. Zeng, "Theoretical studies of singlet fission: Searching for materials and exploring mechanisms", *ChemPlusChem*, **83**, 146–182 (2018).

[282] D. Casanova, "Theoretical modeling of singlet fission", *Chem. Rev.*, **118**, 7164–7207 (2018).

[283] S. W. Eaton, L. E. Shoer, S. D. Karlen, S. M. Dyar, E. A. Margulies, B. S. Veldkamp, C. Ramanan, D. A. Hartzler, S. Savikhin, T. J. Marks, and M. R. Wasielewski, "Singlet exciton fission in polycrystalline thin films of a slip-stacked perylenediimide", *J. Am. Chem. Soc.*, **135**, 14701–14712 (2013).

[284] A. K. Le, J. A. Bender, and S. T. Roberts, "Slow singlet fission observed in a polycrystalline perylenediimide thin film", *J. Phys. Chem. Lett.*, **7**, 4922–4928 (2016).

[285] A. M. Alvertis, S. Lukman, T. J. H. Hele, E. G. Fuemmeler, J. Feng, J. Wu, N. C. Greenham, A. W. Chin, and A. J. Musser, "Switching between coherent and incoherent singlet fission via solvent-induced symmetry breaking", *J. Am. Chem. Soc.*, **141**, 17558–17570 (2019).

[286] I. Papadopoulos, M. J. Álvaro-Martins, D. Molina, P. M. McCosker, P. A. Keller, T. Clark, A. Sastre-Santos, and D. M. Guldi, "Solvent-dependent singlet fission in diketopyrrolopyrrole dimers: A mediating charge trasnfer versus a trapping symmetry-breaking charge separation", *Adv. Energy Mater.*, **10**, 2001496:1–11 (2020).

[287] A. V. Luzanov, D. Casanova, X. Feng, and A. I. Krylov, "Quantifying charge resonance and multiexciton character in coupled chromophores by charge and spin cumulant analysis", *J. Chem. Phys.*, **142**, 224104:1–16 (2015).

[288] S. A. Bäppler, F. Plasser, M. Wormit, and A. Dreuw, "Exciton analysis of many-body wave functions: Bridging the gap between the quasiparticle and molecular orbital pictures", *Phys. Rev. A*, **90**, 052521:1–12 (2014).

[289] R. J. Bell, "The dynamics of disordered lattices", *Rep. Prog. Phys.*, **35**, 1315–1409 (1972).

[290] D. J. Thouless, "Electrons in disordered systems and the theory of localization", *Phys. Rep.*, **13**, 93–142 (1974).

[291] B. Kramer and A. MacKinnon, "Localization: Theory and experiment", *Rep. Prog. Phys.*, **56**, 1469–1564 (1993).

[292] S. Tretiak and S. Mukamel, "Density matrix analysis and simulation of electronic excitations in conjugated and aggregated molecules", *Chem. Rev.*, **102**, 3171–3212 (2002).

[293] T. Meier, Y. Zhao, V. Chernyak, and S. Mukamel, "Polarons, localization, and excitonic coherence in superradiance of biological antenna complexes", *J. Chem. Phys.*, **107**, 3876–3893 (1997).

[294] S. Mukamel, S. Tretiak, T. Wagersreiter, and V. Chernyak, "Electronic coherence and collective optical excitations of conjugated molecules", *Science*, **277**, 781–787 (1997).

[295] A. Ishizaki and G. R. Fleming, "Quantum superpositions in photosynthetic light harvesting: Delocalization and entanglement", *New J. Phys.*, **12**, 055004:1–14 (2010).

[296] W. Barford and M. Marcus, "Theory of optical transitions in conjugated polymers. I. Ideal systems", *J. Chem. Phys.*, **141**, 164101:1–13 (2014).

[297] W. Barford and O. R. Tozer, "Theory of exciton transfer and diffusion in conjugated polymers", *J. Chem. Phys.*, **141**, 164103:1–14 (2014).

[298] B. Rice, A. A. Y. Guilbert, J. M. Frost, and J. Nelson, "Polaron states in fullerene adducts modeled by coarse-grained molecular dynamics and tight binding", *J. Phys. Chem. Lett.*, **9**, 6616–6623 (2018).

[299] R. J. Bell and P. Dean, "Atomic vibrations in vitreous silica", *Discuss. Faraday Soc.*, **50**, 55–61 (1970).

[300] J. T. Edwards and D. J. Thouless, "Numerical studies of localization in disordered systems", *J. Phys. C: Solid State*, **5**, 807–820 (1972).

[301] F. Wegner, "Inverse participation ratio in $2 + \varepsilon$ dimensions", *Z. Phys. B*, **36**, 209–214 (1980).

[302] A. M. M. Pruisken, "Participation ratio in the nonlinear σ-model representation of localization", *Phys. Rev. B*, **31**, 416–419 (1985).

[303] G. D. Scholes and C. Smyth, "Perspective: Detecting and measuring exciton delocalization in photosynthetic light harvesting", *J. Chem. Phys.*, **140**, 110901:1–8 (2014).

[304] R. Pastor-Satorras and C. Castellano, "Distinct types of eigenvector localization in networks", *Sci. Rep.*, **6**, 18847:1–9 (2016).

[305] M. Cho, G. R. Fleming, S. Saito, I. Ohmine, and R. M. Stratt, "Instantaneous normal mode analysis of liquid water", *J. Chem. Phys.*, **100**, 6672–6683 (1994).

[306] J. M. Herbert and J. E. Harriman, "Comparison of two-electron densities reconstructed from one-electron density matrices", *Int. J. Quantum Chem.*, **90**, 355–369 (2002).

[307] M. Marcus, O. R. Tozer, and W. Barford, "Theory of optical transitions in conjugated polymers. II. Real systems", *J. Chem. Phys.*, **141**, 164102:1–14 (2014).

[308] J. H. Burroughes, D. D. C. Bradley, A. R. Brown, R. N. Marks, K. Mackay, R. H. Friend, P. L. Burns, and A. B. Holmes, "Light-emitting diodes based on conjugated polymers", *Nature*, **347**, 539–541 (1990).

[309] G. Grem, G. Leditzky, B. Ullrich, and G. Leising, "Realization of a blue-light-emitting device using poly(*p*-phenylene)", *Adv. Mater.*, **4**, 36–37 (1992).

[310] D. D. C. Bradley, "Conjugated polymer electroluminescence", *Synthetic Met.*, **54**, 401–415 (1993).

[311] S. Karg, W. Riess, V. Dyakonov, and M. Schwoerer, "Electrical and optical characterization of poly(phenylene-vinylene) light emitting diodes", *Synthetic Met.*, **54**, 427–433 (1993).

[312] W. Barford and N. Paiboonvorachat, "Excitons in conjugated polymers: Wavefunctions, symmetries, and quantum numbers", *J. Chem. Phys.*, **129**, 164716:1–10 (2008).

[313] N. Kirova, "Understanding excitons in optically active polymers", *Poly. Int.*, **57**, 678–688 (2008).

[314] M. Rohlfing and S. G. Louie, "Electron-hole excitations and optical spectra from first principles", *Phys. Rev. B*, **62**, 4927–4944 (2000).

[315] S. Sharifzadeh, "Many-body perturbation theory for understanding optical excitations in organic molecules and solids", *J. Phys.: Condens. Matt.*, **30**, 153002:1–12 (2018).

[316] S. Tretiak, V. Chernyak, and S. Mukamel, "Two-dimensional real-space analysis of optical excitations in acceptor-substituted carotenoids", *J. Am. Chem. Soc.*, **119**, 11408–11419 (1997).

[317] S. Tretiak, K. Igumenshchev, and V. Chernyak, "Exciton sizes of conducting polymers predicted by time-dependent density functional theory", *Phys. Rev. B*, **71**, 033201:1–4 (2005).

[318] K. I. Igumenshchev, S. Tretiak, and V. Y. Chernyak, "Excitonic effects in a time-dependent density functional theory", *J. Chem. Phys.*, **127**, 114902:1–9 (2007).

[319] E. Zojer, P. Buchacher, F. Wudl, J. Cornil, J. P. Calbert, J. L. Brédas, and G. Leising, "Excited state localization in organic molecules consisting of conjugated and nonconjugated segments", *J. Chem. Phys.*, **113**, 10002–10012 (2000).

[320] J. Rissler, H. Bässler, F. Gebhard, and P. Schwerdtfeger, "Excited states of ladder-type poly-*p*-phenylene oligomers", *Phys. Rev. B*, **64**, 045122:1–11 (2001).

[321] J. Rissler, "Effective conjugation length of π-conjugated systems", *Chem. Phys. Lett.*, **395**, 92–96 (2004).

[322] L. Romaner, G. Heimel, H. Wiesenhofer, P. Scandiucci de Freitas, U. Scherf, J.-L. Brédas, E. Zojer, and E. J. W. List, "Ketonic defects in ladder-type poly(*p*-phenylene)s", *Chem. Mater.*, **16**, 4667–4674 (2004).

[323] E. Hennebicq, C. Deleener, J.-L. Brédas, G. D. Scholes, and D. Beljonne, "Chromophores in phenylenevinylene-based conjugated polymers: Role of conformational kinks and chemical defects", *J. Chem. Phys.*, **125**, 054901:1–16 (2006).

[324] S. A. Mewes, F. Plasser, A. Krylov, and A. Dreuw, "Benchmarking excited-state calculations using exciton properties", *J. Chem. Theory Comput.*, **14**, 710–725 (2018).

[325] S. A. Mewes, F. Plasser, and A. Dreuw, "Communication: Exciton analysis in time-dependent density functional theory: How functionals shape excited-state characters", *J. Chem. Phys.*, **143**, 171101:1–5 (2015).

[326] S. A. Mewes, J.-M. Mewes, A. Dreuw, and F. Plasser, "Excitons in poly(*para* phenylene vinylene): A quantum-chemical perspective based on high-level *ab initio* calculations", *Phys. Chem. Chem. Phys.*, **18**, 2548–2563 (2016).

[327] S. A. Mewes, F. Plasser, and A. Dreuw, "Universal exciton size in organic polymers is determined by nonlocal orbital exchange in time-dependent density functional theory", *J. Phys. Chem. Lett.*, **8**, 1205–1210 (2017).

[328] X. Feng, A. V. Luzanov, and A. I. Krylov, "Fission of entangled spins: An electronic structure perspective", *J. Phys. Chem. Lett.*, **4**, 3845–3852 (2013).

[329] S. Matsika, X. Feng, A. V. Luzanov, and A. I. Krylov, "What we can learn from the norms of one-particle density matrices, and what we can't: Some results for interstate properties in model singlet fission systems", *J. Phys. Chem. A*, **118**, 11943–11955 (2014).

[330] N. Mardirossian and M. Head-Gordon, "ωB97X-V: A 10-parameter, range-separated hybrid, generalized gradient approximation density functional with nonlocal correlation, designed by a survival-of-the-fittest strategy", *Phys. Chem. Chem. Phys.*, **16**, 9904–9924 (2014).

[331] L. Kronik and S. Kümmel, "Dielectric screening meets optimally tuned density functionals", *Adv. Mater.*, **30**, 1706560:1–14 (2018).

[332] S. Tretiak, V. Chernyak, and S. Mukamel, "Localized electronic excitations in phenylacetylene dendrimers", *J. Phys. Chem. B*, **102**, 3310–3315 (1998).

[333] G. C. Bazan, W. J. Oldham, Jr., R. J. Lachicotte, S. Tretiak, V. Chernyak, and S. Mukamel, "Stilbenoid dimers: Dissection of a paracyclophane chromophore", *J. Am. Chem. Soc.*, **120**, 9188–9204 (1998).

[334] B. M. Wong, "Optoelectronic properties of carbon nanorings: Excitonic effects from time-dependent density functional theory", *J. Phys. Chem. C*, **113**, 21921–21927 (2009).

[335] J.-L. Jin, H.-B. Li, Y. Geng, Y. Wu, Y.-A. Duan, and Z.-M. Su, "Theoretical insight into the origin of large Stokes shift and photophysical properties of anilido-pyridine boron difluoride dyes", *ChemPhysChem*, **13**, 3714–3722 (2012).

[336] T. Le Bahers, C. Adamo, and I. Ciofini, "A qualitative index of spatial extent in charge-transfer excitations", *J. Chem. Theory Comput.*, **7**, 2498–2506 (2011).

[337] P. M. Zimmerman, C. B. Musgrave, and M. Head-Gordon, "A correlated electron view of singlet fission", *Acc. Chem. Res.*, **46**, 1339–1347 (2013).

[338] A. F. Morrison and J. M. Herbert, "Evidence for singlet fission driven by vibronic coherence in crystalline tetracene", *J. Phys. Chem. Lett.*, **8**, 1442–1448 (2017).

[339] H. Kim and P. M. Zimmerman, "Coupled double triplet state in singlet fission", *Phys. Chem. Chem. Phys.*, **20**, 30083–30094 (2018).

[340] M. J. Y. Tayebjee, A. A. Gray-Weale, and T. W. Schmidt, "Thermodynamic limit of exciton fission solar cell efficiency", *J. Phys. Chem. Lett.*, **3**, 2749–2754 (2012).

[341] M. J. Y. Tayebjee, D. R. McCamey, and T. W. Schmidt, "Beyond Shockley–Queisser: Molecular approaches to high-efficiency photovoltaics", *J. Phys. Chem. Lett.*, **6**, 2367–2378 (2015).

[342] W.-L. Chan, M. Ligges, and X.-Y. Zhu, "The energy barrier in singlet fission can be overcome through coherent coupling and entropic gain", *Nat. Chem.*, **4**, 840–845 (2012).

[343] W.-L. Chan, T. C. Berkelbach, M. R. Provorse, N. R. Monahan, J. R. Tritsch, M. S. Hybertsen, D. R. Reichman, J. Gao, and X.-Y. Zhu, "The quantum coherent mechanism for singlet fission: Experiment and theory", *Acc. Chem. Res.*, **46**, 1321–1329 (2013).

[344] M. J. Y. Tayebjee, R. G. C. R. Clady, and T. W. Schmidt, "The exciton dynamics in tetracene thin films", *Phys. Chem. Chem. Phys.*, **15**, 14797–14805 (2013).

[345] S. T. Roberts, "Singlet to triplet and back again", *Nat. Chem.*, **7**, 764–765 (2015).

[346] H. L. Stern, A. Cheminal, S. R. Yost, K. Broch, S. L. Bayliss, K. Chen, M. Tabachnyk, K. Thorley, N. Greenham, J. M. Hodgkiss, J. Anthony, M. Head-Gordon, A. J. Musser, A. Rao, and R. H. Friend, "Vibronically coherent ultrafast triplet-pair formation and subsequent thermally activated dissociation control efficient endothermic singlet fission", *Nat. Chem.*, **9**, 1205–1212 (2017).

[347] N. R. Monahan, D. Sun, H. Tamura, K. W. Williams, B. Xu, Y. Zhong, B. Kumar, C. Nuckolls, A. R. Harutyunyan, G. Chen, H.-L. Dai, D. Beljonne, Y. Rao, and X.-Y. Zhu, "Dynamics of the triplet-pair state reveals the likely coexistence of coherent and incoherent singlet fission in crystalline hexacene", *Nat. Chem.*, **9**, 341–346 (2017).

[348] R. Tempelaar and D. R. Reichman, "Vibronic exciton theory of singlet fission. III. How vibronic coupling and thermodynamics promote rapid triplet generation in pentacene crystals", *J. Chem. Phys.*, **148**, 244701:1–9 (2018).

[349] A. F. Morrison and J. M. Herbert, "Analytic derivative couplings and first-principles exciton/phonon coupling constants for an *ab initio* Frenkel-Davydov exciton model: Theory, implementation, and application to compute triplet exciton mobility parameters for crystalline tetracene", *J. Chem. Phys.*, **146**, 224110:1–12 (2017).

[350] C. B. Dover, J. K. Gallaher, L. Frazer, P. C. Tapping, A. J. Petty II, M. J. Crossley, J. E. Anthony, T. W. Lee, and T. W. Schmidt, "Endothermic singlet fission is hindered by excimer formation", *Nat. Chem.*, **10**, 305–310 (2018).

[351] Z. L. Cai, K. Sendt, and J. R. Reimers, "Failure of density-functional theory and time-dependent density-functional theory for large extended π systems", *J. Chem. Phys.*, **117**, 5543 (2002).

[352] Y.-L. Wang and G.-S. Wu, "Improving the TDDFT calculation of low-lying excited states for polycyclic aromatic hydrocarbons using the Tamm–Dancoff approximation", *Int. J. Quantum Chem.*, **108**, 430–439 (2008).

[353] C. Adamo and D. Jacquemin, "The calculations of excited-state properties with time-dependent density functional theory", *Chem. Soc. Rev.*, **42**, 845–856 (2013).

[354] M. Ehara, R. Fukuda, C. Adamo, and I. Ciofini, "Chemically intuitive indices for charge-transfer excitation based on SAC-CI and TD-DFT calculations", *J. Comput. Chem.*, **34**, 2498–2501 (2013).

[355] T. Le Bahers, E. Brémond, I. Ciofini, and C. Adamo, "The nature of vertical excited states of dynes containing metals for DSSC applications: Insights from TD-DFT and density based indexes", *Phys. Chem. Chem. Phys.*, **16**, 14435–14444 (2014).

[356] C. Adamo, T. Le Bahers, M. Savarese, L. W. and G. García, R. Fukuda, M. Ehara, N. Rega, and I. Ciofini, "Exploring excited states using time dependent density functional theory and density-based indexes", *Coord. Chem. Rev.*, **304–305**, 166–178 (2015).

[357] D. Jacquemin and C. Adamo, "Computational molecular electronic spectroscopy with TD-DFT", in *Density-Functional Methods for Excited States*, N. Ferré and M. Filatov, Eds., Vol. 368 of *Topics in Current Chemistry;* Springer: Switzerland, 2016; pages 347–376.

[358] J. S. García, F. Maschietto, M. Campetella, and I. Ciofini, "Using density based indexes and wave function methods for the description of excited states: Excited state proton transfer reactions as a test case", *J. Phys. Chem. A*, **122**, 375–382 (2018).

[359] L. Huet, A. Perfetto, F. Muniz-Miranda, M. Campetell, C. Adamo, and I. Ciofini, "General density-based index to analyze charge transfer phenomena: From models to butterfly molecules", *J. Chem. Theory Comput.*, **16**, 4543–4553 (2020).

[360] F. Maschietto, M. Campetella, J. S. García, C. Adamo, and I. Ciofini, "Chasing unphysical TD-DFT excited states in transition metal complexes with a simple diagnostic tool", *J. Chem. Phys.*, **154**, 204102:1–12 (2021).

[361] A. D. Laurent, C. Adamo, and D. Jacquemin, "Dye chemistry with time-dependent density functional theory", *Phys. Chem. Chem. Phys.*, **16**, 14334–14356 (2014).

[362] C. A. Guido, P. Cortona, and C. Adamo, "Effective electron displacements: A tool for time-dependent density functional theory computational spectroscopy", *J. Chem. Phys.*, **140**, 104101:1–9 (2014).

[363] T. Etienne, "Probing the locality of excited states with linear algebra", *J. Chem. Theory Comput.*, **11**, 1692–1699 (2015).

[364] W. Graupner, M. Mauri, J. Stampfli, G. Leising, U. Scherf, and K. Mullen, "Photo-excited and doping-induced electronic states in a poly(*para*-phenylene)-type ladder polymer", *Solid State Commun.*, **91**, 7–12 (1994).

[365] C. Jamorski, J. B. Foresman, C. Thilgen, and H.-P. Lüthi, "Assessment of time-dependent density-functional theory for the calculation of critical features in the absorption spectra of a series of aromatic donor–acceptor systems", *J. Chem. Phys.*, **116**, 8761–8771 (2002).

[366] C. J. Jamorski and M. E. Casida, "Time-dependent density-functional theory investigation of the fluorescence behavior as a function of alkyl chain size for the 4-(N,N-dimethylamino)benzonitrile-like donor–acceptor systems 4-(N,N-diethylamino)benzonitrile and 4-(N,N-diisopropylamino)benzonitrile", *J. Phys. Chem. B*, **108**, 7132–7141 (2004).

[367] A. A. Taka, J. M. Herbert, and L. M. McCaslin, "Ground state orbital analysis predicts S_1 charge transfer in donor–acceptor materials", *J. Phys. Chem. Lett.*, **14**, 11063–11068 (2023).

[368] M. J. G. Peach, C. R. Le Sueur, K. Ruud, M. Guillaume, and D. J. Tozer, "TDDFT diagnostic testing and functional assessment for triazene chromophores", *Phys. Chem. Chem. Phys.*, **11**, 4465–4470 (2009).

[369] M. J. G. Peach and D. J. Tozer, "Illustration of a TDDFT spatial overlap diagnostic by basis function exponent scaling", *J. Mol. Struct. (Theochem)*, **914**, 110–114 (2009).

[370] X. Gui, C. Holzer, and W. Klopper, "Accuracy assessment of *GW* starting points for calculating molecular excitation energies using the Bethe–Salpeter formalism", *J. Chem. Theory Comput.*, **14**, 2127–2136 (2018).

[371] J. Plötner, D. J. Tozer, and A. Dreuw, "Dependence of excited state potential energy surfaces on the spatial overlap of the Kohn–Sham orbitals and the amount of nonlocal Hartree–Fock exchange in time-dependent density functional theory", *J. Chem. Theory Comput.*, **6**, 2315–2324 (2010).

[372] B. Moore, II, H. Sun, N. Govind, K. Kowalski, and J. Autschbach, "Charge-transfer versus charge-transfer-like excitations revisited", *J. Chem. Theory Comput.*, **11**, 3305–3320 (2015).

[373] P.-F. Loos, M. Comin, X. Blase, and D. Jacquemin, "Reference energies for intramolecular charge-transfer excitations", *J. Chem. Theory Comput.*, **17**, 3666–3686 (2021).

[374] M. Campetella, F. Maschietto, M. J. Frisch, G. Scalmani, I. Ciofini, and C. Adamo, "Charge transfer excitations in TDDFT: A ghost-hunter index", *J. Comput. Chem.*, **38**, 2151–2156 (2017).

[375] W. Humphrey, A. Dalke, and K. Schulten, "VMD—Visual molecular dynamics", *J. Molec. Graphics*, **14**, 33–38 (1996).

[376] T. Lu and F. Chen, "Multiwfn: A multifunctional wavefunction analyzer", *J. Comput. Chem.*, **33**, 580–592 (2012).

[377] E. Epifanovsky, A. T. B. Gilbert, X. Feng, J. Lee, Y. Mao, N. Mardirossian, P. Pokhilko, A. F. White, M. P. Coons, A. L. Dempwolff, Z. Gan, D. Hait, P. R. Horn, L. D. Jacobson, I. Kaliman, J. Kussmann, A. W. Lange, K. U. Lao, D. S. Levine, J. Liu, S. C. McKenzie, A. F. Morrison, K. D. Nanda, F. Plasser, D. R. Rehn, M. L. Vidal, Z.-Q. You, Y. Zhu, B. Alam, B. J. Albrecht, A. Aldossary, E. Alguire, J. H. Andersen, V. Athavale, D. Barton, K. Begam, A. Behn, N. Bellonzi, Y. A. Bernard, E. J. Berquist, H. G. A. Burton, A. Carreras, K. Carter-Fenk, R. Chakraborty, A. D. Chien, K. D. Closser, V. Cofer-Shabica, S. Dasgupta, M. de Wergifosse, J. Deng, M. Diedenhofen, H. Do, S. Ehlert,

P.-T. Fang, S. Fatehi, Q. Feng, T. Friedhoff, J. Gayvert, Q. Ge, G. Gidofalvi, M. Goldey, J. Gomes, C. E. González-Espinoza, S. Gulania, A. O. Gunina, M. W. D. Hanson-Heine, P. H. P. Harbach, A. Hauser, M. F. Herbst, M. Hernández Vera, M. Hodecker, Z. C. Holden, S. Houck, X. Huang, K. Hui, B. C. Huynh, M. Ivanov, A. Jász, H. Ji, H. Jiang, B. Kaduk, S. Kähler, K. Khistyaev, J. Kim, G. Kis, P. Klunzinger, Z. Koczor-Benda, J. H. Koh, D. Kosenkov, L. Koulias, T. Kowalczyk, C. M. Krauter, K. Kue, A. Kunitsa, T. Kus, I. Ladjánszki, A. Landau, K. V. Lawler, D. Lefrancois, S. Lehtola, R. R. Li, Y.-P. Li, J. Liang, M. Liebenthal, H.-H. Lin, Y.-S. Lin, F. Liu, K.-Y. Liu, M. Loipersberger, A. Luenser, A. Manjanath, P. Manohar, E. Mansoor, S. F. Manzer, S.-P. Mao, A. V. Marenich, T. Markovich, S. Mason, S. A. Maurer, P. F. McLaughlin, M. F. S. J. Menger, J.-M. Mewes, S. A. Mewes, P. Morgante, J. W. Mullinax, K. J. Oosterbaan, G. Paran, A. C. Paul, S. K. Paul, F. Pavošević, Z. Pei, S. Prager, E. I. Proynov, A. Rák, E. Ramos-Cordoba, B. Rana, A. E. Rask, A. Rettig, R. M. Richard, F. Rob, E. Rossomme, T. Scheele, M. Scheurer, M. Schneider, N. Sergueev, S. M. Sharada, W. Skomorowski, D. W. Small, C. J. Stein, Y.-C. Su, E. J. Sundstrom, Z. Tao, J. Thirman, G. J. Tornai, T. Tsuchimochi, N. M. Tubman, S. P. Veccham, O. Vydrov, J. Wenzel, J. Witte, A. Yamada, K. Yao, S. Yeganeh, S. R. Yost, A. Zech, I. Y. Zhang, X. Zhang, Y. Zhang, D. Zuev, A. Aspuru-Guzik, A. T. Bell, N. A. Besley, K. B. Bravaya, B. R. Brooks, D. Casanova, J.-D. Chai, S. Coriani, C. J. Cramer, G. Cserey, A. E. DePrince III, R. A. DiStasio Jr., A. Dreuw, B. D. Dunietz, T. R. Furlani, W. A. Goddard III, S. Hammes-Schiffer, T. Head-Gordon, W. J. Hehre, C.-P. Hsu, T.-C. Jagau, Y. Jung, A. Klamt, J. Kong, D. S. Lambrecht, W. Liang, N. J. Mayhall, C. W. McCurdy, J. B. Neaton, C. Ochsenfeld, J. A. Parkhill, R. Peverati, V. A. Rassolov, Y. Shao, L. V. Slipchenko, T. Stauch, R. P. Steele, J. E. Subotnik, A. J. W. Thom, A. Tkatchenko, D. G. Truhlar, T. Van Voorhis, T. A. Wesolowski, K. B. Whaley, H. L. Woodcock III, P. M. Zimmerman, S. Faraji, P. M. W. Gill, M. Head-Gordon, J. M. Herbert, and A. I. Krylov, "Software for the frontiers of quantum chemistry: An overview of developments in the Q-Chem 5 package", *J. Chem. Phys.*, **155**, 084801:1–59 (2021).

[378] Ohio Supercomputer Center (http://osc.edu/ark:/19495/f5s1ph73), accessed 2023-12-12.